Optical Characterization of Wide-Gap Detector-Grade Semiconductors

A dissertation submitted in partial fulfillment of the requirements for the Degree of
Doctor of Philosophy
at
Virginia Commonwealth University

By

Ezzat S. Elshazly

MSc. Material Science, London University, UK, 1999
MSc. Metallurgical Engineering, Cairo University, EGYPT, 2005

Director: **Gary C. Tepper**
Professor, Department of Mechanical Engineering

Virginia Commonwealth University
Richmond, Virginia, USA
August, 2010

UMI Number: 3413846

UMI

Dissertation Publishing

ProQuest®

المنارة للاستشارات

www.manaraa.com

Virginia Commonwealth University
School of Engineering
Department of Mechanical Engineering

This is to certify that the dissertation prepared by **Ezzat Salah El-Din Elshazly** entitled **Optical Characterization of Wide Bandgap Detector-Grade Semiconductors** has been approved by his or her committee as satisfactory completion of the dissertation requirement for the degree of **Doctor of Philosophy**

Gary C. Tepper, PhD., Dissertation Advisor, Department of Mechanical Engineering.

Supriyo Bandyopadhyay, PhD., Committee Member, Department of Elec. & Comp. Engineering.

Ramana M. Pidaparti, PhD., Committee Member, Department of Mechanical Engineering.

James T. McLeskey, PhD., Committee Member, Department of Mechanical Engineering.

Gary M. Atkinson, PhD., Committee Member, Department of Elec. & Comp. Engineering.

Vishnu B. Sundaresan, PhD., Committee Member, Department of Mechanical Engineering.

Gary C. Tepper, PhD., Chair, Department of Mechanical Engineering.

Russell D. Jamison, PhD., Dean of School of Engineering.

F. Douglas Boudinot, PhD., Dean of the Graduate School.

8 / 2010

ACKNOWLEDGEMENT

convey my gratitude to them for being generous in advising me regarding various issues and difficulties that I faced. They generously supported me to be success and independent.

I owe a special debt to Dr. Karla Mossi, our graduate coordinator, who helped in every possible way. I would like to thank her for continuous support. Her advices helped me not only in my work but also in my life.

I am also thankful for Dr. Dmitry Pestov for his valued help and his continuous support; he highlighted me with his knowledge and enthusiasm that motivated me to the end.

Thank you also to all the members of my research group, past and present, who have all been a vital part of my graduate studies.

My heartfelt thanks to my family and friends for their continuous spiritual support and patience. Their assistance in immeasurable ways and their faith in me have enlightened my entire life.

I would like to dedicate my thesis

to my beloved mother

TABLE OF CONTENTS

LIST OF ABBREVIATIONS

- Electron-Hole pair   ehp
- Electron Detrapping Rate D_e
- Hole Detrapping Rate D_h
- Applied Electric Field   E
- Intrinsic Fermi Level E_i
- Trap Energy E_t
- Electron Volt   eV
- Boltzmann Constant   k
- Electron concentration   n
- Intrinsic carrier concentration n_i
- Electron concentration at thermal equilibrium n_{no}
- Trap Concentration N_t
- Hole concentration at thermal equilibrium p_{no}
- Electron Trapping Rate T_e
- Hole Trapping Rate T_h
- Maximum Drift Time t_d
- Thermal Velocity of an electron or hole v_{th}
- Drift Velocity v_d
- Carrier mobility μ

LIST OF ABBREVIATIONS (Cont.)

- Electron Mobility μ_e

- Hole Mobility μ_h

- Trap capture cross-section for an electron σ_e

- Trap capture cross-section for a hole σ_h

- Carrier Lifetime τ

- Decay Constant τ_o

- Recombination lifetime τ_r

- Absolute Temperature T

- High Pressure Bridgman HPB

- Traveling Heater Method THM

- Physical Vapor Transport PVT

- Thermally stimulated current TSC

- Thermoelectric voltage spectroscopy TEVS

- Thermoelectric emission spectroscopy TEES

- Cadmium Zinc Telluride CZT

- Thallium Bromide TlBr

LIST OF TABLES

LIST OF FIGURES

Abstract

Optical Characterization of Wide Bandgap Detector Grade Semiconductors

By

Ezzat Salah El-Din Elshazly, PhD

A dissertation submitted in partial fulfillment of the requirements for the degree of **Doctor of Philosophy** at Virginia Commonwealth University

Virginia Commonwealth University, 2010

Major Director: **Gary C. Tepper**

Professor, Mechanical Engineering Department

Wide bandgap semiconductors are being widely investigated because they have the potential to satisfy the stringent material requirements of high resolution, room temperature gamma-ray spectrometers. In particular, Cadmium Zinc Telluride ($Cd_{1-x}Zn_xTe$, $x\sim0.1$) and Thallium Bromide (TlBr), due to their combination of high resistivity, high atomic number and good electron mobility, have became very promising candidates for use in X- and gamma-ray detectors operating at room temperature.

In this study, carrier trapping times were measured in CZT and TlBr as a function of temperature and material quality. Carrier lifetimes and tellurium inclusion densities

were measured in detector-grade Cadmium Zinc Telluride (CZT) crystals grown by the High Pressure Bridgman method and Modified Bridgman method. Excess carriers were produced in the material using a pulsed YAG laser with a 1064nm wavelength and 7ns pulse width. Infrared microscopy was used to measure the tellurium defect densities in CZT crystals. The electronic decay was optically measured at room temperature. Spatial mapping of lifetimes and defect densities in CZT was performed to determine the relationship between defect density and electronic decay. A significant and strong correlation was found between the volume fraction of tellurium inclusions and the carrier trapping time.

Carrier trapping times and tellurium inclusions were measured in CZT in the temperature range from 300K to 110K and the results were analyzed using a theoretical trapping model. Spatial mapping of carrier trapping times and defect densities in CZT was performed to determine the relationship between defect density and electronic decay. While a strong correlation between trapping time and defect density of tellurium inclusions was observed, there was no significant change in the trap energy.

Carrier trapping times were measured in detector grade thallium bromide (TlBr) and compared with the results for cadmium zinc telluride (CZT) in a temperature range from 300K to 110K. The experimental data was analyzed using a trapping model. In CZT, because the majority carrier concentration is close to the intrinsic carrier concentration, the trapping time increases exponentially as the temperature decreases below about 160K. While, in TlBr, the majority carrier concentration is many orders of magnitude greater than

the intrinsic carrier concentration and the trapping time followed a $\left(\sqrt{\frac{1}{T}}\right)$ temperature dependence over the range of temperatures studied. The results of the model suggest that a moderately deep compensation center, located approximately 200 meV from the middle of the bandgap, could be used to significantly increase the room temperature trapping time in TlBr. The results of this model demonstrate that the room temperature trapping time in TlBr can, in principle, approach 0.1ms through the introduction of a moderately deep compensation level but without decreasing the overall trap concentration. This strategy is not possible in CZT, because the band gap is too small to use a moderately deep compensation level while still maintaining high material resistivity.

Carrier trapping times were measured in three polycrystalline TlBr samples produced by melting commercial TlBr beads in a sealed quartz ampoule for two hours at three different temperatures near the melting point. The trapping time decreased with increasing melting temperature, presumably due to the thermal generation of a trap state.

Chapter (1)

Introduction and Background

CHAPTER (1)
INTRODUCTION AND BACKGROUND

1.1. Semiconductor Materials

Semiconductor materials are materials that possess an intermediate electrical conductivity between conductors, which easily conduct electrical current, and insulators, which do not conduct electrical current under normal conditions [1-3]. Materials with zero bandgap are metals or semimetals; while those materials with an energy gap larger than 3eV are more frequently known as insulators. There are some exceptions to these definitions, such as diamond (whose energy gap is about 6eV), semi-insulating GaAs (with a 1.5eV energy gap), and GaN (with energy gap of 3.5eV). A true semiconductor material, in its pure state, is neither a good conductor nor a good insulator.

The energy gap, by definition, is the minimum energy required for electron to move from its bound state to a free state where it can participate in conduction [4, 5]. Insulators have a wide bandgap and require significant energy to move from the electron from the valence band to the conduction band. Conductors or metals have either small or have non

2

existing bandgap and electrons can move easily from the valence band to the conduction band. While semiconductors have a bandgap with an intermediate energy gap between insulators and conductors, thereby thermally excited electrons can move from the valence band to the conduction band. Figure (1.1) is a schematic diagram of the electronic band structure of conductors, semiconductors and insulators. The energy needed for the movement of electrons is the difference between their energy in the conduction band and their energy in the valence band [6].
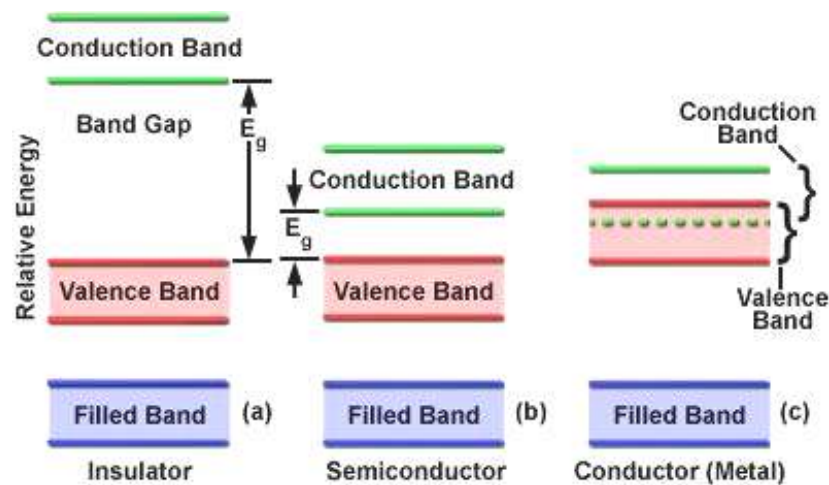
Figure (1.1): Simplified diagram of the electronic band structure of (A) Insulator, (B) Semiconductor, and (C) Metal [7-10].

Semiconductors can be generally classified into elemental semiconductors and compound semiconductors [11]. The elemental semiconductors are composed of single type of atoms such as silicon and germanium, while the compound semiconductors can be derived from elements in groups II to VI of the periodic table as shown in figure (1.2). These compounds can be either binary or ternary compounds. Binary compounds such as gallium arsenide (GaAs) or gallium phosphide (GaP) are formed by combining one

element from group III and one element from group V element. Ternary compound semiconductors such as $Al_xGa_{1-x}As$ and $Hg_{1-x}Cd_xTe$, (the subscript x indicates the fraction of the lower atomic number element component) are more complex and can offer flexibility when choosing material properties [5]. In order to understand and describe semiconductors, it is important to consider their inter-atomic bonding configurations, structural properties, and various imperfections that present in the material.
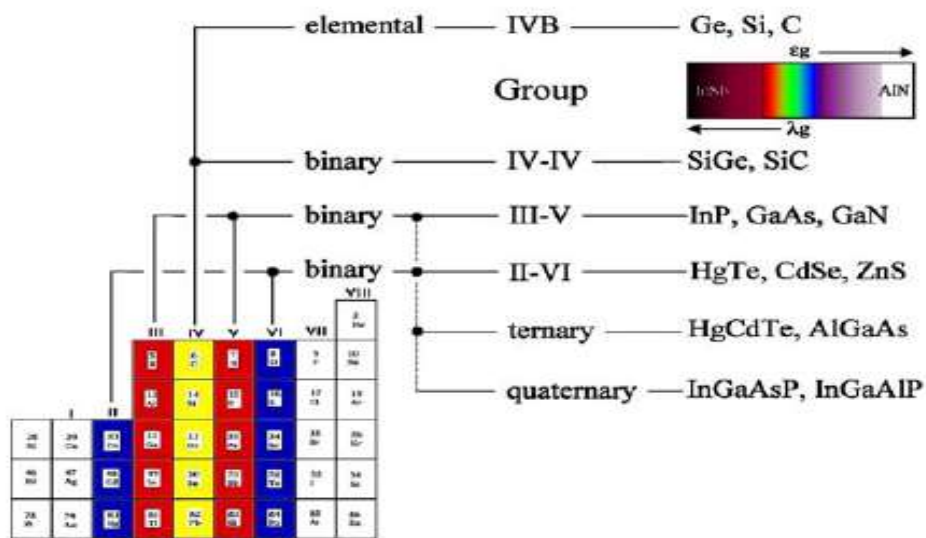
Figure (1.2): Diagram illustrating the elemental and compound semiconductors [12].

1.1.1. Intrinsic and Extrinsic Semiconductors

A semiconductor is considered intrinsic called intrinsic semiconductor if it is chemically pure and does not have energy level of conduction or bandgap. Specifically, if an electron receives enough thermal energy to jump from the valence band to the conduction band, it will leave a hole behind in the valence band. Each hole in the valence band corresponds to an electron in the conduction band, and the number of electrons in the conduction band is exactly equal to the number of holes left in the valence band [13].

4

Electrical properties of semiconductors can be drastically altered by adding trace amounts of suitable impurities to the pure crystals, this process called doping, and this type of semiconductor material is considered extrinsic. A semiconductor containing donor impurities is an n-type semiconductor, since most of the current carriers have a negative charge (electrons), conversely a semiconductor containing acceptor impurities is called a p-type semiconductor and the current carriers have a positive charge (holes) [14], as shown in figure (1.3).
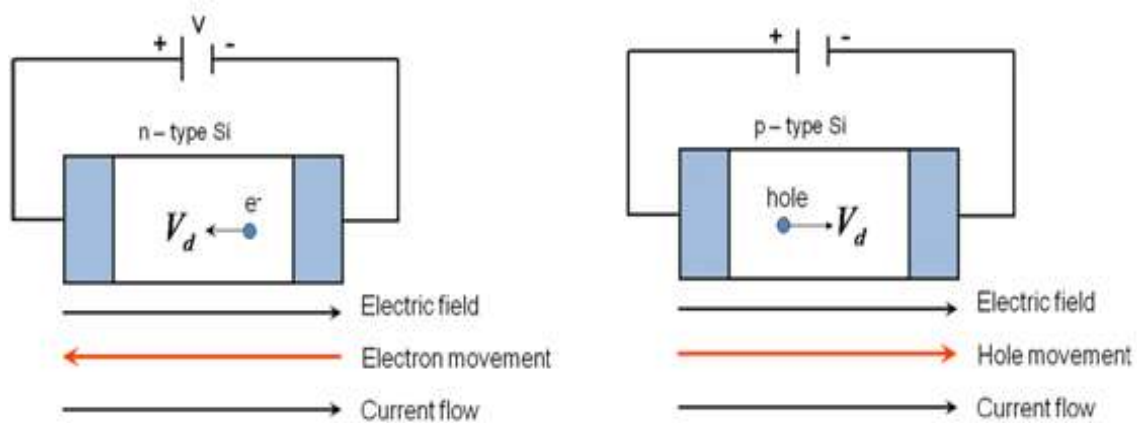
Figure (1.3): Schematic diagram illustrates the current carriers in an n-type and p-type semiconductors.

An n-type semiconductor has more free electrons than holes, while p-type semiconductor has more holes than free electrons. However, the material itself is charge neutral due to the ionized impurities which carry a charge equal and opposite to that of the free carriers [8].

1.1.2. Direct and Indirect Bandgap Semiconductors

As mentioned before, the band gap represents the minimum energy difference between the top of the valence band and the bottom of the conduction band. However, the

5

top of the valence band and the bottom of the conduction band are not generally at the same value of the electron momentum. In a direct band gap semiconductor, the top of the valence band and the bottom of the conduction band occur at the same value of momentum, as in the schematic below. In an indirect band gap semiconductor, the maximum energy of the valence band occurs at a different value of momentum to the minimum in the conduction band energy [15, 16].
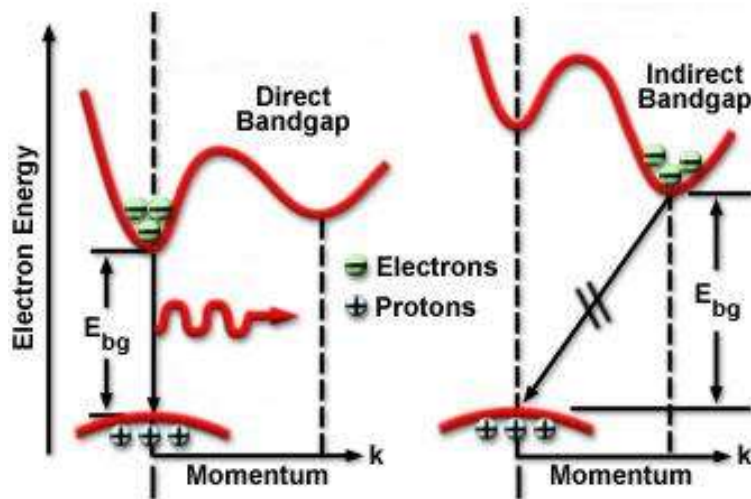
Figure (1.4): Direct and Indirect bandgap semiconductors.

A photon can produce an electron-hole pair in a direct band gap semiconductor quite easily, because the electron does not need to be given very much momentum. However, an electron must also undergo a significant change in its momentum for a photon to produce an electron-hole pair in an indirect band gap semiconductor. This is possible, but it requires such an electron to interact not only with the photon to gain energy, but also with a lattice vibration called a phonon in order to either gain or lose momentum.

6

1.1.3. Wide Bandgap Semiconductors

Wide bandgap semiconductors are semiconducting materials in which the energy of the band-to-band electronic transitions exceeds approximately 2eV. These materials have different kinds of chemical bonds and different crystal lattice structures [17]. This wide bandgap results on a high room temperature resistivity in intrinsic materials due to the small thermalization effects. Wide bandgap semiconductors can potentially satisfy the main requirements for high resolution room temperature gamma-ray radiation spectrometers which are used in various applications including well logging, weapons detection, environmental characterization and medical imaging [18].

The performance of wide band gap semiconductors is directly affected by impurities and defects produced during the growth process. The ability of the defects or impurities to trap a hole or electron can significantly influence the performance of the semiconductor radiation detectors. Many techniques have been used to characterize the performance and identify defects and impurities but few of them are able to quantify the effect of these defects on carrier lifetime.

There are two solid state materials that first come to mind are high purity germanium (HPGe) and sodium iodide (NaI) [19]. Germanium (Ge) presently is processed to a very pure state providing a very sensitive detection material. The generation of the electron-hole pairs by gamma ray absorption of germanium provides exceptional energy resolution that easily identifies the emitting source. The major drawback of germanium is the necessity of cooling to liquid nitrogen temperature (77K) in order to obtain high sensitivity; this will reduce the thermal excitation of electrons in the valence band.

Sodium iodide (NaI) provides detection by scintillation at room temperature; the incident particle energy is converted to visible light. The efficiency of this process is affected by other modes of de-excitation, such as heat, exist and can degrade the excitation energy through other modes. The decay time in sodium iodide is too long (230 ns) which considered as a problem when using sodium iodide detectors for high counting rate applications. A result of the long decay time is that phosphorescence can build up due to multiple overlapping of preceding pulses; this afterglow characteristic is undesirable in high rate applications.
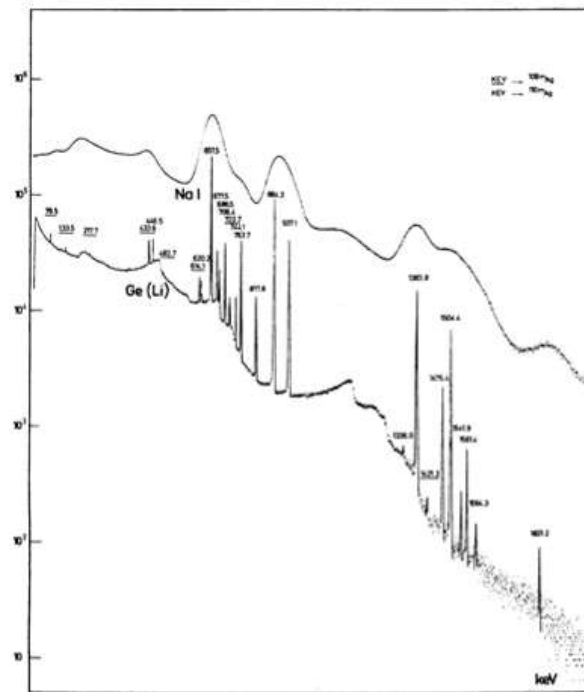
Figure (1.5): Comparative pulse height spectra recorded using a sodium iodide (NaI) scintilator and a Germanium (Ge) detector [20].

Figure (1.5) shows the energy resolution of Ge and NaI and the unresolved multiple peaks in NaI spectrum are easily resolved in the Ge spectrum. The energy resolution difference is apparent when comparing Germanium to sodium iodide.

The broadening of NaI peaks are resolved by Ge. This is one of the drawbacks of sodium iodide which makes it not suitable for the identification of complicated mixtures of gamma ray-producing materials. Therefore, there has been a strong interest in developing semiconductors that have high photon stopping power and can operate at room temperature, without sacrificing the advantages of Ge and NaI detectors.

The main physical properties required for fabrication of room temperature semiconductor detectors are [21-23]:

1) High atomic number and density for high stopping power.

2) A bandgap large enough to keep leakage currents low at room temperature.

3) Large electron and hole mobility-lifetime ($\mu\tau$) product for efficient charge collection.

High atomic number compound semiconductors such as Cadmium Telluride (CdTe), Cadmium Zinc telluride (CZT), Mercuric iodide (HgI_2), Lead Iodide (PbI_2), and Thallium Bromide (TlBr) have been investigated as excellent candidates for nuclear radiation detectors that can operate at room temperature [24-26].

1.2. Cadmium Zinc Telluride (CZT)

Ternary compound Cadmium Zinc Telluride ($Cd_{1-x}Zn_xTe$, x ~ 0.1-0.2) is one of the promising materials for room-temperature gamma-ray radiation detection [22, 27-29]. CdZnTe has a high density (~6 g/cm^3) and atomic number (Cd: 48, Zn: 30, Te: 52) that is sufficient to provide reasonably high gamma-ray stopping power. The bandgap of CZT is wide enough (~1.68 eV) to suppress thermal generation of charge carriers at room temperature and, under proper growth conditions, the material quality can be sufficient to

provide high resistivity (10^{10} Ω.cm) and low leakage currents under applied fields in the 10^3 V/cm range [30]. Table (1.1) provides some basic properties of CZT compared to CdTe [31].

Table (1.1): Some basic properties of CdTe and CdZnTe [31].

	Bandgap,	Resistivity	Electron Mobility	Hole Mobility	Typical Operating Electric Field
	(eV)	*(Ω.cm)*	*($cm^2/V.s^{-1}$)*	*($cm^2/V.s^{-1}$)*	*(V/cm)*
CdTe	1.47	$10^9 - 3x10^9$	1000 – 1100	80	300-500
Cd$_{1-x}$Zn$_x$Te (x~0.1)	1.65	$5x10^{10} - 10^{11}$	1000 – 1100	50	900-1500

The mean free path of the charge carriers, which establishes the maximum detector thickness, is given by the product of the charge carrier mobility, trapping time and applied electric field or $\mu\tau E$. The mean free path of electrons is currently in the range of a few centimeters and there is a significant effort underway to increase the volume and spectroscopic performance of CZT detectors for several applications such as industrial monitoring, gauging and imaging, medical imaging, nuclear safeguards and nonproliferation, transportation security and safety, as well as in a range of scientific applications [27, 32].

Cd$_{1-x}$Zn$_x$Te is actually a ternary alloy of CdTe and Zn. Its properties therefore depend on the concentration of zinc in the bulk, which is the main difference between CdTe and Cd$_{1-x}$Zn$_x$Te, as well as on the surface of the material. For radiation detection purposes the most important parameter is the band gap. Fortunately, the band gap has been found to be very lightly dependent on the concentration of zinc [26]. It was found that

fluctuations of the zinc concentration changes the band gap by only a few milielectron volts (~1.68eV) relative to CdTe (~1.5eV), which is insignificant for most detector related parameters. In general the concentration of zinc in a typical CdZnTe bulk is less than 10% [33, 34]. Empirically, the relationship between the bandgap (E_g) and the zinc fraction (x) can be described by the following equation [12]:

$$E_g(x) = 1.510 + 0.606\,x + 0.139\,x^2 \quad \text{eV} \tag{1.1}$$

The introduction of zinc at levels above x = .07 results in the formation of a p-type material [35]. The p-type semiconductor has a greater concentration of holes than electron carriers. It is necessary to compensate or balance this larger hole concentration with the introduction of a material such as indium or chloride that will introduce electrons. But it is also necessary to take advantage of deep level defects to assist in the pinning of the Fermi level near the middle of the band gap. So, when compensating CZT a balance of shallow and deep energy states is assumed to occur within the semiconductor [19]. An introduction of deep energy levels, from compensation, assists in controlling shallow trapping with an increase in resistance of CZT. But by controlling the shallow trapping states the lifetime of the carriers are influenced by deep energy traps that can also provide recombination sites. Even so, the balancing of semiconductor hole and electron concentration by compensation still provides a good method to control trapping within semiconductors and the ability to optimize detector performance.

Another important property of CZT material is that it can be formed into different shapes and sizes. Large area and complicated geometry CZT detectors can therefore be practically fabricated. CZT detectors have fairly high stopping power and absorption

efficiency due to the high atomic number elements. There are two main disadvantages associated with CZT materials: their low hole mobility (and hence low lifetime) and crystal defects. The crystal defects can be somewhat controlled by using some growth techniques that yield less crystal defects. The low hole mobility, on the other hand, is caused by the hole trapping mechanisms and is more or less intrinsic to the material. The only way to increase the hole lifetime is by increasing the detector bias voltage. Note that crystal defects further deteriorate the hole mobility and should therefore be controlled as much as possible. As known, the direct consequence of low charge carrier lifetime is the loss of signal. Since this loss is not linearly dependent on the amount of deposited energy, it results in nonlinear response of the detector. Another important point to note here is that the charge collection also depends on the depth of the material. For example if the charge is created near the collecting electrode of the detector, the loss of charge will be minimal. On the other hand, if the same charge is produced away from the collecting electrode, the signal loss will be higher. Increasing the bias voltage might not always be practical or even desirable in certain applications. The best way to compensate for the low hole mobility is to use ohmic contacts at the electrodes. The advantage of this method is that the holes get recombined with the electrons released into the material by the ohmic contact. This hole recombination effectively stops the leakage current, while the signal current is carried predominantly by the electrons. Ohmic contacts therefore completely eliminate the need for operating the detector at high voltages or external circuitry to compensate for low hole mobility.

1.3. Thallium Bromide (TlBr)

Thallium Bromide (TlBr) is a particularly attractive and promising compound semiconductor for fabrication of room temperature X- and gamma ray detectors [36-41]. It has a wide bandgap (~2.68eV) which enable it to operate at room temperature with low noise signal. Due to its high atomic number (Tl: 81, Br: 35) and high density (~7.5g/cm3), TlBr exhibits high photon stopping power. Relatively low melting temperature (~480°C) and a simple CsCl cubic lattice structure make TlBr single crystal easy to grow by conventional melt growth techniques [28, 29, 42], Table (1.2) provides some of the important properties of TlBr materials.

Table (1.2): Some important properties of TlBr materials [40].

Property	Value
Atomic Number	81,35
Density, g/cm^3	7.56
Bandgap, eV	2.68
Resistivity, Ω.cm	3×10^{10}
Electron Drift Mobility, cm^2/V.s	40.2
Hole Drift Mobility, cm^2/V.s	11.8
Electron Mobility-Lifetime ($\mu\tau_e$), cm^2/V	1.7×10^{-4}
Hole Mobility-Lifetime ($\mu\tau h$), cm^2/V	6.4×10^{-5}

Recent results have shown that single crystals of TlBr can be grown with a room temperature resistivity above 10^{10} Ω.cm and an electron mobility-lifetime ($\mu\tau$) product in the range of 10^{-4} cm^2/V [43]. The mobility-lifetime ($\mu\tau$) product for electrons in TlBr has

13

been improved by several orders of magnitude in comparison to the values reported just a few years ago [40, 44-46] and has resulted in room temperature radiation detectors with a thickness near 1 cm and an energy resolution better than 2%@662keV [41, 44]. TlBr has been studied for use as a gamma-ray radiation detector for many years [47, 48] for applications in fields such as homeland security, astrophysics [49, 50] and medical X-ray imaging [51], But due to the relatively poor charge transport properties, TlBr detector performance did not meet the desired expectations until very recently.

Multipass horizontal zone refining of commercially available material can improve the charge transport in TlBr crystals [52, 53]. The improvement in the mobility-lifetime ($\mu\tau$) product is presumably due to an improvement in crystal quality which reduces the number of charge traps thereby increasing the carrier trapping time [41]. However, at this time, there is no direct measurements of the carrier trapping time in TlBr have been reported.

1.4. Crystal Growth Methods

There are many crystal growth techniques have been used in the growth of semiconductors such as Bridgman methods [22, 54], traveling heater method [55], and physical vapor growth.

Bridgman methods are the most developed methodologies to grow semiconductor crystals [56, 57]. These methods involve the movement of a crucible containing high purity elemental source materials (99.999% pure) for the crystal formation through a temperature zone (furnace) which is programmed for a specific temperature profile. The heating furnace may be either horizontal or vertical and the growth may proceed by mechanically moving the crucible or by moving the heating furnace. Figure (1.6) presents the horizontal and vertical versions of the Bridgman technique.

The high pressure inhibits the reduction of source material through vaporization with a high over pressure [58]. After crystal growth is complete, it must cooled down slowly in order to avoid internal stress and damage by temperature gradients within the crystal.
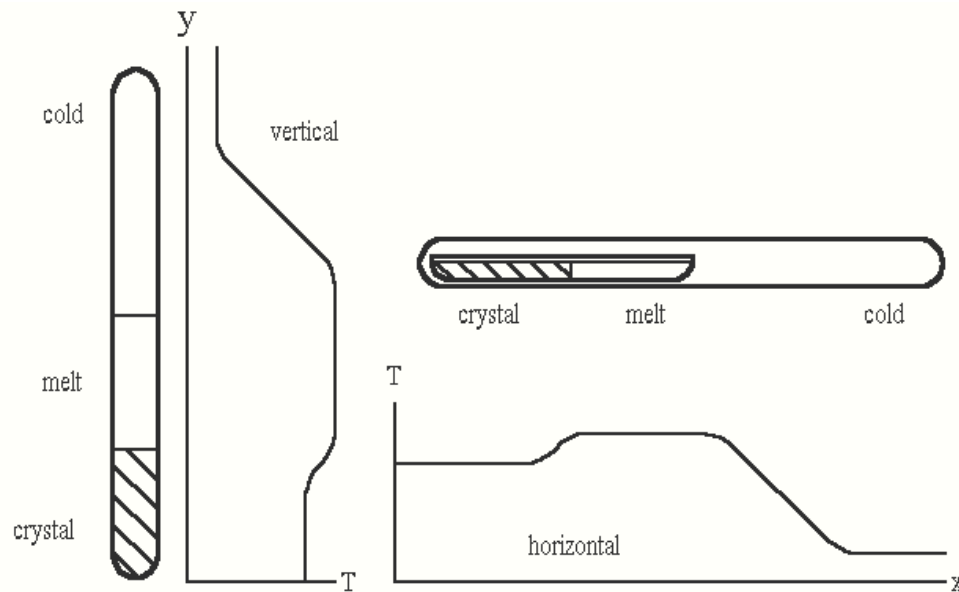
Figure (1.6): Crystal growth by vertical and horizontal Bridgman [59].

Control of the ampoule's cold end temperature is important during the cool down period, in order to have good crystal quality [60]. The crystal quality is maintained when the difference temperature, between the crystal and cold end, stays constant during this stage. The excess cadmium in the system condenses separately and crystallizes at the coldest point in the ampoule.

Traveling heater method (THM) is one of the solution growth techniques which has been applied to the single crystal growth of the semiconductors [61]. It was developed to provide steady-state conditions during the growth process. This method offers some advantages over the near stoichiometric melt techniques such as low temperature

15

www.manaraa.com

environment, low pressure environment, and the capability to synthesis large ingots [62, 63].

Physical vapor transport (PVT) is one of the more successful methods used to grow number of binary compounds used in radiation detection such as HgI_2, and CdTe [64]. The method has some advantages over melt growth techniques like the lower growth temperature and minimal contact area with the containment vessel which can reduce the impurity levels and stress related imperfections. In addition, it should be possible to achieve greater uniformity and better control of the stoichiometry. The method is amenable to either seeded or unseeded growth. As with melt growth a number of variations of the basic method have been developed. In general, the method is characterized by relatively slow growth rates and, in the case of CZT, by smaller boules. Despite significant thermo-chemical and kinetic complications, PVT has been applied with some success to the growth of CZT. As with the Bridgman method, controlled post-growth cooling is frequently employed. The boule diameter is up to 50 mm which is considerably smaller than that obtained using the Bridgman method [65] .

1.5. Crystal Defects

After growth process is completed, the produced ingot has numerous structural defects including grain boundaries, twins, polycrystallinity, cracks, voids, slips, dislocations and precipitates [35, 66] which can interfere with the charge collection and degrade the spectroscopic performance of the wide bandgap semiconductor gamma-ray spectrometers [67, 68]. Every impurity introduced into a crystal has a certain level of solubility, which defines the concentration of that impurity that the solid solution of the host crystal can accommodate. Impurity solubility usually decreases with decreasing

16

temperature. If an impurity is introduced into a crystal at the maximum concentration allowed by its solubility at a high temperature, the crystal will become supersaturated with that impurity once it is cooled down.
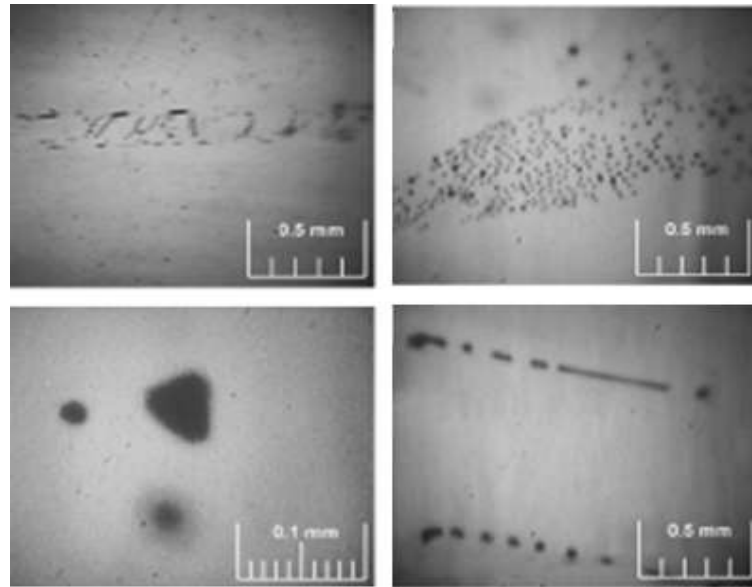
Figure (1.7): IR micrograph of main types of observed structural defects [69].
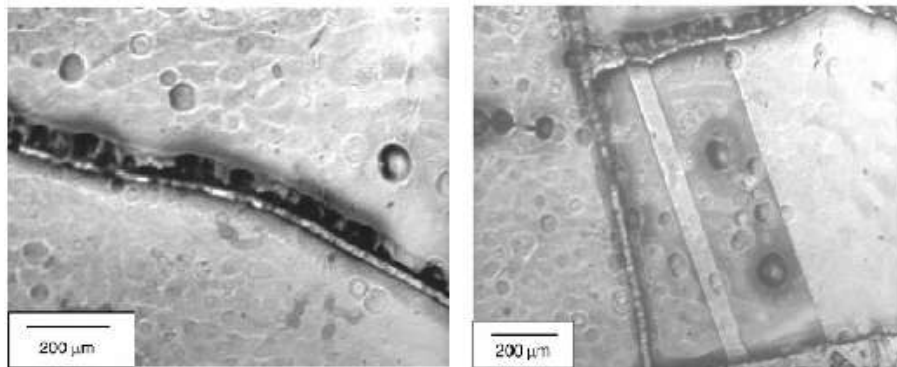
Figure (1.8): Te inclusions and dislocations in CZT crystal grown by THM technique [70].

A crystal under such supersaturated conditions seeks and achieves equilibrium by precipitating the excess impurity atoms into another phase of different composition or structure. Precipitates are considered undesirable because they have been known to act as

sites for the generation of dislocations[71]. Dislocations arise as a means of relieving stress generated by the strain exerted by precipitates on the lattice[72]. Of the numerous defects present in CZT, tellurium inclusions have been shown to have a particularly detrimental impact on detector performance [23, 73].

1.6. Electronic Decay Evaluation Techniques

There are several techniques have been used to measure the electronic properties of wide bandgap semiconductors such as thermally stimulated current (TSC), thermoelectric voltage spectroscopy (TEVS), and thermoelectric emission spectroscopy (TEES). Other techniques such as time of flight methods were used to determine the transport properties, carrier lifetime and mobility. One of the common features of most of these techniques is that it is necessary to apply contacts to the surface of the semiconductor to perform the measurements which means that the actual analysis of the semiconductor surface is not performed and these methods are known as contact methods.

For this reason, since the early 1960's, the microwave cavity perturbation (MCP) technique has been developed for studying the dielectric and magnetic properties of materials at microwave frequency. This technique was pioneered by Slater [74] and still one of the most widely used because of its high sensitivity and relative simplicity.

A microwave resonant cavity is usually fabricated from high-conductivity metal (usually from oxygen-free copper) with dimensions comparable to the wavelength; it might be in rectangular or cylindrical shape. Because of the complicated shape of resonator, it may be nearly impossible to calculate the distribution of electric and magnetic fields.

While in the case of right or simple geometrical form these distributions are well-known and calculated for a long time.

At resonance, the cavity is capable of sustaining microwave oscillations, which form an interference pattern from superposed microwaves multiply reflected from the cavity walls. Each particular cavity size and shape can sustain oscillations in a number of different standing wave configurations called modes.

1.7. Charge Transport of Radiation Detection Operation

When a gamma ray photon is absorbed within a semiconductor, electron-hole pairs are generated, figure 3 shows a schematic diagram of the radiation detection operation. The number of charge carriers, electrons and holes, is proportional to the energy of the incident gamma ray. The generated charge carriers can be transported through the semiconductor through the application of an electric field and the collected charge is converted to a voltage pulse. The amplitude of the pulse is a measure of the gamma ray energy. A key factor in determining if a photon is absorbed or transmitted is the energy of the photon itself. If the Photon energy (E_{ph}) is less than the band gap energy (E_G), it will interact only weakly with the semiconductor, passing through it as if it is transparent. If the Photon energy (E_{ph}) is equal to the band gap energy (E_G), it is just enough to create an electron hole pair and is efficiently absorbed. While, if the Photon energy (E_{ph}) is greater than the band gap energy (E_G), it will be strongly absorbed.
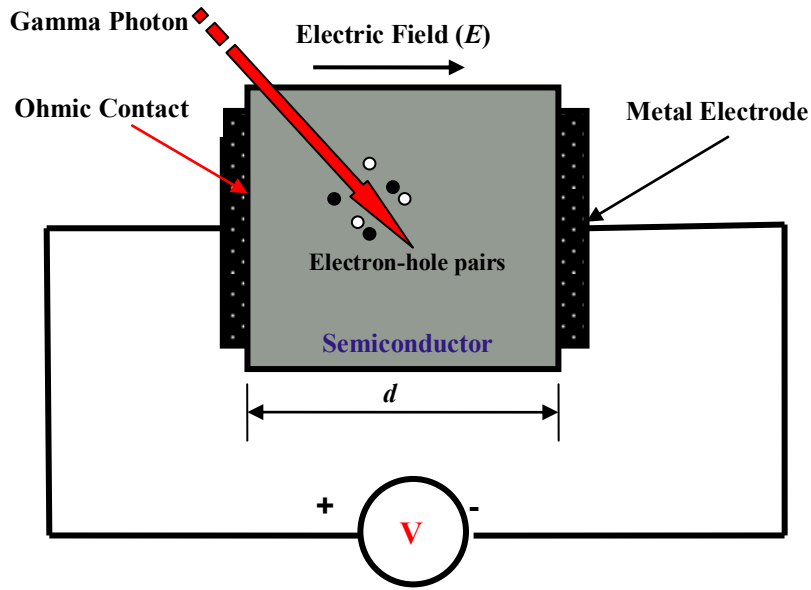
Figure (1.9): Schematic diagram illustrates the radiation detection operation.

The metal electrodes are used to impose an electric field across the semiconductor and collect the charge created by the incident radiation. For the high resistivity materials, the metal-semiconductor contact is preferred to be ohmic, i.e. have a linear current versus voltage relationship. This is the ideal case which only occurs when the mean free path of the charge carriers is long in comparison to the drift length within the semiconductor.

For efficient charge collection, the carrier lifetime (τ) must be long compared to the maximum drift time (t_d) within the detector, which can be expressed in terms of the drift velocity of the charge carriers (v_d) as:

$$t_d = \frac{d}{v_d} \tag{1.2}$$

Where d is the detector thickness or maximum drift length. The drift velocity is proportional to the applied electric field (E) through the relationship $v_d = \mu E$, where the proportionality constant (μ) is the carrier mobility.

20

Applying large electric field will increase the drift velocity and at the same time will increase the leakage current (the leakage current density is directly proportional with the applied electric field). By using high resistive materials, the leakage current can be decreased [75].

Defects can trap charge and reduce the mean free path and prevent efficient charge collection in radiation detector.

1.8. Neutral Trapping Model

Lifetime measurements fall into two categories, recombination and generation. Generation lifetime is essentially the time it takes to generate an electron-hole pair. The recombination lifetime is the measure of time it takes the electron-hole pair to cease to exist on average. These generation and recombination events occur at both the surface and the bulk material [76].

Three possible mechanisms, as shown in figure (1.10), are associated with the bulk recombination process:

1. Band-to-Band (*Radiative*) recombination where the electron hole pairs recombine from band to band with energy carried away by a photon. The radiative lifetime is inversely proportional to the carrier concentration (electron or hole concentration) because in band-to-band processes both electrons and holes must be present simultaneously for a recombination event to occur.

2. Trap-assisted (*Shockley-Read-Hall*) recombination, where electron-hole pairs recombine through deep level impurities. The impurity has a certain concentration,

21

energy and cross-section associated with it. Lattice vibrations or phonons dissipate the energy liberated during recombination event.

3. Auger recombination where three carriers are involved where and an electron and a hole which recombine in a band-to band transition and give off the resulting energy to a third carrier (electron or hole). The Auger lifetime is inversely proportional to the square of the carrier concentration.
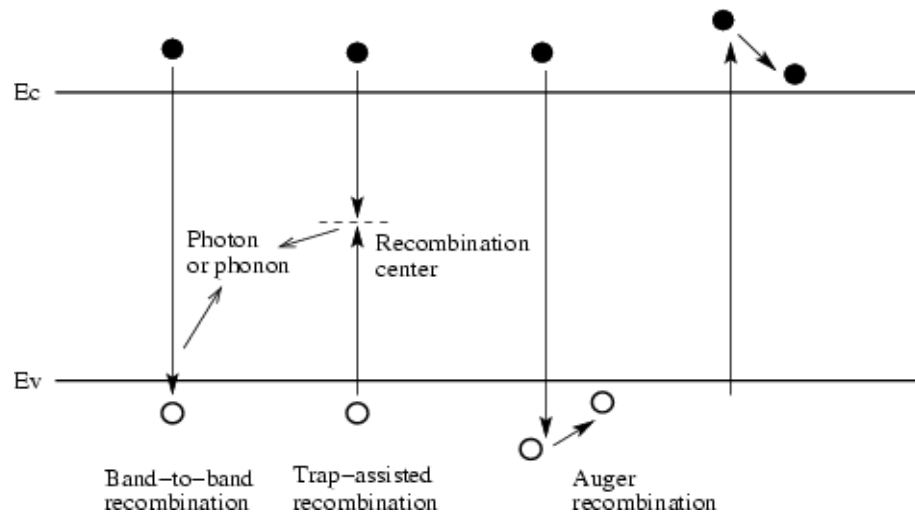
Figure (1. 10): Schematic diagram illustrates the carrier recombination mechanisms: a) Band-to-Band recombination, b) Trap-assisted recombination, and c) Auger recombination [77].

There are various transitions, shown in figure (1.11), that occur in the recombination process through the recombination centers which called emission and capture processes [78, 79]:

1) Hole emission: the process of hole emission from a defect, it can also viewed as promoting an electron from the valence band to the defect level.

2) Electron emission: the electron can proceed to the conduction band and contribute to the current flow (generation current).

3) Electron capture: conversely, a defect state can capture an electron from the conduction band which in turn can capture a hole. This recombination process reduces current flowing in the conduction band.

4) Hole capture: defect levels close to a band edge will capture charge and release it after some time, this process called trapping.
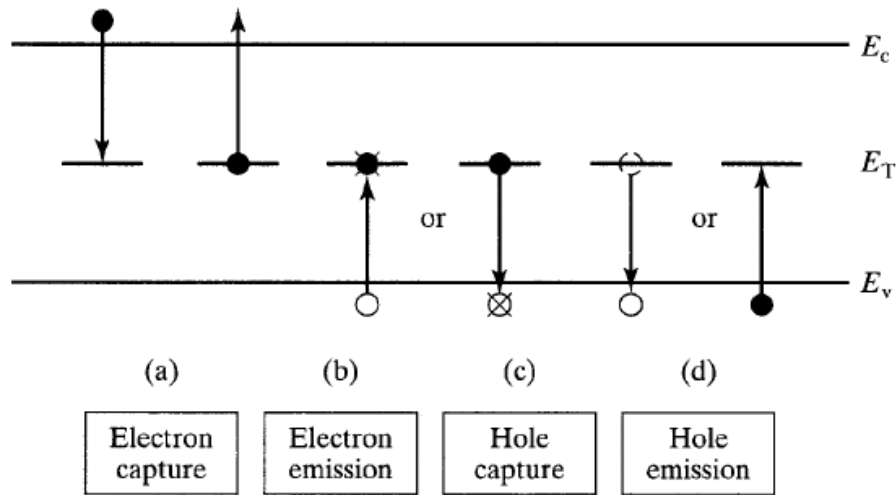
Figure (1.11): Indirect generation-recombination process at thermal equilibrium [80].

The probability of each of these events or processes occurring depends on the numbers of occupied and unoccupied states in the different levels and therefore depends on the position of the Fermi level. However the Fermi level is only a valid concept under equilibrium conditions.

$$np = n_i^2 \qquad (1.3)$$

Probability of electron occupies trap $(f_t) = \dfrac{1}{1+\exp\left(\dfrac{E_t - E_f}{kT}\right)}$ (1.4)

Where E_t is the energy level of the center, E_f is the Fermi level, k is Boltzmann constant and T is the absolute temperature.

Therefore, probability of hole occupies trap $(1 - f_t)$

Number of occupied centers $= N_t f_t$

Number of unoccupied centers $N_t (1 - f_t)$

By assuming that the trapping processes are all first order, i.e. the rate of electron capture is proportional to the number of electrons in the conduction band and to the number of empty trapping energy [81].

$$R_a = n N_t (1 - f_t)$$ (1.5)

$$R_a = v_{th} \sigma_n n N_t (1 - f_t)$$ (1.6)

Where v_{th} is the thermal velocity of electrons ($\sim 10^7$ cm/s), and σ_n is the capture cross section of electrons ($\sim 10^{-15}$ cm^2).

The electron emission rate is proportional to the number of occupied trapping centers (the conduction band is nearly empty).

$$R_b = e_n N_t f_t$$ (1.7)

Where the probability constant e_n is called the emission probability.

For the holes we can write similar equations,

$$R_c = v_{th} \sigma_p p N_t f_t$$ (1.8)

$$R_d = e_p N_t (1 - f_t) \tag{1.9}$$

Under thermal equilibrium, $R_a = R_b$ and $R_c = R_d$

$$v_{th} \sigma_n n N_t (1 - f_t) = e_n N_t f_t \tag{1.10}$$

$$v_{th} \sigma_p p N_t f_t = e_p N_t (1 - f_t) \tag{1.11}$$

As
$$n = n_i \exp\left(\frac{E_f - E_i}{kT} \right) \tag{1.12}$$

$$p = n_i \exp\left(\frac{E_i - E_f}{kT} \right) \tag{1.13}$$

Therefore,

$$v_{th} \sigma_n n_i \exp\left(\frac{E_f - E_i}{kT} \right) N_t (1 - f_t) = e_n N_t f_t \tag{1.14}$$

$$v_{th} \sigma_p ni \exp\left(\frac{E_i - E_f}{kT} \right) N_t f_t = e_p N_t (1 - f_t) \tag{1.15}$$

Also,
$$\frac{1 - f_t}{f_t} = \exp\left(\frac{E_t - E_f}{kT} \right) \tag{1.16}$$

The emission rates can be expressed as:

$$e_n = v_{th} \sigma_n n_i \exp\left(\frac{E_t - E_i}{kT} \right) \quad \text{carriers/s} \tag{1.17}$$

$$e_p = v_{th} \sigma_n n_i \exp\left(\frac{E_i - E_t}{kT} \right) \quad \text{carriers/s} \tag{1.18}$$

The relationship between the capture and emission rates expressed on equations (15) and (16) does not depend on the Fermi level and are valid in non-equilibrium although

25

they were derived using equilibrium assumptions. However, equations which include the

probability of occupation depend on E_f and are only valid in equilibrium.
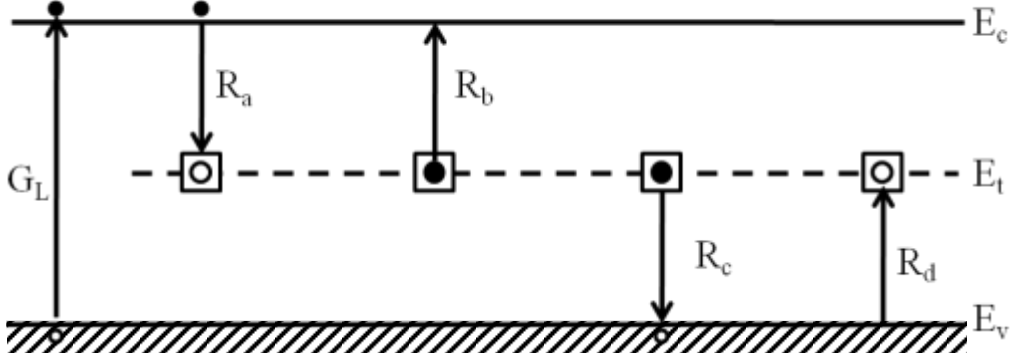
Figure (1.12): Generation-recombination processes under illumination [82].

In steady state (not equilibrium),

$$G_L = R_a - R_b = R_c - R_d \tag{1.19}$$

The numbers of electrons and holes in the conduction band are constant.

$$R_a - R_b = R_c - R_d \tag{1.20}$$

Using the previous expressions for the capture and emission rates,

$$v_{th}\sigma_n nN_t(1-f_t) - e_n N_t f_t = v_{th}\sigma_p pN_t f_t - e_p N_t(1-f_t) \tag{1.21}$$

$$v_{th}\sigma_n nN_t\left[n(1-f_t) - n_i \exp\left(\frac{E_t-E_i}{kT}\right)f_t\right] = v_{th}\sigma_p pN_t\left[pf_t - n_i \exp\left(\frac{E_i-E_t}{kT}\right)(1-f_t)\right] \tag{1.22}$$

For reasons which will become apparent, define

$$\tau_n = \frac{1}{v_{th}\sigma_n N_t} \quad , \quad \tau_p = \frac{1}{v_{th}\sigma_p N_t}$$

Then, $\quad \dfrac{1}{\tau_n}\left[n(1-f_t) - n_i \exp\left(\dfrac{E_t-E_i}{kT}\right)f_t\right] = \dfrac{1}{\tau_p}\left[pf_t - n_i \exp\left(\dfrac{E_i-E_t}{kT}\right)(1-f_t)\right] \tag{1.23}$

26

This equation can be solved for f_t, the occupation probability of the trap level.

$$f_t = \frac{\tau_n \tau_p \left[n + n_i \exp\left(\frac{E_i - E_t}{kT} \right) \right]}{\tau_p \left[n + n_i \exp\left(\frac{E_t - E_i}{kT} \right) \right] + \tau_n \left[p + n_i \exp\left(\frac{E_i - E_t}{kT} \right) \right]} \tag{1.24}$$

The net recombination rate $U = R_1 - R_2$,

$$U = \frac{\left(pn - n_i \right)^2}{\tau_p \left[n + n_i \exp\left(\frac{E_t - E_i}{kT} \right) \right] + \tau_n \left[p + n_i \exp\left(\frac{E_i - E_t}{kT} \right) \right]} \tag{1.25}$$

If we assume that $\tau = \tau_n = \tau_p = \dfrac{1}{v_{th} \sigma N_t}$

The net recombination rate can be simplified to:

$$U = \frac{\left(pn - n_i \right)^2}{\tau \left[n + p + 2n_i \cosh\left(\frac{E_t - E_i}{kT} \right) \right]} \tag{1.26}$$

$$U \cong v_{th} \sigma_o N_t \frac{\left(pn - n_i \right)^2}{1 + \left(\frac{2n_i}{n_{no} + p_{no}} \right) \cosh\left(\frac{E_t - E_i}{kT} \right)} = \frac{p_n - p_{no}}{\tau_r} \tag{1.27}$$

Where τ_r is the recombination lifetime and given by

$$\tau_r = \frac{1 + \left(\frac{2n_i}{n_{no} + p_{no}} \right) \cosh\left(\frac{E_t - E_i}{kT} \right)}{v_{th} \sigma_o N_t} \tag{1.28}$$

To restore the system to equilibrium, carriers must be generated by the generation-recombination centers.

The generation lifetime (τ_g) is;

27

$$\tau_g = \frac{2\cosh\left(\dfrac{E_t - E_i}{kT}\right)}{v_{th}\sigma_o N_t} \tag{1.29}$$

From the last two equations above, equations (26) and (27):

$$\frac{\tau_g}{\tau_r} \cong 2\cosh\left(\frac{E_t - E_i}{kT}\right) \tag{1.30}$$

By assuming low injection conditions for an n-type semiconductor (i.e. $p_n \ll n_i$ and

$n_n < n_i$), the recombination lifetime can be calculated:

$$\tau_r \cong \left(\frac{1}{v_{th}\sigma_o N_t}\right)\left[1 + \left(\frac{2n_i}{n_o}\right)\cosh\left(\frac{E_t - E_i}{kT}\right)\right] \tag{1.31}$$

1.9. Dissertation Objectives

The main objectives of this study can be summarized as follows:

a. Characterize the electronic decay behavior of wide bandgap compound semiconductors to assist in the fabrication of room temperature gamma-ray detectors.

b. Determine the effect of the crystal growth technique on the electronic decay measurements of CZT crystals have been grown by different growth techniques.

c. Studying the effect of the crystal defects resulted from the growth process of CZT crystals on the carrier lifetime.

d. Studying the kinetics of the electronic decay process in wide bandgap semiconductors as a function of temperature.

e. Investigating other room temperature semiconductors such as detector grade Thallium Bromide.

1.10. Dissertation Organization

This study focused on the Optical Characterization of Wide Bandgap Detector Grade Semiconductors and falls in six chapters. The first chapter has provided background information from the relevant literature and listed the main objectives and expected contributions of this dissertation. Chapter 2 discusses the materials and the experimental procedures used in this study. Chapter 3 presents a quantitative study of the defects resulted during the crystal growth process; while Chapter 4 focuses on the correlation between between the volume fraction of the tellurium inclusions and the carrier trapping time in CdZnTe crystals. Chapter 5 presents the measurements of the carrier trapping time in single crystal CZT and TlBr as a function of temperature, whereas chapter 6 provides the recommendations for future research.

Chapter (2)

Materials and Experimental Procedures

CHAPTER (2)

MATERIALS AND EXPERIMENTAL PROCEDURES

2.1. IR Imaging Microscopy System

Te precipitates or inclusions are one of these defects resulted during the crystal growth process in the ternary compound cadmium zinc telluride (CdZnTe). These inclusions are considered as one of the factors limiting the performance of the radiation detector. Since CZT crystals are opaque to visible light but transparent if illuminated with infrared light while the internal defects such as tellurium inclusions are not. Te inclusions will act to either scatter or absorb the infrared light and show up as distinct black spots.

An infrared (IR) microscope imaging system has been established and developed and was used for measuring the Te inclusions in the CZT crystals. The system mainly consists of:

- An infra red back light,

31

- 3D translation stage,

- IR sensitive CCD camera with long objective microscope lens and a $7.8 \times 10.6 \ mm^2$ sensor with 2208×3000 pixels, and

- The 3D translation stage.
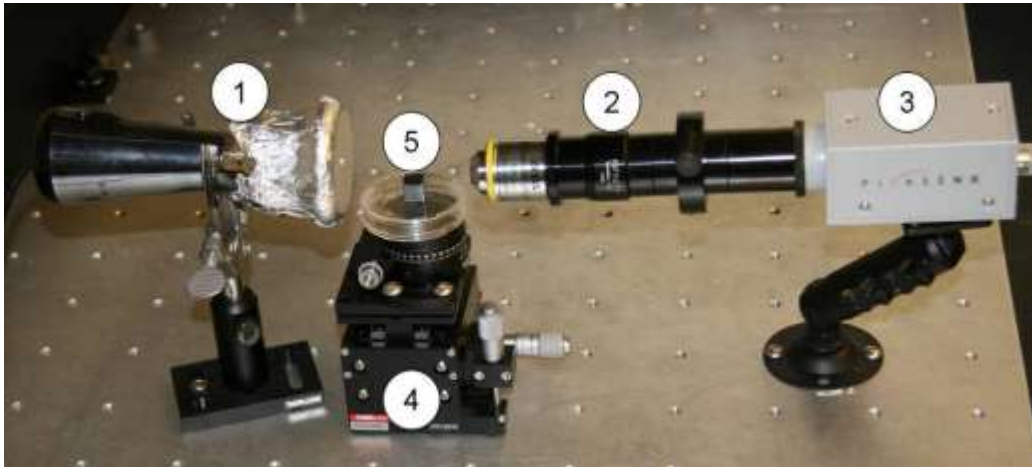
Figure (2.1): Photograph of the IR microscope imaging system setup: (1) IR light, (2) Long objective length, (3) CCD camera, (4) 3D translation stage, (5) The sample.

By using the 3D translation stage, the system can perform a one, two, or three dimensional scan. At each XYZ position of the crystal, an image of the area is taken and saved, and then the translation stage moves to the next position where this is repeated. The system setup allowed us to acquire stacks of images, each focused at a different depth of the crystal. IR images were saved as monochrome high-resolution jpeg files and *Image-pro Plus 6.0* software was used to calculate the sizes and concentrations of Te precipitates in the crystal.

2.2. Nd:YAG Laser

Neodymium:Yttrium-Aluminum-Garnet (Nd:YAG) pulsed laser was used to generate the laser energy that pumped into the wide bandgap semiconductors. There are four wavelengths are available to choose from, the fundamental at 1064nm and three harmonics at, 532, 355 and 266 nm respectively; therefore, a wide spectrum of energies is available. The used wavelength depends on the bandgap of semiconductor material. The excitation wavelength of the laser is below the bandgap energy of the semiconductor material so that most of the carrier generation will be from the midgap energy states within the bulk of the crystal. For the proceeding experiments, the 1064 nm wavelength and 7ns as a pulse width was primarily used to excite carriers in the CZT material, while the 532 nm wavelength was used for the TlBr material.

2.2.1. Laser Theory

The generation of the laser beam is as follows. The flash lamp, filled with xenon, is electrically pulsed and the generated light from the excited xenon in turn excites the neodymium in the YAG rod. The excited neodymium atoms remain in an excited lasing level for a fraction of a millisecond. To obtain maximum benefit from the laser light stored in the YAG rod, the laser oscillation is held off in a process called Q-switching [83].

The Q-switching process allows for a buildup of excited atoms in the rod. The Q-switch is open very briefly (nanosecond) and the stored energy is emitted in a short intense pulse. The polarization vector of the light beam can be rotated if the appropriate electric field is applied to the proper orientation of the crystal. A high voltage Marx bank circuit

applies a voltage of approximately 3500 Volt; this voltage is the quarter wave voltage for KDP at 1064 nm.

The xenon flash lamp pumps the laser rod and atoms are driven to higher electronic levels. The laser does not oscillate because the Q-switch is closed; the light passing through the polarizer orients the laser beam to a vertical polarization vector. Then the laser beam passes through the potassium dihydrogen phosphate crystal (KDP) without any electric field applied. The light continues through a quarter wave plate and hits a high reflector and passes the quarter wave plate a second time, the light beam is now polarized horizontally. In other words when the light interacts with the polarizer on the return trip from the high reflector, the light is polarized vertically preventing it from reentering the rod, also known as hold off. The rod stores optical energy since it is not depleted during hold off. The time when maximum storage has occurred (100μs after lamp pumping the rod) the Marx bank voltage is applied to the KDP. The light undergoes a 90-degree rotation of polarization so it can pass through the polarizer and laser rod. The laser is now free to oscillate between the high reflector and output coupler. The light undergoes enough roundtrips to build up enough gain to overcome the losses imposed in the cavity. The resulting pulse is on the order of 7ns with a high peak power per pulse [83].

A tunable solid-state yttrium-iron-garnet (YIG) oscillator was used to provide microwave energy with a frequency of 4-8 GHz with a maximum power of 100 mW. The microwave energy is directed through a waveguide and entered the resonant cavity containing semiconductor sample. The frequency of the microwave signal was matched to the cavity resonant frequency by a tuning adjustment built into the cavity. The cavity and sample were critically coupled to minimize the power reflected back toward the source.

The resonant frequency of the cavity/sample was determined by its size and dielectric constant of the sample material. When a photon of light is absorbed by the sample, electron-hole pairs are generated and the conductivity of the sample momentarily increases. Since the energy of the microwave photons are much less than the band gap of the material, the microwaves can only lose energy to the free charge carriers generated by the ionizing radiation. The absorption event causes a perturbation, disturbance in energy balance, in the cavity coupling and some microwave power is reflected back towards the source.

The reflected power passed through a 30dB preamplifier before entering a double balanced mixer detector, this assists in the comparison of the base line power compared to the perturbed power condition. The mixer output signal is input to a custom built preamplifier with a response 1µs. An oscilloscope monitors the preamplifier and YIG outputs. The Oscilloscope was interfaced with a GPIB connection to a computer to capture the signals.

The contactless technique involves establishing a natural resonant condition in a highly reflective cavity. The procedure for creating the desired resonant condition is well documented and the theory and design is presented below. The cavity has been fabricated in a cylindrical design for experimentation at a desired electromagnetic mode for a certain microwave frequency. For its cylindrical design, the field distributions in the cavity need to be determined. There are two modes of cavity; transverse electric (TE_{lmn}) and transverse magnetic (TM_{lmn}) mode. The integers l, m, and n prescribe the number of full period variations in the transverse electric (TE) or transverse magnetic (TM) fields for the three principle directions in the cylindrical coordinate system.

35
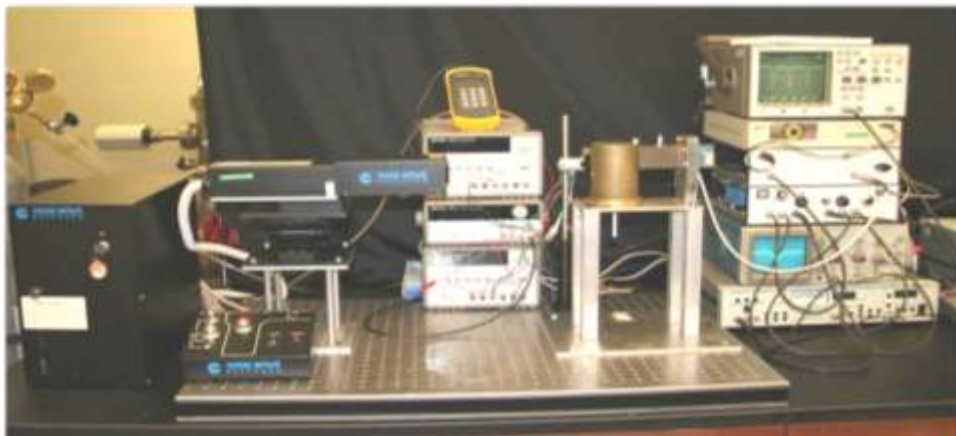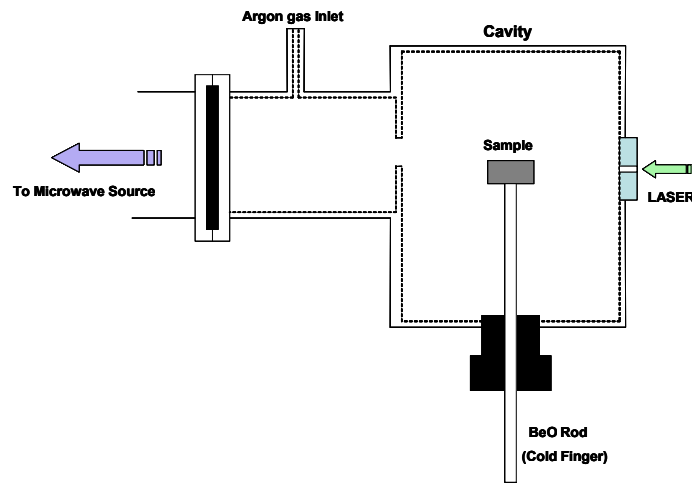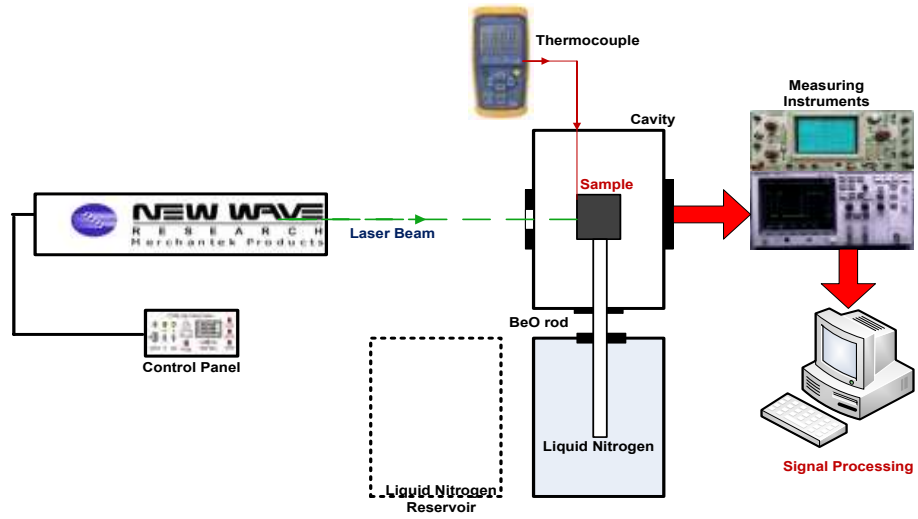
Figure (2.2): The basic experimental setup.

The cylindrical cavity, TE_{011}, was machined out of brass and silver plated to provide a high quality factor (Q). A high Q or sharp resonance allows small changes in cavity properties to be resolved. One method of calculating Q of a resonating cavity is to take the resonant frequency (f) and divide by its width (df) or $Q = f / \Delta f$. The unloaded or empty cavity, Q, and resonant frequency are calculated in the current cavity to be about 15000 at 4.6 GHz. The TE_{011} cavity has electric field strength at a minimum in the center of the cavity where the TM_{010} cavity has an electric field maximum. The magnitude of the electric field that is established at the sample location is a function of several parameters including microwave power and quality factor.

The semiconductor crystals are placed in the center of the cavity using a BeO rod that is inserted axially through the center of the cavity. The BeO rod is an electrical insulator that does not significantly load the cavity compared to the semiconductor crystal. The BeO rod also has a high thermal conductivity which is important at low temperature measurements. Controlling the temperature of the sample is achieved by placing the external end of the BeO rod in a liquid nitrogen reservoir. By this way, the sample's temperature can be controlled without directly placing the temperature source inside the cavity. A continuous flow of inert gas (i.e. argon gas) can be used to avoid any condensation occurred inside the cavity.

2.3. Materials

Three highly polished surface CZT single crystals, one Thallium Bromide (TlBr) single crystal, and three polycrystalline TlBr samples have been used in this study. The general specifications and designations of these materials have been summarized in Table (2.1).

Table (2.1): The general specifications and designations of the used materials.

Crystal	Dimensions (mm)	Growth Technique	Vendor
CZT1	10x10x10	High Pressure Bridgman	eV-Products
CZT2	10x10x10	High Pressure Bridgman	eV-Products
CZT3	8x8x15	Modified Bridgman	Yinnel Tech.
TlBr-SC	10x10x2.6	Travelling Molten Zone	Bruker Baltic Ltd.,
TlBr480	7.5x15 (D x L)	Traditional melting	_____
TlBr500	7.5x15 (D x L)	Traditional melting	_____
TlBr520	7.5x15 (D x L)	Traditional Melting	_____

Chapter (3)

Defect Density in Cadmium Zinc Telluride Crystals

CHAPTER (3)

DEFECT DENSITY IN CADMIUM ZINC TELLURIDE CRYSTALS

3.1. Introduction

3.1.1. Crystal Defects

As we mentioned earlier in Chapter 1, there are many kinds of defects such as grain boundaries, twin boundaries, pipes, voids, and second phase precipitates resulted during the crystal growth process [71, 84]. Tellurium precipitates/inclusions in the cadmium zinc telluride crystals grown by high pressure Bridgman method are typical. The presence of these Te inclusions cause large fluctuations in the collected charge and degrade the spectroscopic performance of CZT gamma-ray spectrometers [67]. Tellurium inclusions can be described as non-stoichiometric defects that form during the melt growth of the crystal [56, 85, 86]; differ from Te precipitates which are formed during crystal cooling as a result of the nucleation of native defects. Te inclusions/precipitates are formed based on

40

its solubility in reference to the Cd-Te phase diagram [87]. The spatial distribution of the precipitates/inclusions is normally one of three types: dispersed, cellular, or segregated along grain and twin boundaries [88, 89]. However, the likely explanation of how are the Te precipitates formed is that Te antisites are actually Te atoms located at Cd vacancies. By increasing the Te overpressure supplied by excess Te, the CZT crystal became Te rich [35]. In this process, small amounts of Cd vacancies are formed first and the density of Cd vacancies start to increase due to the higher Te overpressure and consequently Te atoms begin to occupy some of the vacancy sites. After both the Cd vacancies and Te antisites (Te_{Cd}) reach the densities determined by thermodynamics, complexes such as Te precipitates begin to form [72]. The observed precipitates/inclusions dispersed in CZT appear to have little effect on the electrical properties [22, 68, 90]. These defects behave as ordinary traps associated with point defects, native or impurities, in the material [91, 92]. Since tellurium has a narrow bandgap (~ 0.3eV), Te precipitates have higher electrical conductivity which affect the detector leakage current and distort the electric field distribution and carrier transport in CZT devices. Conversely, the concentration of Te precipitates in the as-grown material can be high, which may affect the mobility-lifetime product ($\mu\tau$) for both holes and electrons [90, 93].

3.2. Te Inclusion Density in CZT Crystals

In this chapter, we report on the size and concentrations of tellurium inclusions in detector grade $Cd_{1-x} Zn_x Te$ (x ~ 0.1-0.2). The crystals used in these measurements were acquired from two vendors: eV Products and Yinnel Tech, Inc., representing two different growth techniques.

Two crystals of 10x10x10mm^3 grown by the High Pressure Bridgman method at eV Products, and one crystal of 8x8x15mm^3 grown by the Modified Bridgman method at Yinnel Tech, Inc. All of the three crystals posses a highly polished surface. Table (3.1) shows the general specifications and designations of the CZT crystals.

Table (3.1): General specifications of the used CZT crystals

Crystal	Vendor	Dimensions (mm)	Growth Technique
CZT1	eV-Products	10x10x10	High Pressure Bridgman
CZT2	eV-Products	10x10x10	High Pressure Bridgman
CZT3	Yinnel Tech, Inc	8x8x15	Modified Vertical Bridgman

CdZnTe crystals are opaque to visible light but transparent when illuminated with infrared light, while the internal defects such as tellurium inclusions are not. Te inclusions will either scatter or absorb the infrared light and show up as distinct black spots. Infrared image microscopy system consists of an IR back light, 3D translation stage, and IR sensitive CCD camera was used to determine and calculate the size and concentrations of Te inclusions in CZT crystals. Images were captured and saved as monochrome high resolution jpeg files. IMAGE-PRO Plus software v.6 was used to calculate the size and the concentration of Te precipitates in the crystal. The IR image microscopy system was described in details earlier in the experimental chapter. Figures (3.1), (3.2), and (3.3) show composite IR images obtained at 10x magnification from typical 3.0x2.25 mm^2 planes within CZT1, CZT2, and CZT3 respectively.
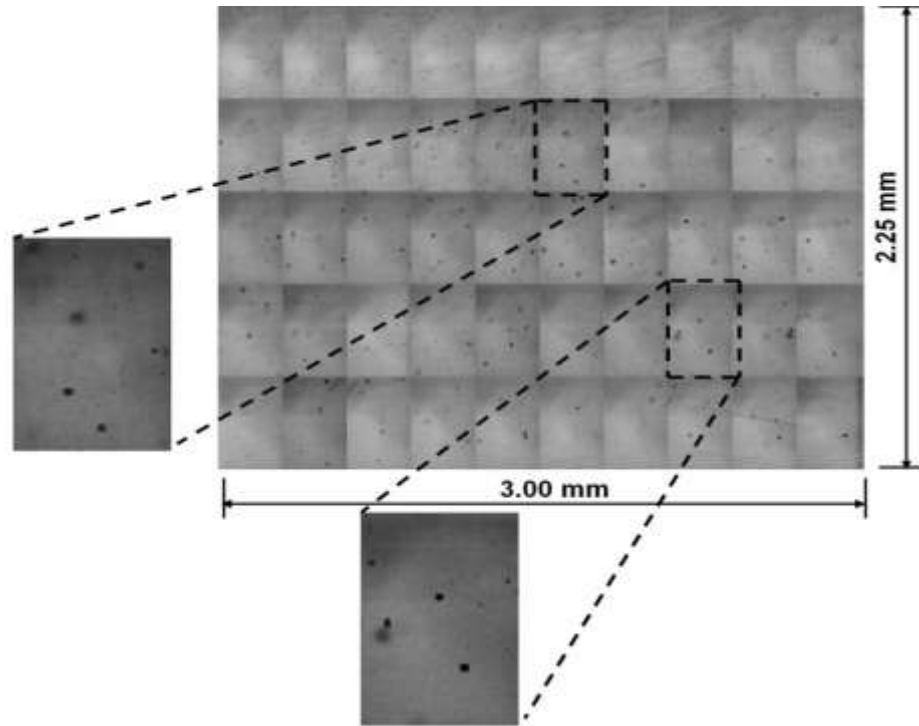
Figure (3.1): IR images of the CZT 1 at 10x magnification.
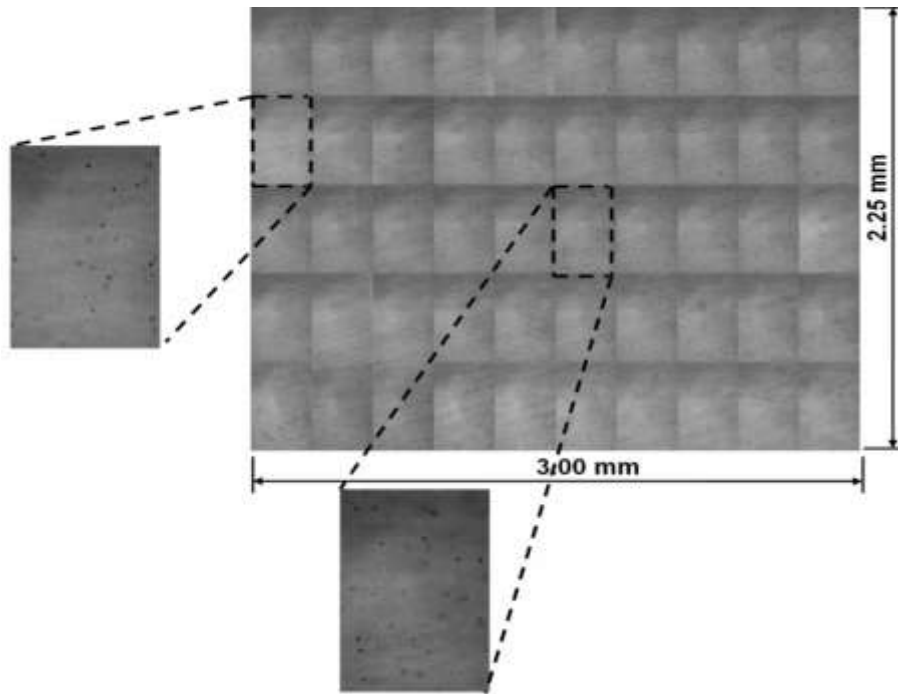
Figure (3.2): IR images of the CZT 2 at 10x magnification.
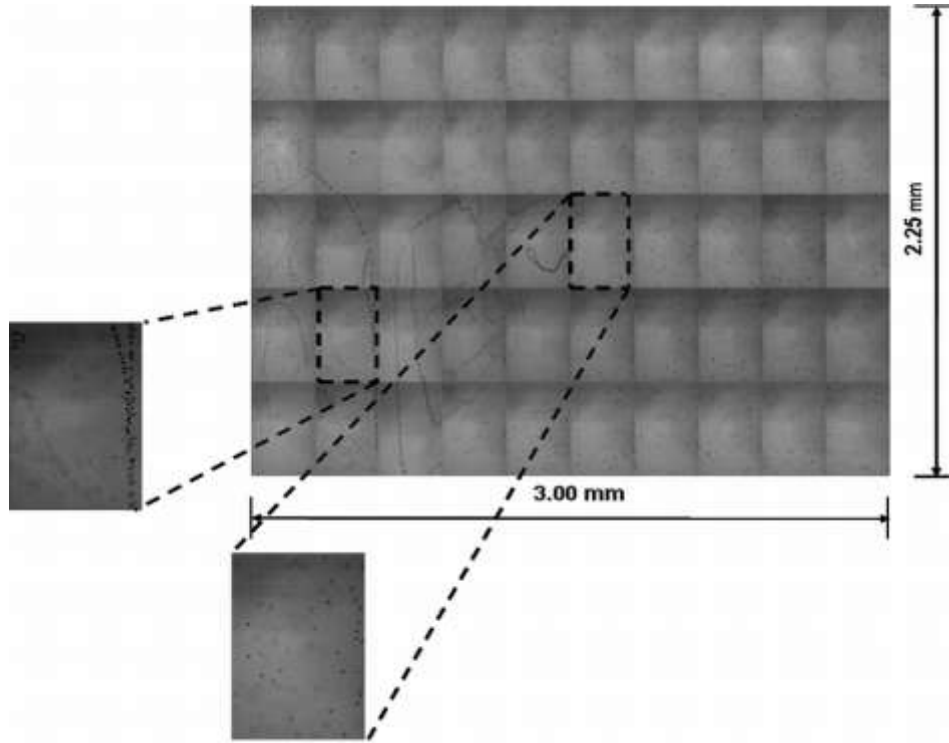
Figure (3.3): IR images of the CZT 3 at 10x magnification.

The tellurium planar defect density was calculated and determined to be 89 inclusions/mm^2 with an average inclusion diameter of 27µm in the sample CZT1; sample CZT2 has a planar defect density of 108 inclusions/mm^2 with an average inclusion diameter of 18µm. On the other hand, sample CZT3 has a planar defect density of 167 inclusions/mm^2 with an average inclusion diameter of 20µm. Because the depth of field of our imaging system (3.9µm) is smaller than the average defect diameter, the volume density of the tellurium inclusions was estimated assuming that the defects are spherical and using the average defect diameter to represent the thickness of the imaging plane in each crystal. We then estimated the volume fraction (fractional crystal volume occupied by tellurium inclusions) for CZT1, CZT2, and CZT3 as 3.4%, 1.8%, and 2.8% respectively. The obtained results of the three samples are summarized in table (3.2).

Crystal	Average Size of Te inclusions (μm)	Defect Density ($incl./mm^2$)	Volume Fraction of Te inclusions (%)
CZT1	27	89	3.4
CZT2	18	108	1.8
CZT3	20	167	2.8

Utilizing the XYZ translation stage of the IR imaging system setup allowed us to acquire stacks of images, each focused at different depth (different planes) of the each crystal. From figure (3.4) and the obtained data, Te inclusions were clearly found to be distributed uniformly throughout the bulk of the CZT crystals.
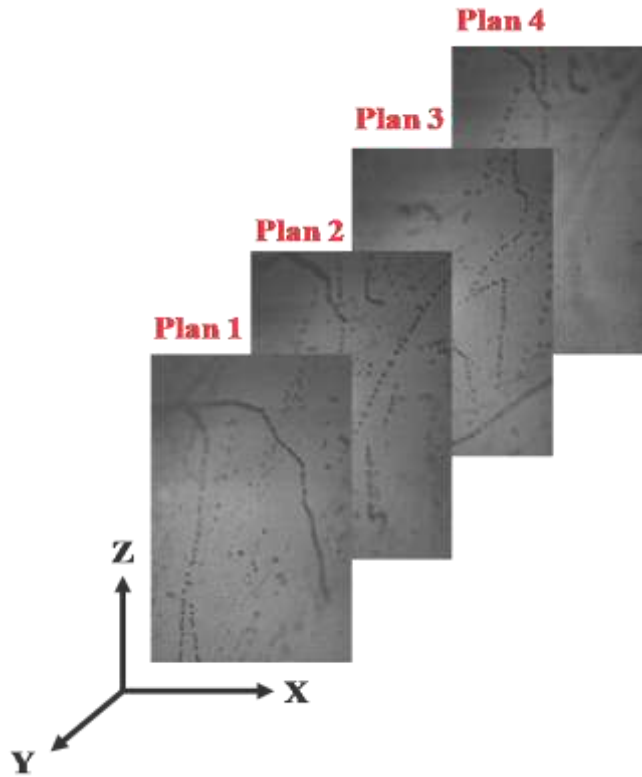
Figure (3.4): IR images along CZT crystal in four different planes.

The histogram of the size distribution of tellurium inclusions was generated and compiled from two arbitrary planes in each sample, figure (3.5). Variations of the concentration of Te inclusions within a crystal have been obtained and thus can be used to characterize the quality of the CZT material in terms of the growth technique that used to grow the crystal. However, such variations are strongly associated with the presence of many other kinds of defects.
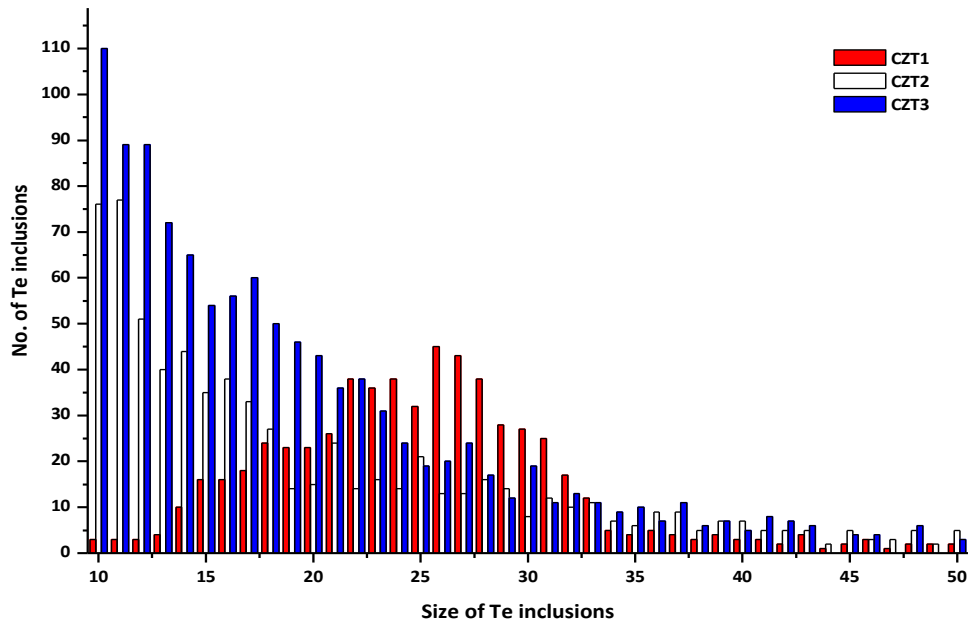
Figure (3.5): The histogram of the Te inclusion size distribution of the three CZT crystals.

3.3. Conclusion

In summary, Te inclusions and precipitates are strongly associated with the presence of many other kinds of defects and charge traps in CZT, and the presence of large diameter Te inclusions may simply be a measure of the overall crystal quality.

Te inclusions or precipitates as one of these kinds of internal defects is expected to produce non-uniform charge transport and degrade the spectroscopic performance of radiation

detectors fabricated from such materials. The correlation between the size and concentrations of Te inclusions and the carrier trapping time in detector grade CZT will be discussed - in details - in the next Chapter.

Chapter (4)

Lifetime Measurements Cadmium Zinc Telluride Crystals

CHAPTER (4)

LIFETIME MEASUREMENTS ON CADMIUM ZINC TELLURIDE CRYSTALS

4.1. Introduction

It is well known that Semiconductor materials must have high resistivity, on the order of 10^9 Ω.cm or greater [94], and high mobility-lifetime ($\mu\tau$) product to be suitable for room temperature radiation detection applications [66, 95]. This high resistivity is needed to minimize the noise resulting from the high leakage current [29]. Also to maximize the charge collection and signal, it must has a large electron and hole drift length [18, 96].

Cadmium zinc telluride (CZT) is one of these semiconductor materials that possess good kinetic charge-carrier parameters (mobility and lifetime) [97] with relatively large concentrations of impurities and native defects resulted during the growth process resulting in low resistivity. Of the various defects present in CZT, tellurium inclusions have been shown to have a particularly detrimental impact on charge collection and spectroscopic performance. A correlation has been established between the size and number density of tellurium inclusions and detector leakage

current and spectroscopic performance. Detectors fabricated from CZT with a large number of Te inclusions exhibited higher leakage current and lower energy resolution in comparison with detectors fabricated from higher quality material. In addition, high resolution x-ray mapping studies have recently shown that charge collection is specifically impeded along crystallographic trajectories containing tellurium inclusions. However, charge collection studies require sample metallization and do not require a direct measurement of the carrier lifetime, making it challenging to directly relate the tellurium inclusions to the carrier trapping time.

To compensate for the impurities and defects, often additional impurities or native defects are introduced to increase the room temperature resistivity of the CZT materials [94]. Compensation refers to the presence of relatively large concentration of deep energy levels which partially ionize and pin the Fermi level near the middle of the energy gap [98]. This is an effective method of increasing the resistivity of semiconductors plagued by shallow defect levels. Unfortunately, these deep energy levels will trap the free charge carriers and reduce the carrier lifetime which degrades the detector performance [99, 100]. Balance between compensation and trapping is required to optimize the performance of the radiation detector based on these materials [101, 102].

The electrical properties of CZT semiconductors are largely determined by the electron and the hole traps [103, 104]. Several techniques such as thermoelectric emission spectroscopy (TEES), thermally stimulated current (TSC) and current voltage measurements (I-V) have been used to characterize the traps in CZT semiconductor. These techniques were described in details in Chapter 1.

In this chapter, we are studying the correlation between the volume fraction of the tellurium inclusions and the carrier trapping time in detector grade $Cd_{1-x}Zn_xTe$ (x~0.1) using a

contactless microwave perturbation (MCP) technique which does not require any electrical contacts.

4.2. Tellurium Inclusion and Carrier Trapping Time

To measure the trapping time, the cubic CZT crystal was mounted on a ceramic BeO rod and inserted axially into the center of a cylindrical TE_{011} microwave resonant cavity with a resonant frequency near 5 GHz and a maximum power of 100 mW. The loaded cavity was critically coupled, and the reflected microwave power was monitored as a function of time during pulsed laser excitation of the sample. A pulsed neodymium-doped yttrium aluminum garnet laser with wavelength of 1064 nm and a pulse width of 7 ns was used to excite carriers in the CZT crystal through a 1 mm diameter aperture in the cavity wall. The excitation wavelength of the laser is below the bandgap energy of the CZT so that carrier generation is from midgap energy states within the bulk of the crystal. Specified details of the experimental setup were described in Chapter 2.

Figures (4.1), (4.2) and (4.3) show a set of decay curves (normalized reflected microwave power versus time) obtained after pulsed excitation of the three CZT samples at random locations. The reflected microwave pulse is a measure of the free charge carrier density as a function of time after laser excitation. The carrier trapping time (decay time) was determined by fitting a linear region of the decay curves (from 0.85 to 0.6 of the y-axis) to an exponential function with an adjustable time constant. The laser probes a cylindrical volume of the sample, 1 mm in diameter and 10 mm long and is, therefore, a measurement of the cumulative effect of charge traps within the measurement volume.
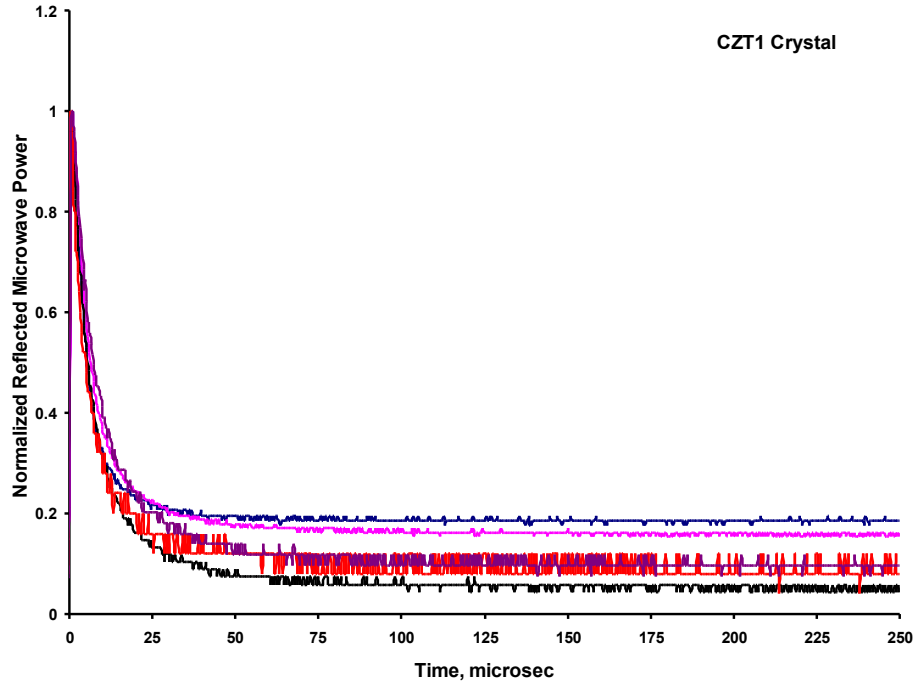
Figure (4.1): Normalized Reflected microwave power versus time for CZT1 crystal at room temperature.
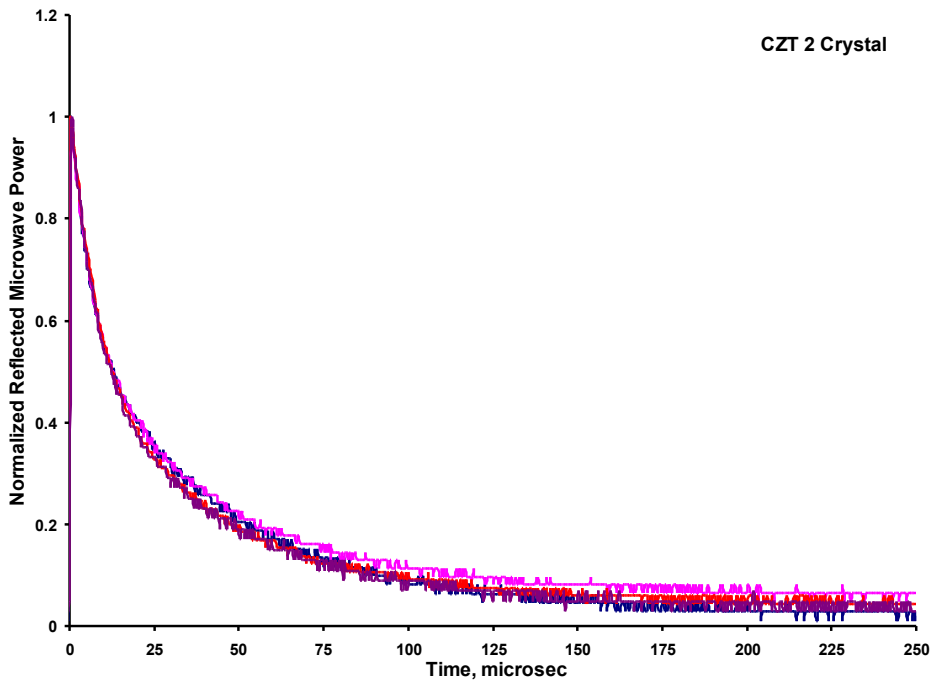
Figure(4.2): Normalized Reflected microwave power versus time for CZT2 crystal at room temperature.
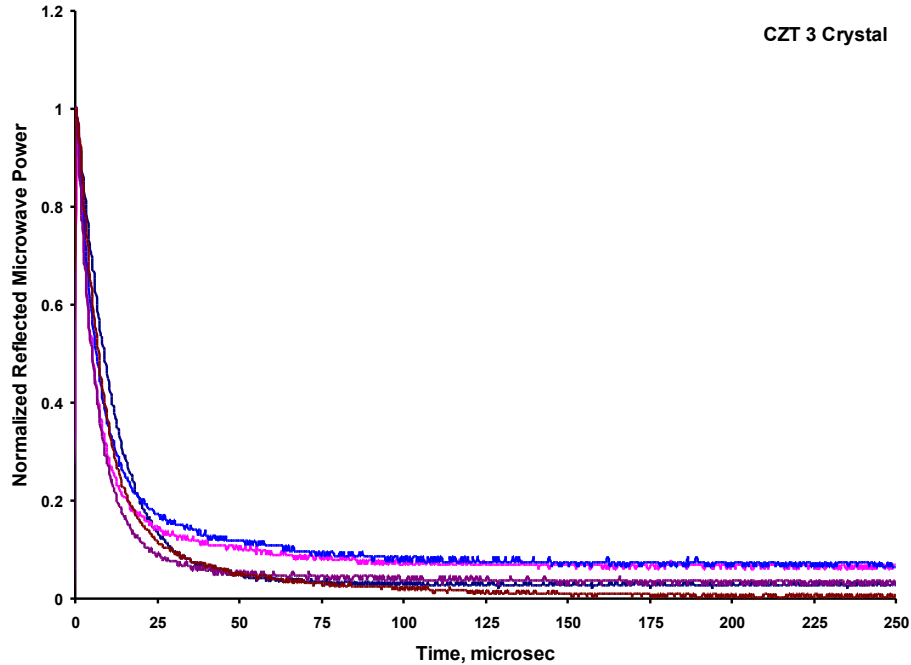
Figure (4.3): Normalized Reflected microwave power versus time for CZT3 crystal at room temperature.

The first sample, CZT1, had an average decay time of 5.5μs, the second sample, CZT2, had an average decay time of 16.9μs and, while the third sample, CZT3, had an average decay time of 3.25μs. For each sample, the decay time did not vary significantly throughout the volume of the crystal and is, therefore, considered to be representative.

There appears to be a correlation between the volume fraction of the tellurium inclusions, obtained in Chapter (3) and the carrier trapping time in CZT. Sample CZT1 has a volume averaged trapping time of 5.5μs and a tellurium inclusion volume fraction of 3.4%. On the other hand, sample CZT2 has a volume averaged trapping time of 16.9μs and a tellurium inclusion volume fraction of 1.8%, while CZT3 has a volume averaged trapping time of 3.25μs and a tellurium inclusion volume fraction of 2.8%. That is, the carrier trapping time is significantly longer in the sample with a lower volume fraction of tellurium inclusions. Table below shows the summary of the obtained results of the three CZT crystals.

While it is tempting to conclude that this correlation is a direct result of the Te inclusions acting as highly efficient trapping sites, there are other possible explanations for this correlation that cannot be ruled out at this time. Te inclusions are intensely studied, in part because they are so readily visible in CZT.

Table (4.1): Summary of the results obtained for the three CZT crystals.

Crystal	Average Size of Te inclusions (μm)	Defect Density ($incl./mm^2$)	Volume Fraction of Te inclusions (%)	Average Lifetime (μm)
CZT1	27	89	3.4	5.5
CZT2	18	108	1.8	16.9
CZT3	20	167	2.8	3.25

4.3. Temperature dependence Measurements of CZT

To measure the trapping time at low temperatures, semiconductor samples were mounted on a ceramic BeO rod and inserted axially into the center of a cylindrical TE_{011} microwave resonant cavity with a resonant frequency near 5 GHz and a maximum power of 100 mW, the other end of the BeO rod is dipped into a Dewar of liquid nitrogen. By this way, the sample's temperature can be controlled without directly placing the temperature source inside the cavity. A continuous flow of inert gas (Argon gas) was used to avoid any condensation occurred inside the cavity

Figures (4.4), (4.5), and (4.6) are a set of decay curves, the normalized reflected microwave power versus time of the three cadmium zinc telluride crystals, CZT1, CZT2, and CZT3 respectively that obtained after pulsed excitation at different temperatures.
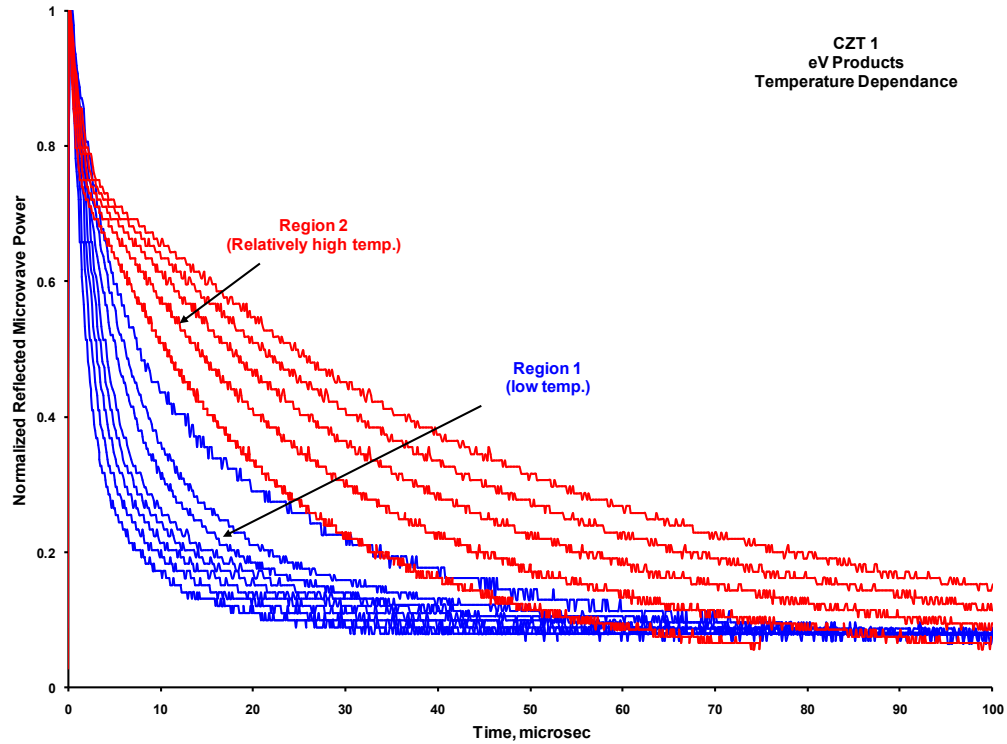
Figure (4.4): Normalized reflected microwave power versus time of both two temperature regions for CZT1.
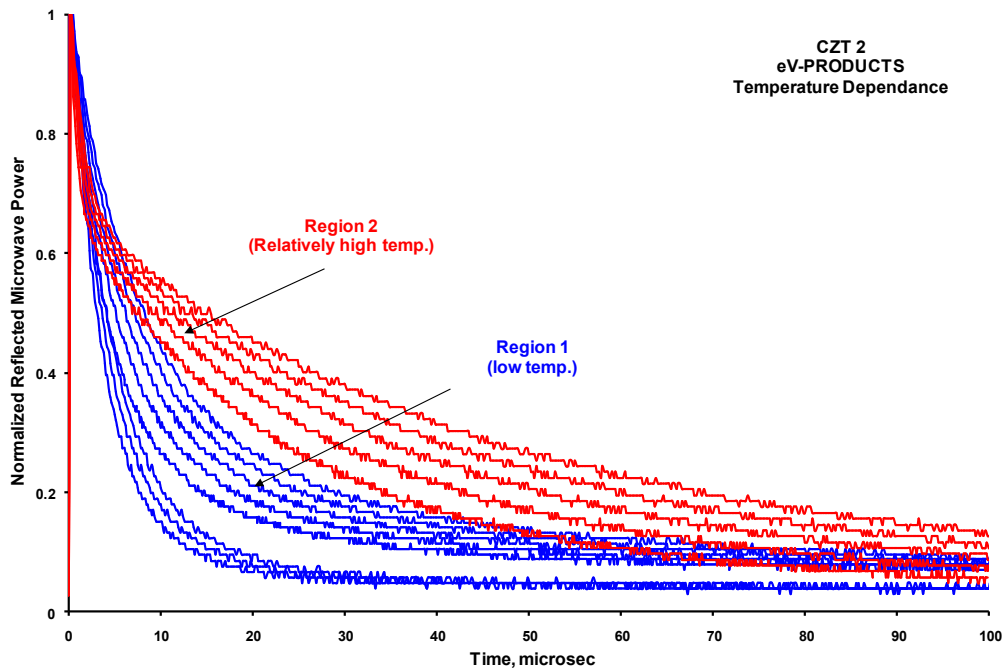
Figure (4.5): Normalized reflected microwave power versus time of both two temperature regions for CZT2.
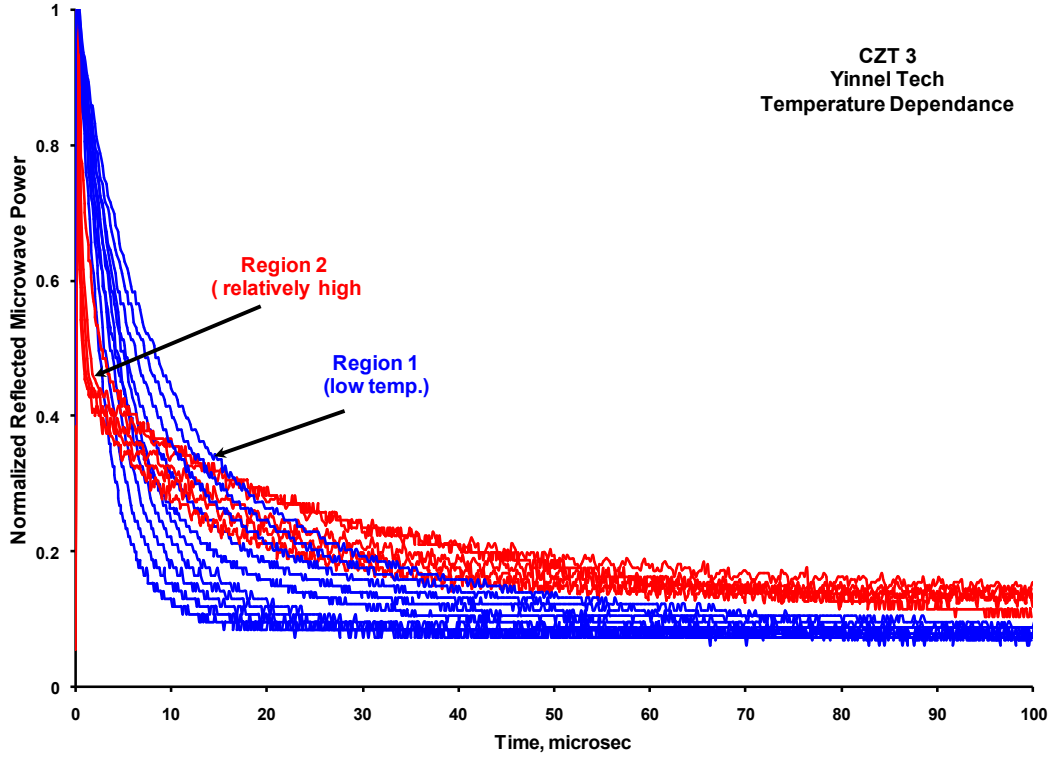
Figure (4.6): Normalized reflected microwave power versus time of both two temperature regions for CZT3.

Analysis of decay curves, shown in the figures above, indicate that there are two distinct temperature regions: a region of fast decay (covers the low temperature region from 150K down to 100K) followed by a region of relatively slow decay (covers the relatively high temperature region from 300K down to 160K). The fast region was assigned to a charge trap at energy Et1 corresponding to a decay time constant τ1, while the relatively slow region was assigned to a charge trap at energy Et2 corresponding to a decay time constant τ2. These time constants, τ1 and τ2, were determined for both regions at a series of temperatures by fitting the sample exponential function to the corresponding region of the curve. The developments of a trapping/recombination model can be summarized in the equation below:

$$\tau = \tau_o \left(\sqrt{\frac{300}{T}} \right) \left[1 + \left(\frac{2n_i}{n_{no}} \right) \cosh \left(\frac{E_t - E_i}{kT} \right) \right] \qquad (4.1)$$

Where: τ_o is the minimum carrier lifetime (the carrier lifetime at room temperature), E_i is the mid-gap energy, E_t is the trap energy, k is the Boltzmann constant, and T is the absolute temperature.

Based on the resistivity measurements of the single crystal CZT that obtained from the I-V measurements and was found to be 10^{10} Ω.cm, we estimate that the majority carrier concentration (n_{no}) is between 10 and 100 times greater than the intrinsic carrier concentration, which is approximately 10^4 carrier/cm^3. Therefore, the coefficient ($2n_i/n_{no}$) was determined to be 10^{-2}.
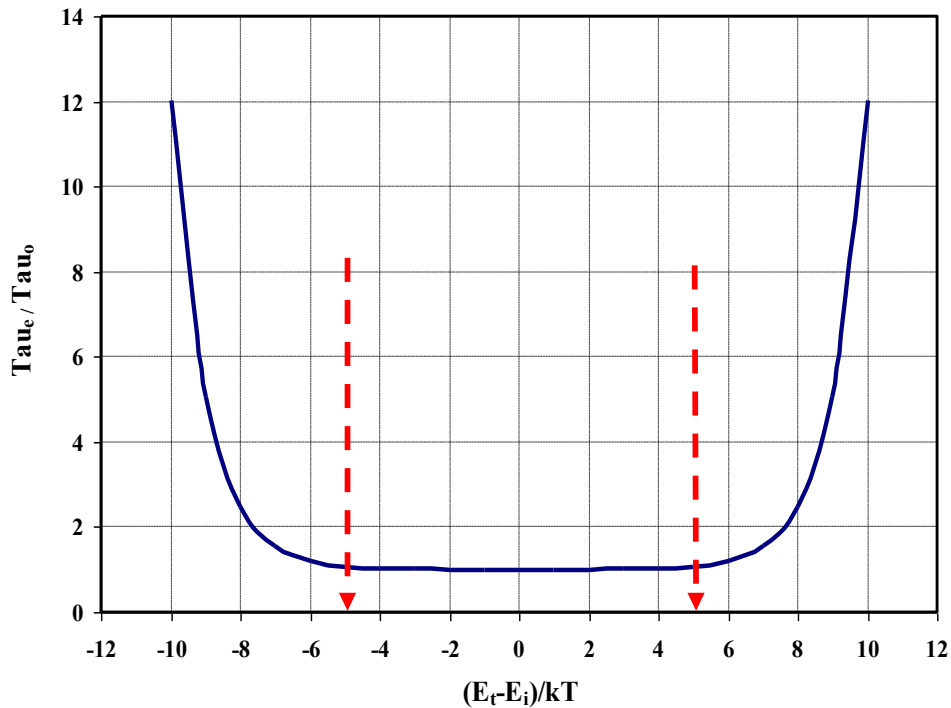
Figure (4.7): Decay time versus trap energy.

The equation above predicts a strong temperature dependence of the recombination lifetime when the argument of the hyperbolic cosine function exceeds a value of 5.

By plotting (τ/τ_o) versus $(E_t - E_i)/kT$, as shown in figure, it shows that the decay time is strongly dependant on the trap energy and the sample temperature and the decay time expected to be nearly independent of the trap energy range and equal to the minimum lifetime time τ_o as long as the trap energy is in the range of 5kT of the midgap energy.

The trap energies E_{t1} and E_{t2} for the three CZT samples were determined by fitting the model equation to the experimental data, shown in the figures below, figures (4.8), (4.9), and (4.10).
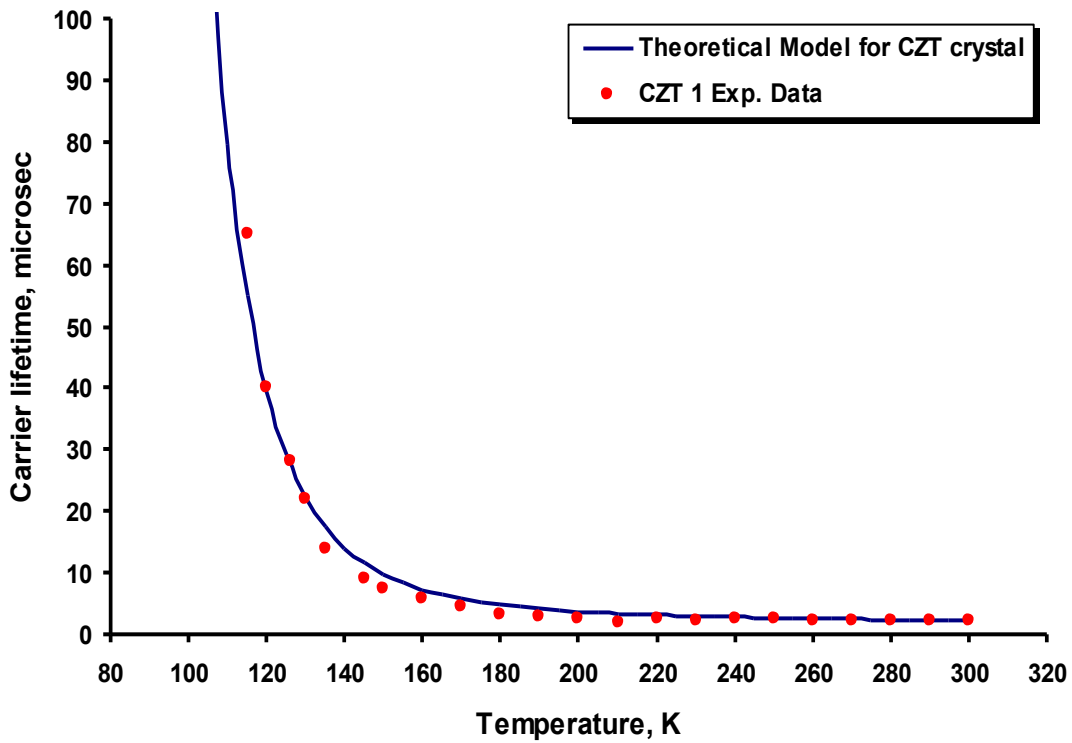
Figure (4.8): Decay time versus temperature for the two temperature regions for CZT1.
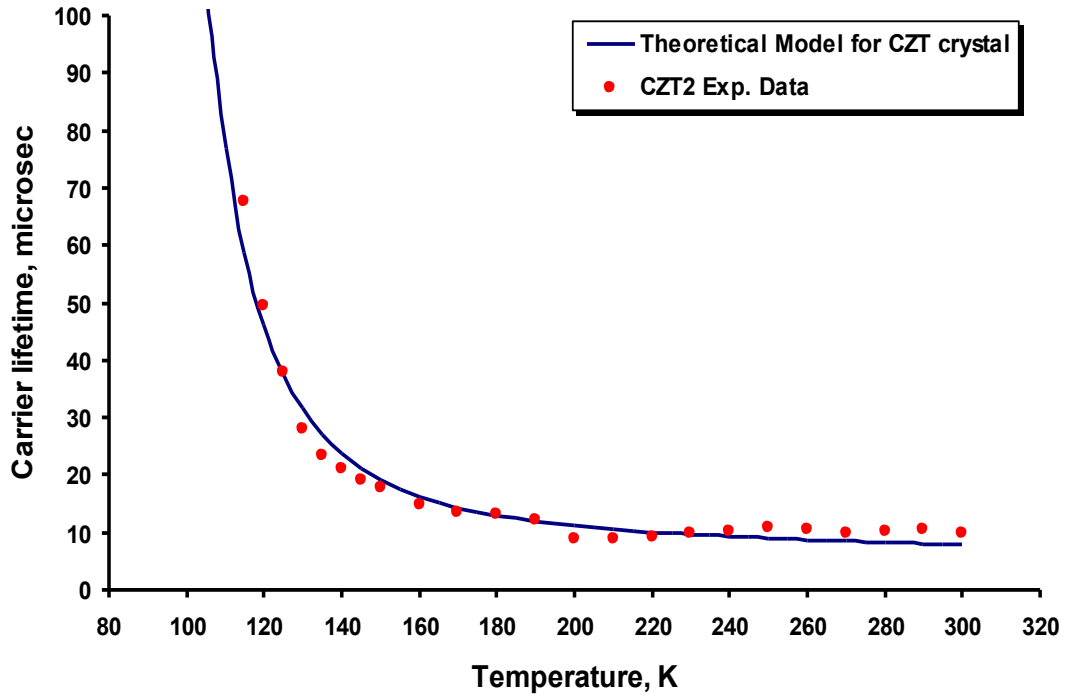
Figure (4.9): Decay time versus temperature for the two temperature regions for CZT2.
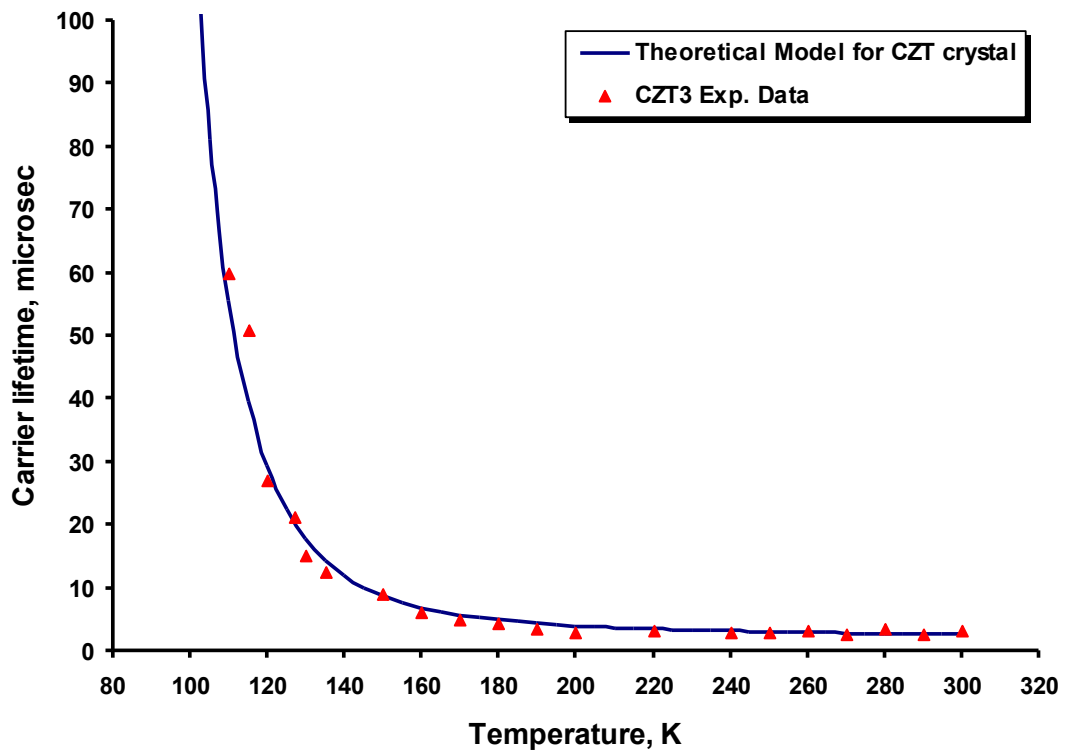
Figure (4.10): Decay time versus temperature for the two temperature regions for CZT3.

The best fit of the experimental data with the model is summarized in the table below, Table (4.2). There is a significant relationship between both of the volume fractions of the Te inclusions and the average size of Te inclusions, which discussed in the previous section. While there is no significant correlation reported between the trap energy and the volume fraction of Te inclusions.

Table (4.2): Summary of the fit of the experimental data with the model.

Crystal	Av. Size of Te inclusions	Vol. Fraction of Te inclusions	Av. Lifetime	(E_t-E_i)
	(μm)	*(%)*	*(μm)*	*(meV)*
CZT1	27	3.4	5.5	80
CZT2	18	1.8	16.9	66
CZT3	20	2.8	3.25	75

The decay data shown in figures above can fit to a mathematical equation of the sum of two exponential functions with two time constants, τ_1 and τ_2, and two independent amplitudes, A and B.

$$\frac{I}{I_o} = A \exp\left(\frac{t}{\tau_1}\right) + B \exp\left(\frac{t}{\tau_2}\right)$$

(4.3)

Where A and B represent the relative contribution of the specific charge trap at different energies E_{t1} and E_{t2} respectively. Also, the two corresponding time constants for each trap and the two amplitudes both are temperature dependant. By adjusting the values of the two independent amplitudes, A and B, the relative contribution of each trap at three different temperatures, 125, 150, 200, 225, and 250K, were determined.
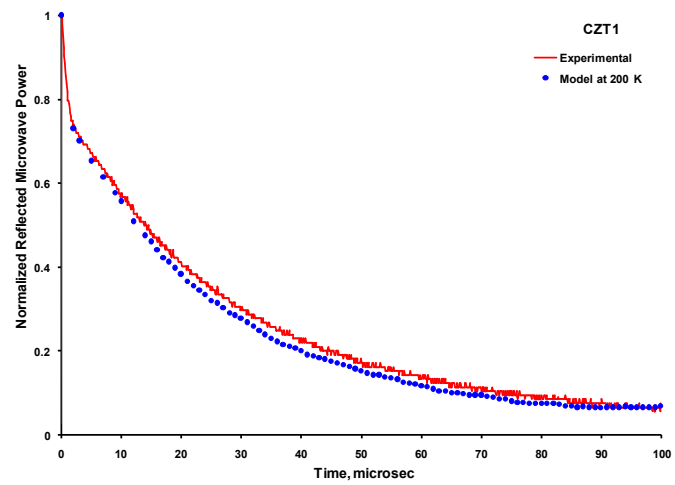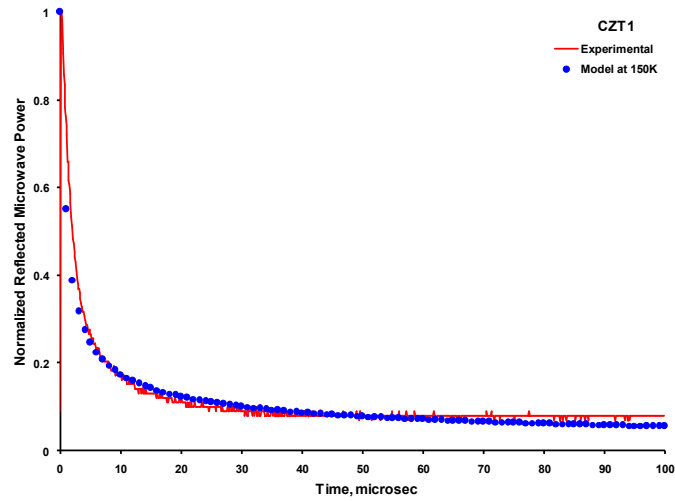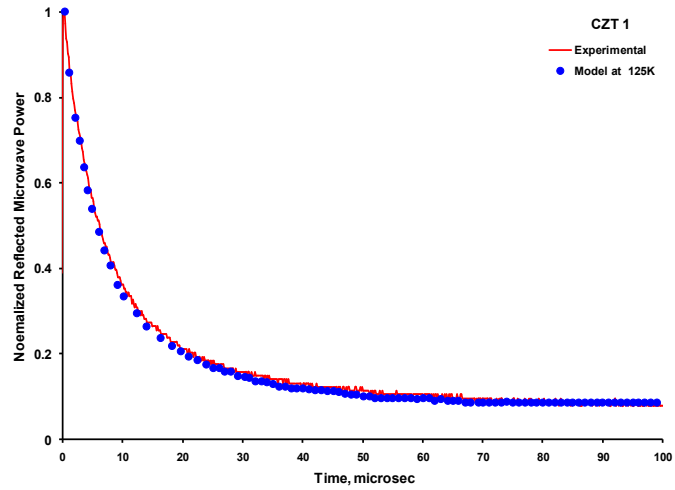
Figure (4.11): Decay Curves of CZT1 at three different temperatures.

61
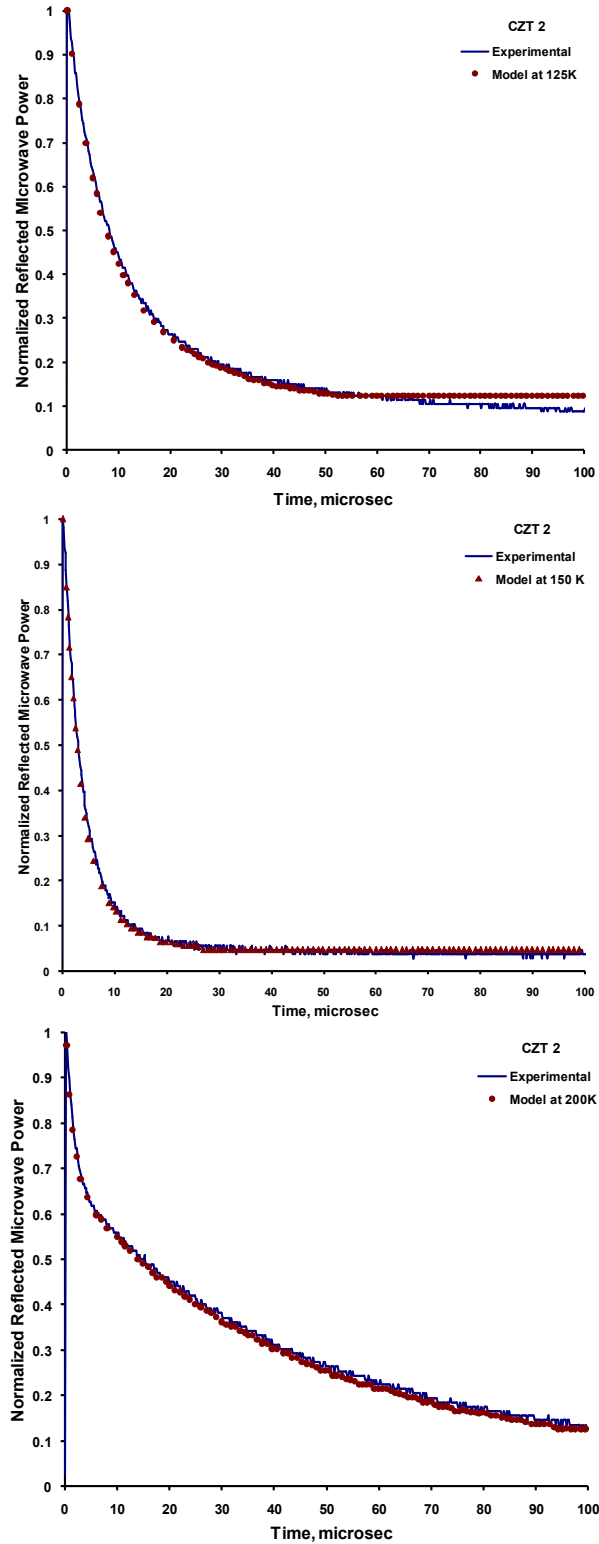
Figure (4.12): Decay Curves of CZT2 at three different temperatures.
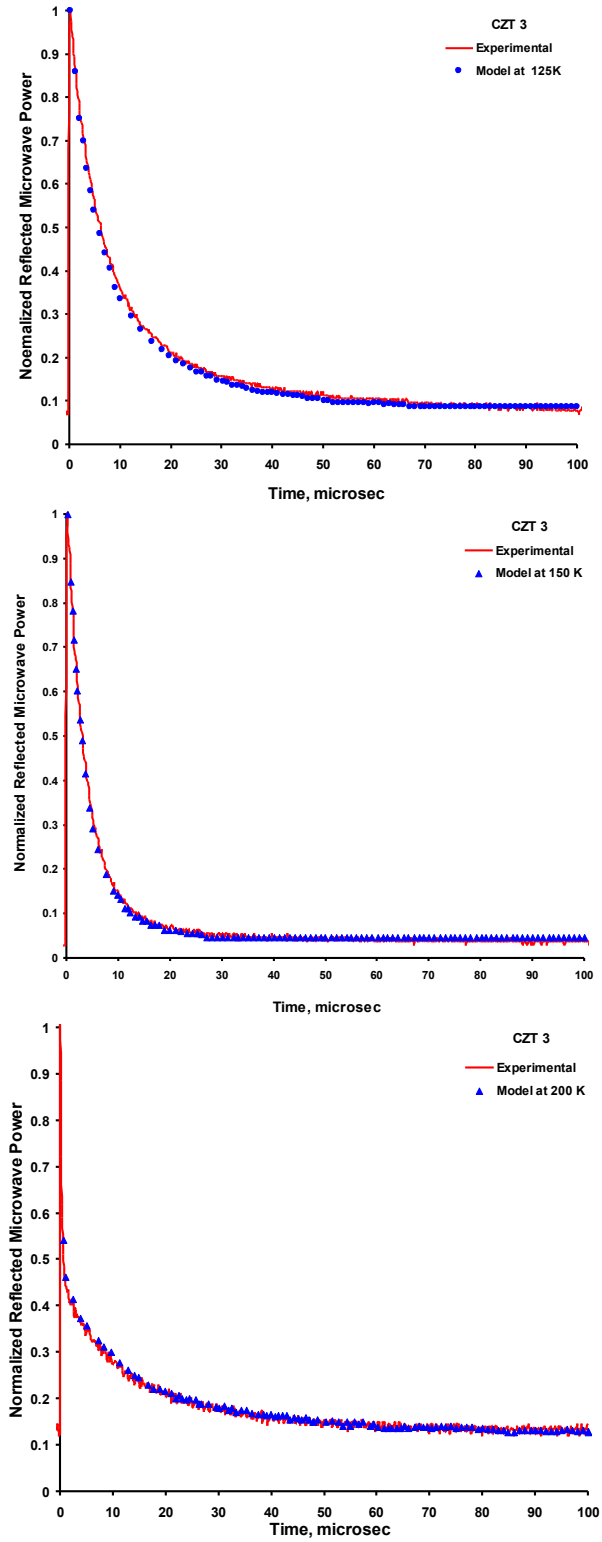
Figure (4.13): Decay Curves of CZT3 at three different temperatures.

Based on the best fit at each temperature shown in figure (4.14), it is shown that the decay process is mainly governed by two dominant deep recombination. It also shows that τ_1 is dominant at low temperature region and τ_2 is dominant at the relatively high temperature region. Also, it is noted that the contribution of the trap τ_1 relative to trap τ_2 increase with decreasing temperature consistently with the deactivation process explained below.
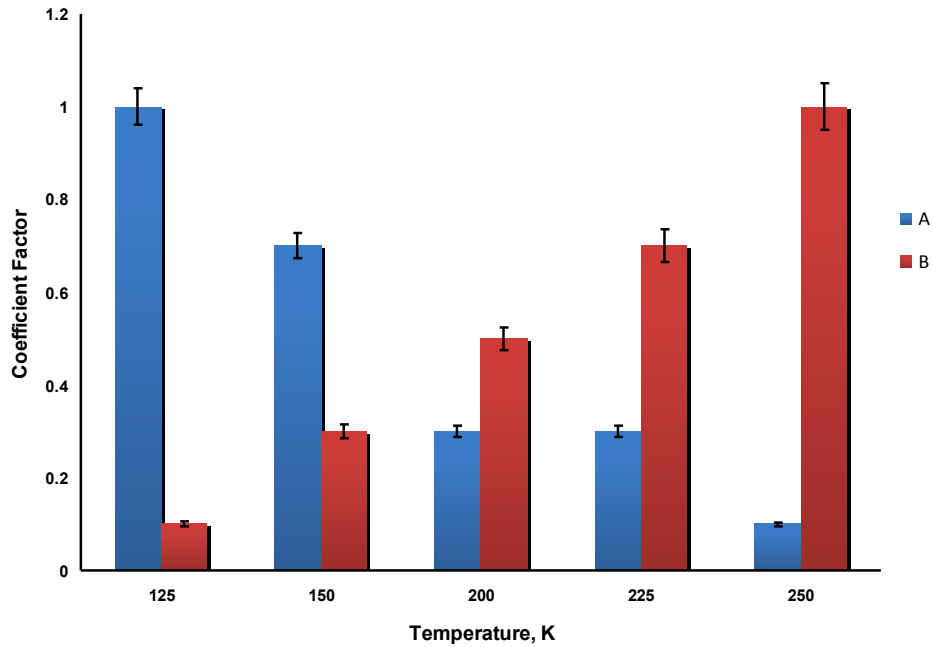
Figure (4.14): The average model amplitude coefficients at three different temperatures.

From the all results obtained we can conclude a strong temperature dependence of the electronic decay of CZT sample and this can be explained by the following sequence:

- At room temperature, the trap energy E_{t1} is within a certain value of the midgap (~5kT), while the trap energy E_{t2} is quite more 5kT away from the midgap and both of these trap energies are relatively effective recombination centers.

- Since the temperature is lowered, the shallower trap E_{t2} became thermally deactivated ($E_{t2}-E_i$ > 5kT) and the decay time of region 2 starts to increase.

64

- As the temperature continues to decrease, the deep trap E_{t1} also became thermally deactivated and the decay time of region 1 starts to also increases.

- At very low temperature, both traps are completely out of 5kT range and the overall decay time increased significantly.

Although their nature is not well known yet, the existence of the deep-level traps is consistent with the optical properties of the semi-insulating CdZnTe. If the deep levels are not close to the middle of the bandgap of CdZnTe, this will result a low resistivity p-type due to the presence of native defects such as Cd vacancies which is always associated with the CdZnTe grown from slightly Te rich melt. To bring the material to high resistive state, deep levels need to be introduced to pin the Fermi level close to the middle of the bandgap.

4.4. Conclusion

There appears to be a correlation, therefore, between the volume fraction of the tellurium inclusions and the carrier trapping time in CZT. Sample CZT1 has a volume averaged trapping time of 5.5μs and a tellurium inclusion volume fraction of 3.4%. On the other hand, sample CZT2 has a volume averaged trapping time of 16.9μs and a tellurium inclusion volume fraction of 1.8%, while CZT3 has a volume averaged trapping time of 3.25μs and a tellurium inclusion volume fraction of 2.8%. That is, the carrier trapping time is significantly longer in the sample with a lower volume fraction of tellurium inclusions.

While it is tempting to conclude that this correlation is a direct result of the Te inclusions acting as highly efficient trapping sites, there are other possible explanations for this correlation

that cannot be ruled out at this time. Te inclusions are intensely studied, in part because they are so readily visible in CZT.

Both the lifetime and defect measurements reported here were performed using simple, contactless optical methods and do not require any specific sample preparation or metallization. We, therefore, believe that these lifetime/defect density measurements can be used as a rapid material characterization / screening tool to select materials for specific detector applications.

Also, the electronic decay of the detector grade CZT, as a function of temperature, has been investigated using a contactless pulsed laser microwave cavity perturbation technique. The results obtained indicate that the electronic decay process in the bulk is dominated by a single deep hole trap at energy above the valence band.

Chapter (5)

Charge Trapping in Detector Grade Thallium Bromide and Cadmium Zinc Telluride

CHAPTER (5)

CHARGE TRAPPING IN DETECTOR GRADE THALLIUM BROMIDE AND CADMIUM ZINC TELLURIDE

5.1. Introduction:

The need for a room temperature gamma radiation detector with high energy resolution and good detection efficiency has motivated the investigation of gas, liquid and solid-state detection media capable of providing a combination of high room temperature resistivity, high atomic number and efficient charge transport [23, 105-107]. The compound semiconductors cadmium zinc telluride (CZT) and thallium bromide (TlBr) both have the potential to satisfy these requirements, but the detector efficiency is still limited.

Cadmium Zinc Telluride ($Cd_{1-x}Zn_xTe$, x ~ 0.1) detectors with a thickness near 1cm are commercially available from several companies and, through the use of single polarity charge sensing strategies, can provide a room temperature energy resolution near 1% at 662keV [108]. Recent results have shown that high-resistivity single crystals of TlBr can be grown with an

electron mobility-lifetime ($\mu\tau$) product in the range of 10^{-3} cm^2/V [42, 109]. The $\mu\tau$ product for electrons in TlBr has been improved by several orders of magnitude in comparison to the values reported just a few years ago [41, 53] and has resulted in room temperature radiation detectors with a thickness near 1 cm and an energy resolution better than 2%@662keV [41, 53]. Table (5.1) lists the important material properties of CZT and TlBr.

Table (5.1): Important material properties of CZT and TlBr.

Material	Atomic Number	Density (g/cm^3)	Bandgap (eV)	Resistivity (Ω.cm)	Electron Mobility (cm^2/V.s$^-$)^1	Hole Mobility (cm^2/V.s$^-$)^1
CZT	48,30,52	6	1.68	10^{10}	1000	100
TlBr	81,35	7.56	2.68	10^{10}	40	12

The continuous improvement in the performance of CZT and TlBr radiation detectors is largely due to a simultaneous increase in the material resistivity and $\mu\tau$ product. A high resistivity is necessary in order to reduce the detector leakage current under bias, while a large $\mu\tau$ product is required for efficient charge collection. Both the resistivity and $\mu\tau$ product are strongly influenced by the crystal quality and, specifically, the energy level and concentration of charge traps. The highest theoretical resistivity in CZT or TlBr would occur in an intrinsic material free of defects, impurities and mid-gap energy levels. However, because the quality of these compound semiconductors is far from intrinsic, high resistivity is achieved using compensation methods whereby a deep trap level is intentionally introduced in order to pin the Fermi level near the middle of the band gap. Compensation has been successfully used in CZT to produce materials with a resistivity very close to the intrinsic level. However, the deep traps used as compensation levels to increase the material resistivity are also the most efficient recombination

centers and can significantly reduce the carrier lifetime and μτ product. Therefore, crystal growers must attempt to control the concentration of the deep traps so that they are close to the minimum value necessary to compensate for the shallow traps.

Herein we present measurements of the carrier trapping time in single crystal CZT and TlBr as a function of temperature. Our results suggest that, due to its much larger band gap, there may be an alternative method for achieving both a high resistivity and a large μτ product in TlBr, which is not possible in CZT. We show that the temperature dependence of the trapping times in CZT and TlBr differ significantly primarily because the majority carrier concentration in CZT is close to the intrinsic carrier concentration while for TlBr, the majority carrier concentration is very large in comparison to the intrinsic carrier concentration.

During the standard operation of a semiconductor gamma-ray detector a strong electric field is used to dissociate the electron-hole pairs generated by the absorption of a gamma-ray photon. Therefore, electron-hole recombination is accomplished primarily through interactions with charge traps. The time constant associated with trap-assisted recombination depends on the concentration, cross section and energy level of the traps, but is usually significantly longer than the time constant associated with direct recombination.

In this chapter, the carrier lifetime measurements were performed in the presence of a microwave field and the term "trapping time" is, therefore, used to denote trap assisted recombination.

The single crystal TlBr sample was provided by Bruker Baltic Ltd., measured $10 \times 10 \times 2.6 mm^3$ and had a room temperature resistivity on the order of 10^{10} Ω.cm and a μτ product of 1.3×10^{-4} cm^2/V. The μτ product in this sample was determined by measuring the pulse height (a measure of the collected charge) versus bias voltage under alpha particle excitation and

fitting the data using the Hecht relationship. The single crystal CZT sample was obtained from eV Products, measured 10x10x10mm³, had a room temperature resistivity on the order of 10^{10} Ω.cm and was grown using the high pressure Bridgman method.

Cylindrical polycrystalline samples, 7.5 mm in diameter, were formed by melting high purity (99.999% from Sigma Aldrich) TlBr beads at temperatures near the melting point. Resistivity and mobility-lifetime product (μτ) measurements were not performed on the polycrystalline samples.

The trapping times were measured as a function of sample temperature using a contactless pulsed laser microwave cavity perturbation method described earlier, in detail, in the chapter of the experimental procedures.

5.2. Charge Trapping in Detector Grade TlBr and CZT

Figure (5.1) shows photographs of the CZT, TlBr and polycrystalline TlBr samples. Remnants of the electrical contacts, used to measure the material resistivity and mobility-lifetime (μτ) product, are still visible on the TlBr sample.
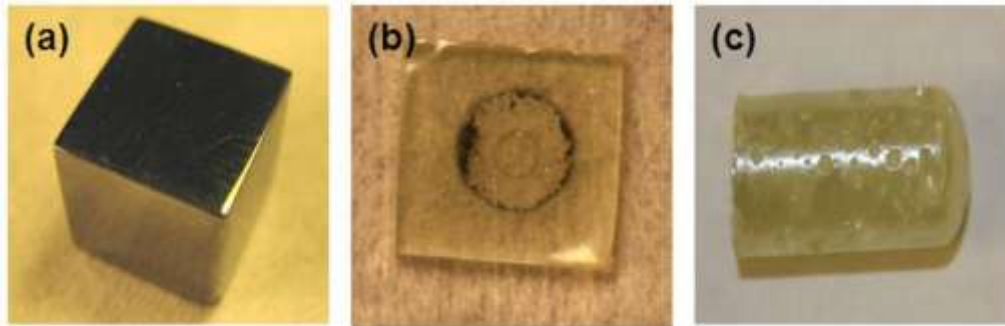
Figure (5.1): Photograph of (a) single crystal CZT and (b) single crystal TlBr, and (c) Polycrystalline TlBr.

Figures (5.2) and (5.3) are a set of room temperature decay curves showing the reflected microwave power (a measure of the semiconductor conductivity) versus time after pulsed laser

excitation of the single crystal CZT and TlBr sample at several different locations. The sample was placed in the center of the microwave cavity and the laser pulse was passed through a 1mm diameter aperture in the cavity wall. The excitation pulse width was approximately 7 ns and the excitation wavelength was 532 nm.

An excitation wavelength of 532 nm was selected for TlBr because it is below the band gap absorption edge and results in uniform bulk carrier generation throughout a 1mm diameter cylinder within the TlBr sample. Figure (5.4) shows the UV absorption spectrum of TlBr single crystal, the absorption edge is found to be approximately at 450 nm; therefore the bandgap of TlBr single crystal can be calculated to be approximately 2.68 eV.
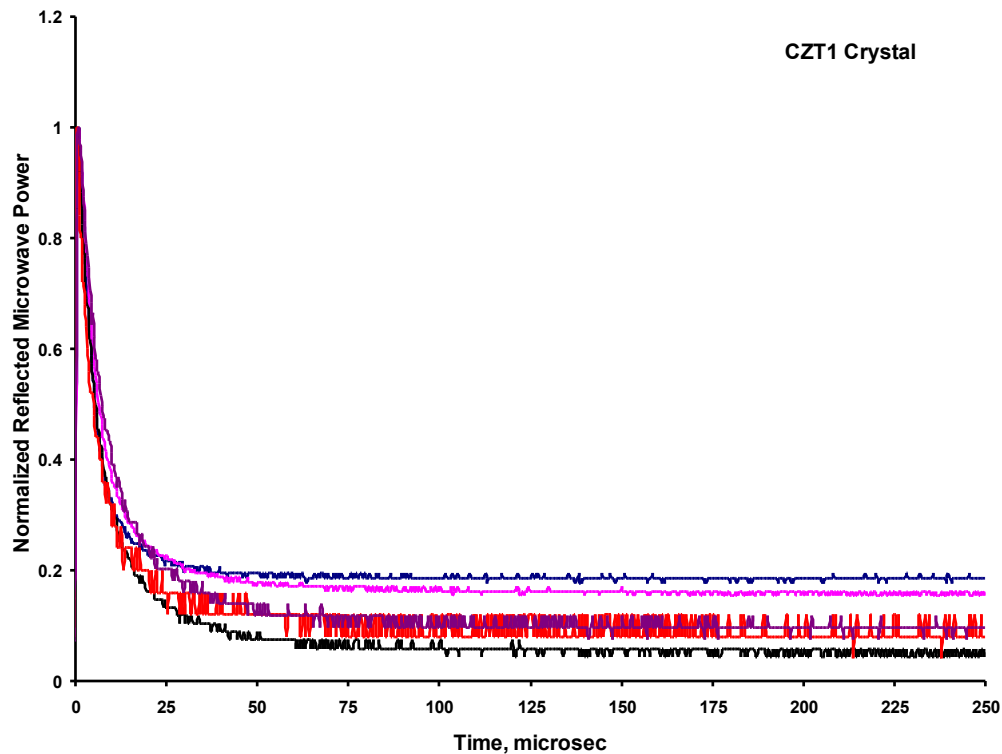
Figure (5.2): Normalized Reflected microwave power versus time for CZT crystal.
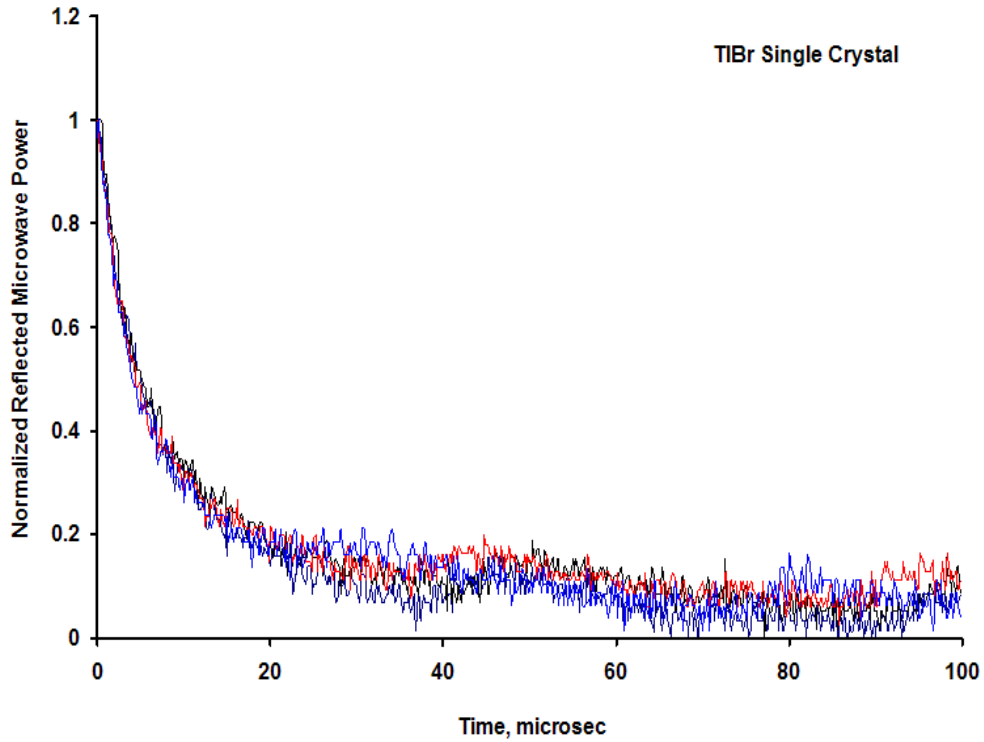
Figure (5.3): Normalized Reflected microwave power versus time for TlBr Single crystal at room temperature.
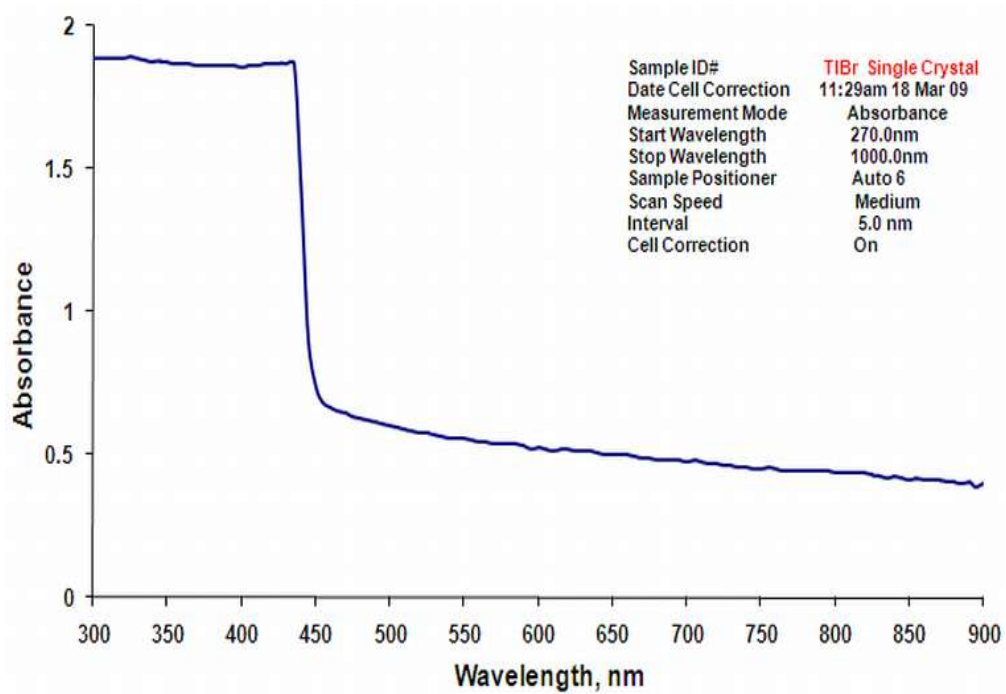
Figure (5.4): UV absorbance spectrum of TlBr single crystal.

The carrier trapping time was determined by fitting an exponential function to the experimental decay curves and the sample temperature could be varied from about 110K to 300K using a Beryllium Oxide cold finger. Similar decay curves were obtained for the CZT sample but at an excitation wavelength of 1064nm. The longer wavelength excitation (1064nm) was used in the CZT sample due to its smaller band gap.

Figure (5.5) is a plot of the carrier trapping time in the CZT crystal as a function of temperature from room temperature down to about 110K. The dots are the experimental data points and the solid line is the results of a theoretical trapping model.

Assuming low injection conditions and equal electron and hole capture cross sections, the temperature dependence of the trapping time is given by [82]:

$$\tau = \tau_{300}\left(\sqrt{\frac{300}{T}}\right)\left[1+\left(\frac{2n_i}{n_{no}}\right)\cosh\left(\frac{E_t-E_i}{kT}\right)\right] \tag{5.1}$$

Where:

n_i is the intrinsic carrier concentration,

n_{no} is the majority carrier concentration (because our trapping time measurements are not sensitive to the charge polarity, this symbol will be used to denote the majority carrier concentration, but this does not imply that the sample is necessarily n-type),

E_t is the energy level of the charge trap,

E_i is the mid-gap energy and k is the Boltzmann constant, and

τ_{300} is the minimum trapping time at 300K.

The minimum trapping time is given by: $\qquad \tau_o = \dfrac{1}{v_{th}\sigma N_t} \tag{5.2}$

Where:

σ is the trap capture cross section,

N_t is the trap concentration, and

v_{th} is the thermal drift velocity of the charge carriers given by $\sqrt{\dfrac{3kT}{m_e}}$.

Therefore, the $\left(\sqrt{\dfrac{1}{T}}\right)$ term in equation (5.1) reflects the temperature dependence of the thermal

drift velocity.
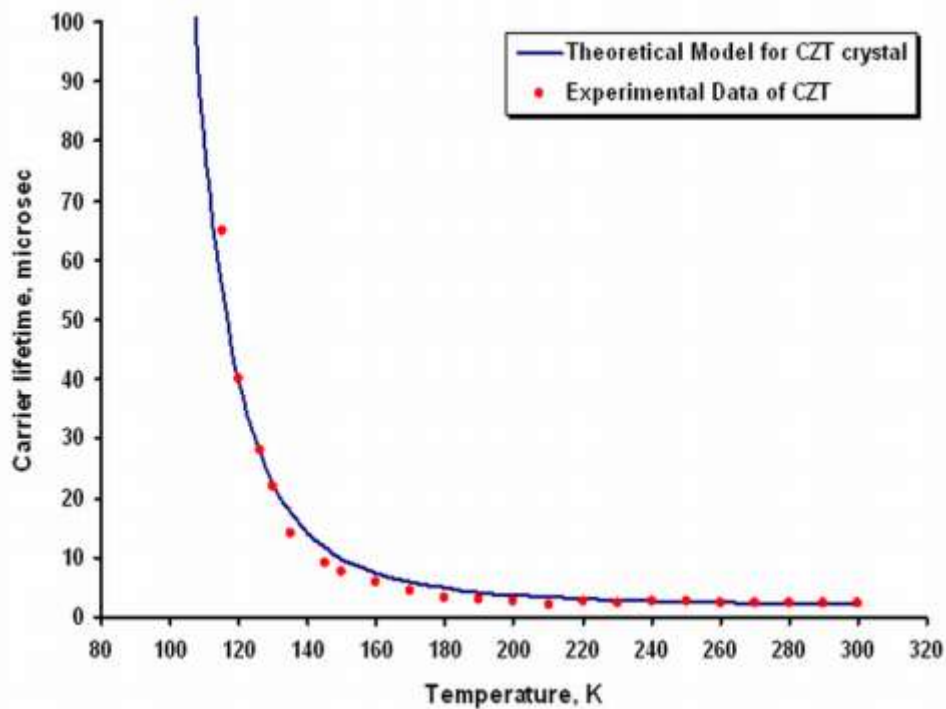
Figure (5.5): Trapping time versus temperature for single crystal CZT (theory and experiment).

The dependence of the trapping time on the trap energy is governed by the hyperbolic

cosine term in equation (5.1). Deep trap levels, because they are equally accessible to both

electrons and holes, are the most efficient recombination centers and the hyperbolic cosine term

goes to zero as the energy level of the charge trap (E_t) approaches the mid-gap energy (E_i).

Therefore, in order to increase the carrier trapping time, one must either decrease the trap concentration (N_t) or maximize the contribution of the hyperbolic cosine term. As mentioned previously, a certain minimum deep trap concentration is required in both CZT and TlBr in order to compensate for the shallow traps and to increase the material resistivity. The coefficient in front of the hyperbolic cosine term is the ratio of the intrinsic carrier concentration to the majority carrier concentration and this coefficient gets small when the majority carrier concentration is significantly larger than the intrinsic concentration reflecting the fact that carrier/trap interactions have a higher probability when the majority carrier concentration is large. For semiconductor materials where the majority carrier concentration is close to the intrinsic carrier concentration, the temperature dependence of the trapping time can be significantly influenced by the hyperbolic cosine term in equation (5.1), particularly at low temperatures where the argument of the function becomes large. High resistivity, detector grade CZT is an example of a material that satisfies this criterion. The measured resistivity (obtained from I-V measurements) of this single crystal CZT sample is on the order of 10^{10} Ω.cm. Based on this resistivity measurement, we estimate that the majority carrier concentration (n_{no}) is between 10 and 100 times greater than the intrinsic carrier concentration, which is approximately 10^4 carrier/cm^3 in CZT [94, 96, 104]. The theoretical line in figure (5.5), was obtained with $\left(\dfrac{2n_i}{n_{no}}\right) = 10^{-2}$, $(E_t - E_i) = 0.08$eV and $\tau_{300} = 2.3$ µs (the experimentally measured room temperature trapping time). In the model, the trap energy level was adjusted in order to obtain the best fit between the experimental and theoretical data [29]. A trap energy level of 0.08eV suggests that charge trapping in this CZT crystal is dominated by a very deep trap close to the middle of the energy gap. This result is consistent with a compensated material where high resistivity is achieved through the introduction of a deep trap which pins the Fermi level near the

middle of the band gap.

Figure (5.6) is a plot of the carrier trapping time in the TlBr crystal as a function of temperature from room temperature down to about 110 K. The trapping times were determined directly at each temperature by fitting an exponential function to the reflected microwave signal after pulsed laser excitation. The reflected microwave signal intensity is proportional to the free carrier concentration and the time constant of the exponential fit is, therefore, a direct measurement of the carrier trapping time. Like CZT, TlBr has a measured room temperature resistivity in the 10^{10} Ω.cm range, but due to its larger bandgap (2.7eV versus 1.7eV) TlBr has a much lower intrinsic carrier concentration and the majority carrier concentration is not close to the intrinsic value.
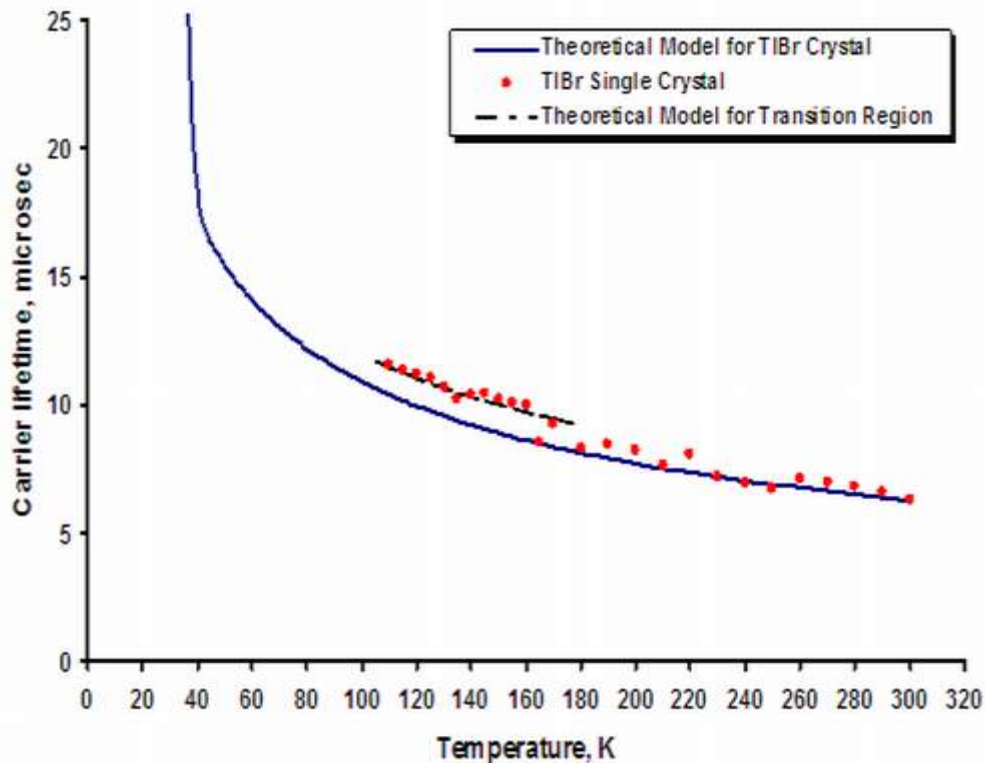
Figure (5.6): Trapping time versus temperature for single crystal TlBr (theory and experiment).

The solid line in figure (5.6) represent the curve fits obtained using equation (5.1) with $\left(\dfrac{2n_i}{n_{no}}\right) = 10^{-11}$, $(E_t - E_i) = 80$ meV and $\tau_{300} = 6.3$ μs (the measured room temperature trapping time). While the majority carrier concentration in TlBr is similar to that of CZT (similar resistivity), it is very large in comparison to the intrinsic carrier concentration. Because of this important difference the coefficient before the hyperbolic cosine term in equation (5.1) is negligibly small for TlBr and this term does not influence the trapping time over the temperature range investigated here. For the theoretical curve shown in figure 4 the CZT trap energy of 0.08eV was arbitrarily used since the trap energy level does not influence the model over the range of our experimental data.

We found that for TlBr the trapping time is equal to the minimum value (given by equation 2) and varies as $\left(\dfrac{1}{\sqrt{T}}\right)$ due to the temperature dependence of the drift velocity. The theoretical temperature dependence of the trapping time is shown as the solid line in figure (5.6).

The theoretical line fits the experimental data very well from 300K down to about 180K at which point there is a discontinuity in the temperature dependence of the trapping time. The crystal structure of TlBr changes from a cubic CsCl type at room temperature to an orthorhombic thallium iodide type upon cooling [110, 111]. It is, therefore, possible that the observed discontinuity in the trapping time is caused by this change in crystal structure with temperature. However, temperature dependent x-ray diffraction measurements would be needed in order to confirm this hypothesis but is beyond the scope of the present study.

Figure (5.7) shows the TlBr experimental data compared to the trapping model at four different trap energies $(E_t - E_i)$: (50 meV, 80 meV, 150 meV and 200 meV).

It is well shown that, in a material where the ratio of the intrinsic carrier concentration to the majority carrier concentration is very small, the temperature dependence of the carrier trapping time is relatively unaffected by the trap energy over a very large temperature range. In the TlBr crystal, for example, the trapping time only begins to increase exponentially at temperatures below 100K, even when the trap energy is far from the intrinsic energy level.

Our results suggest that, because of its relatively large band gap, it may be possible to significantly increase the room temperature trapping time in TlBr while at the same time maintaining a very high resistivity.
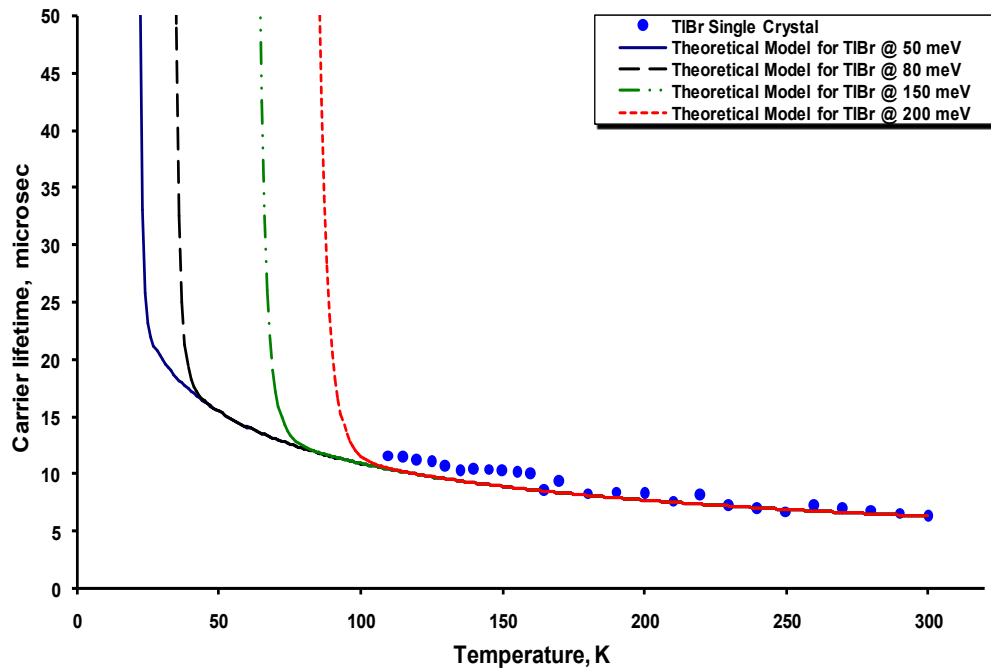
Figure (5.7): Trapping time versus temperature in single crystal TlBr (experimental data versus theoretical model at four trap energies).

The combination of a very long trapping time and very high resistivity at room temperature would represent an important achievement in gamma radiation detection. Unlike CZT, TlBr, because of its much larger bandgap, has an acceptably high room temperature

79

resistivity despite the fact that the majority carrier concentration is many orders of magnitude larger than the intrinsic carrier concentration [112]. At a resistivity of 10^{10} Ω.cm, the Fermi level in TlBr is approximately 0.7eV from the mid-gap region. If a deep compensation level was introduced to move the Fermi level closer to the middle of the energy gap, the majority carrier concentration would decrease thereby increasing the coefficient in front of the hyperbolic cosine term in equation (5.1). However, if the compensation level was too deep (e.g. E_t=E_i) it would act as an efficient charge trap and would reduce the value of the hyperbolic cosine function itself. However, because of the large band gap in TlBr, it should be possible to significantly increase the room temperature trapping time in TlBr through the introduction of a moderately deep trap (compensation level) located approximately 200meV from the mid-gap level. A moderately deep trap level would reduce the majority carrier concentration and increase the coefficient in front of the hyperbolic cosine term without decreasing the argument of the function to the point where there is no net benefit.

Figure (5.8) is a plot of equation 1 for TlBr with a trap energy level of 200meV (from the mid gap energy level) and at several different values of the coefficient $\left(\dfrac{2n_i}{n_{no}} \right)$. The results of this model demonstrates that the room temperature trapping time in TlBr can, in principle, approach 0.1 ms through the introduction of a moderately deep compensation level. This strategy is not possible in CZT, because the band gap it too small to use a moderately deep compensation level while still maintaining high material resistivity.
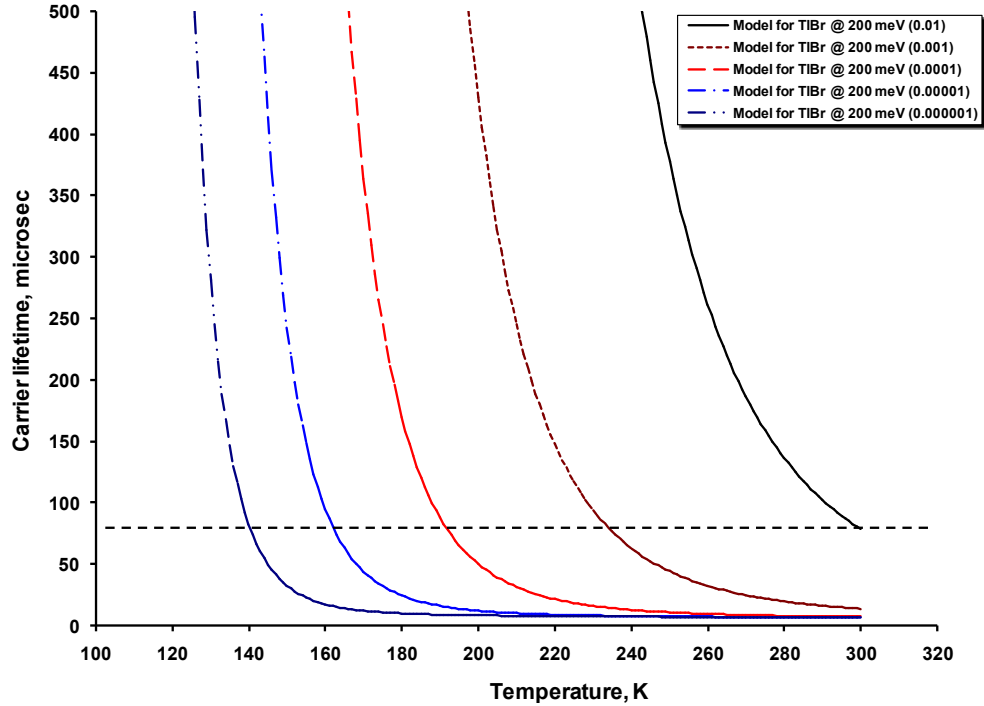
Figure (5.8): Trapping time versus temperature in TlBr for a trap energy level of 200meV and at several different majority carrier concentrations.

5.3. Polycrystalline Thallium Bromide

Because of the low melting temperature of TlBr, three polycrystalline samples were produced by melting commercial TlBr beads in a sealed quartz ampoule for two hours at 480°C, 500°C and 520°C respectively. In each case, the furnace temperature was raised and lowered gradually over two hours to minimize any internal stresses in the samples. Figures (5.9), (5.10) and (5.11) are a set of room temperature decay curves showing the reflected microwave power (a measure of the semiconductor conductivity) versus time after pulsed laser excitation at 532nm wavelength of the three polycrystalline TlBr samples at several different locations. The room temperature trapping time increased monotonically from 5.9μs to 8.8μs to 14μs as the melting temperature decreased from 520°C to 500°C to 480°C.
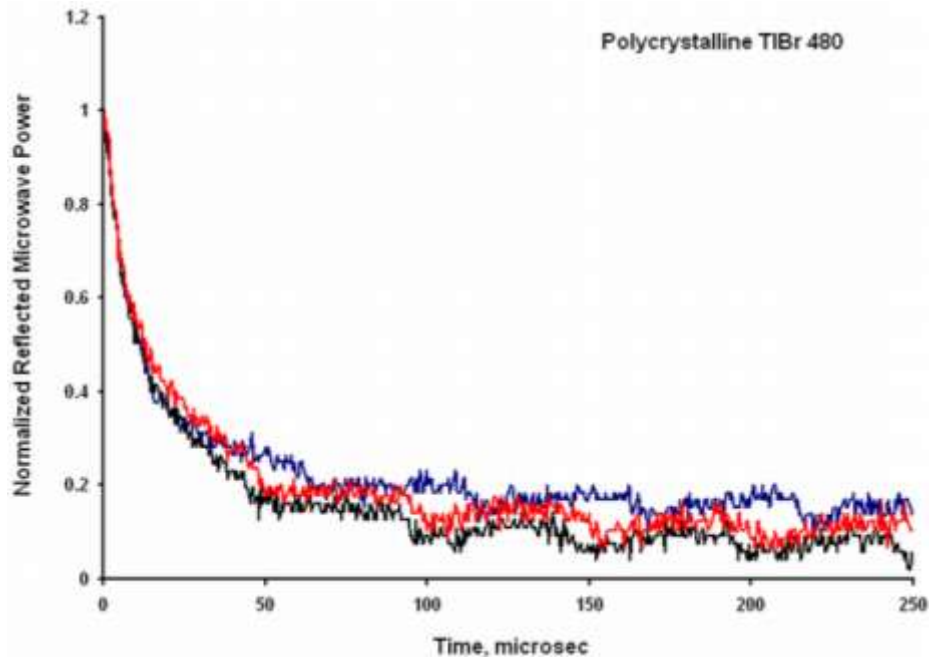
Figure (5.9): Normalized Reflected microwave power versus time for polycrystalline TlBr480 sample at room temperature.
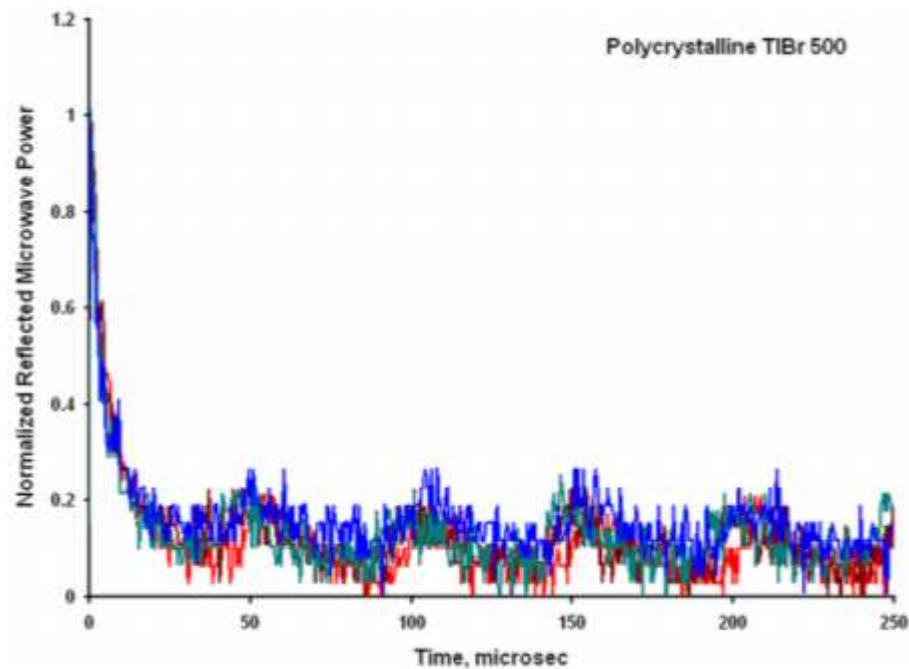
Figure (5.10): Normalized Reflected microwave power versus time for polycrystalline TlBr500 sample at room temperature.

82
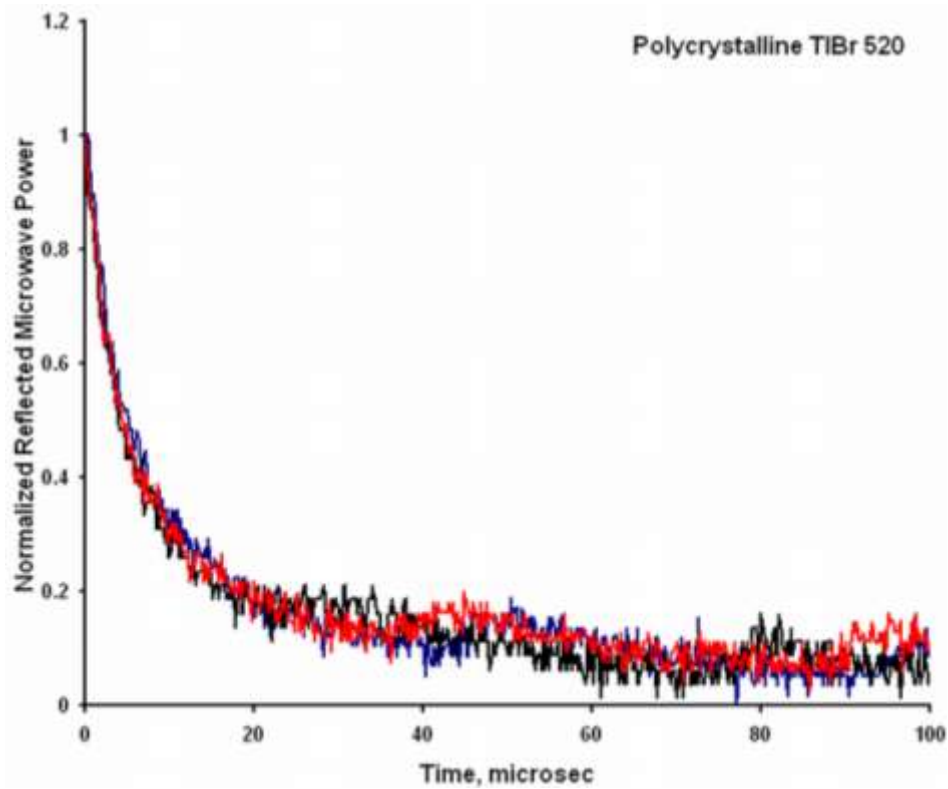
Figure (5.11): Normalized Reflected microwave power versus time for polycrystalline TlBr520 sample at room temperature.

Figures (5.12), (5.13) and (5.14) show the temperature dependence of the trapping time in three polycrystalline TlBr samples, melted at three different temperatures.

The polycrystalline sample melted at 520°C exhibited a room temperature trapping time very close to the value of the single crystal sample and the temperature dependence of the trapping time for all samples followed the expected $\left(\dfrac{1}{\sqrt{T}}\right)$ dependence.

Assuming that the thermal drift velocity, v_{th}, and trap cross section, σ, in equation (5.2) are not significantly influenced by the melting temperature, we conclude that the observed increase in trapping time with decreasing melt temperature is due to a corresponding decrease in the trap concentration N_t.

83
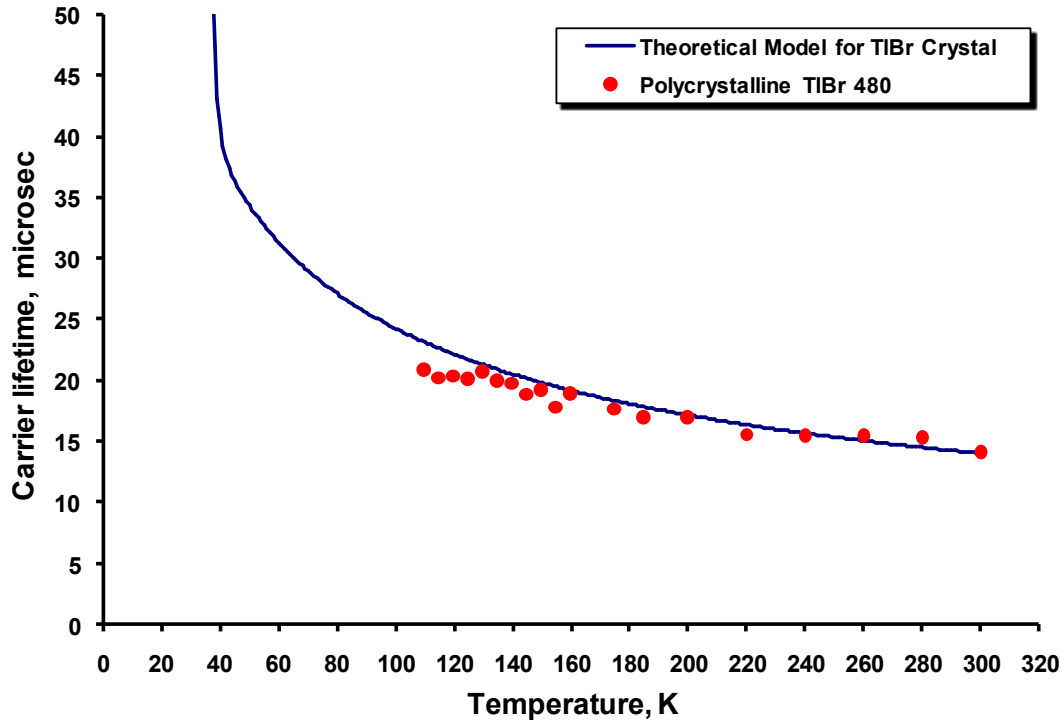
Figure (5.12): Trapping time versus temperature for polycrystalline TlBr melted at 480°C (theory and experiment).
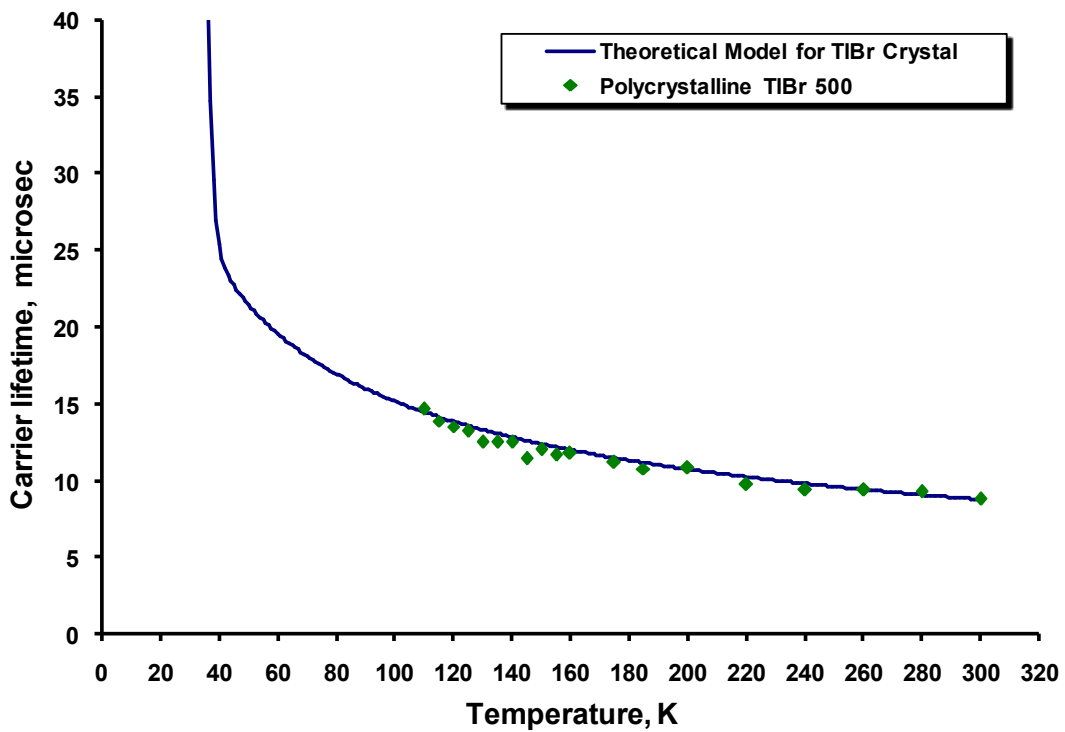
Figure (5.13): Trapping time versus temperature for polycrystalline TlBr melted at 500°C (theory and experiment).
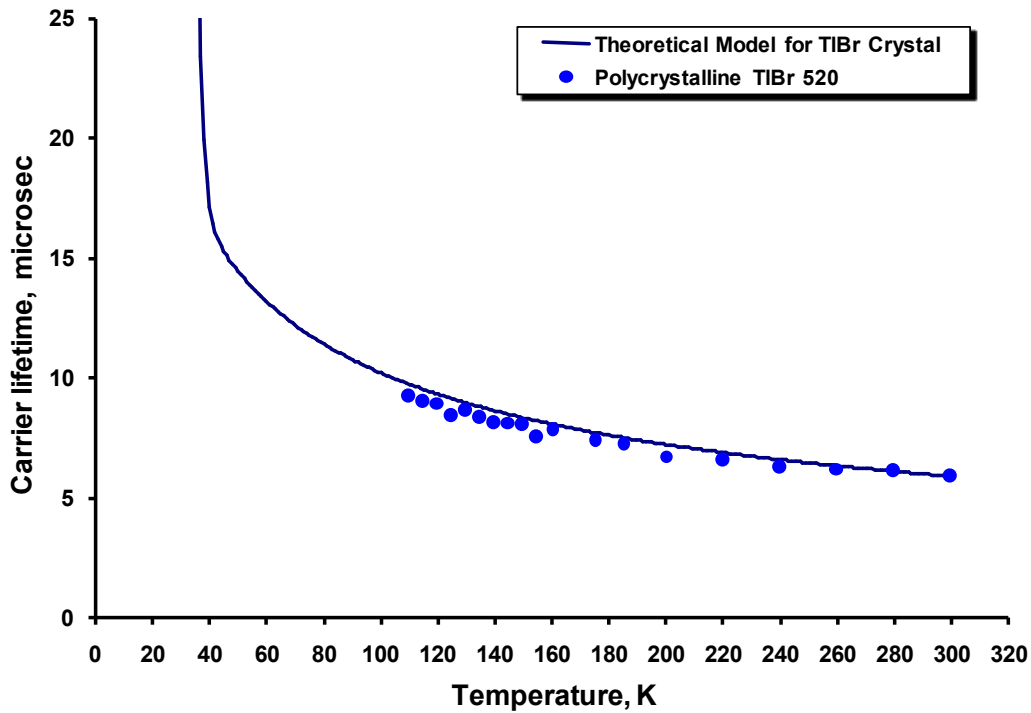
Figure (5.14): Trapping time versus temperature for polycrystalline TlBr melted at 520°C (theory and experiment).

Furthermore, because no additional purification was performed on these samples and they contain approximately the same concentration of extrinsic impurities, we assume that the increase in trap concentration with increasing melt temperature is due primarily to an increase in the concentration of intrinsic crystal defects such as vacancies, voids and interstitials. It is well established that the concentration of intrinsic crystalline defects depends strongly on the thermodynamics of the solidification process. However, a study of the relationship between processing conditions and the defect structure in TlBr is beyond the scope of this study. Our results indicate that the intrinsic trap concentration in TlBr depends strongly on the processing temperature (a 58% decrease in N_t over 40°C).

85

5.4. Conclusion

The carrier trapping time in single crystalline CZT and TlBr was measured as a function of temperature and the results were interpreted using a theoretical trapping model. The results of the trapping model suggest that the room temperature trapping time in TlBr can be significantly increased through the introduction of a moderately deep compensation level located approximately 200meV from the middle of the band gap.

The results of this model demonstrate that the room temperature trapping time in TlBr can, in principle, approach 0.1ms through the introduction of a moderately deep compensation level but without decreasing the overall trap concentration. This strategy is not possible in CZT, because the band gap is too small to use a moderately deep compensation level while still maintaining high material resistivity.

The polycrystalline samples did not exhibit a notable discontinuity in the lifetime-temperature curve. The discontinuity observed in the single crystal TlBr sample was attributed to a change in cubic lattice structure and the polycrystalline samples would be expected to exhibit the same transition since the average grain size is relatively large. At this time we do not have an explanation for this discrepancy.

Literature Cited

[1]   Schieber, M., Lund, J.C., Olsen, R.W., McGregor, D.S., VanScyoc, J.M., James, R.B.,
        and Soria, E., *Material properties and room temperature nuclear detector response of
        wide band gap semiconductors (vol 377, pg 492, 1996).* Nuclear Instruments & Methods
        in Physics Research Section a-Accelerators Spectrometers Detectors and Associated
        Equipment, 1997. **389**(3): p. 523-523.

[2]   Schieber, M., James, R.B., Lund, J.C., McGregor, D.S., Gilbert, T.S., VanScyoc, J.M.,
        Olsen, R.W., Pontau, A.E., Schlesinger, T.S., and Toney, J., *State of the art of wide-
        bandgap semiconductor nuclear radiation detectors.* Nuovo Cimento Della Societa
        Italiana Di Fisica a-Nuclei Particles and Fields, 1996. **109**(9): p. 1253-1260.

[3]   Yu, P.Y. and Cardona, M., *Fundamentals of Semiconductors: Physics and Material
        Properties*. 3rd ed. 2001: Springer.

[4]   Smith, R.A., *Semiconductors*. 2nd ed. Vol. . 1978, Cambridge: Cambridge University
        Press.

[5]   Singh, J., *Semiconductor Devices: Basic Principles*. 2001, New York: John Wiley and
        Sons.

[6]   Cardona, P.Y.Y.a.M., *Fundamentals of Semiconductors: Physics and Material
        Properties*. 3rd ed. 2001: Springer.

[7]   Kittel, C., *Introduction to Solid State Physics*. 1996, New York: Wiely.

[8]   Colinge, J.-P., Colinge, C. A., *Physics of Semiconductor Devices*. 2002: Kluwer
        Academic Publishers.

[9]   Yacobi, B.G., *Semiconductor Materials: An Introduction to Basic Principles*. 2004, New
        York: Kluwer Academic.

[10]   McKelvey, J.P., *Solid State and Semiconductor Physics*. 1966: Harper International.

[11]   Neamen, D.A., *Semiconductor Physics and Devices: Basic Principles*. 3 ed. 2003: McGraw-Hill.

[12]   Owens, A. and Peacock, A., *Compound Semiconductor Radiation Detectors*. Nuclear Instruments & Methods in Physics Research Section A-Accelerators Spectrometers Detectors and Associated Equipment, 2004. **531**: p. 18-37.

[13]   Rockett, A., *The Materials Science of Semiconductors*. 2008: Springer.

[14]   Sze, S.M. and Kwok, K.N., *Physics of Semiconductor Devices*. 3 ed. 2007: John Wiley & Sons,.

[15]   Singh, J., *Semiconductor Devices: Basic Principles*. 1 ed. 2000: Wiley.

[16]   Yu, P.Y. and Cardona, M., *Fundamentals of Semiconductors: Physics and Materials Properties*. 3 ed. 2005, New York: Springer.

[17]   Vavilov, V.S., *Physics and applications of wide bandgap semiconductors*. Physics Uspekhi, 1994. **37**: p. 269-277.

[18]   Kessick, R.F., *Evaluating Electronic Decay in Wide Bandgap Semiconductors Using ContactlessThermally Stimulated Lifetime Measurements*, in *Chemical Engineering*. 2002, Virginia Commonwealth University: Richmond, USA.

[19]   Knoll, G.F., *Semiconductor Diode Detectors. Radiation Detection and Measurement*. 3 ed. 1999, New York: John Wiley & Sons, Inc.

[20]   Philippot, J.C., *Automatic Processing of Diode Spectrometry Results*. IEEE Transactions on Nuclear Science, 1970. **17**(3): p. 446 - 488.

[21]   Rose, A., *Concepts in Photoconductivity and Allied Problems*. 1963, New York: Wiley.

[22]   Schlesinger, T.E., Toney, J.E., Yoon, H., Lee, E.Y., Brunett, B.A., Franks, L., and James, R.B., *Cadmium zinc telluride and its use as a nuclear radiation detector material.* Materials Science & Engineering R-Reports, 2001. **32**(4-5): p. 103-189.

[23]   Schlesinger, T.E. and James, R.B., *Semiconductors for Room Temperature Nuclear Detector Applications.* Vol. 43. 1995: Academic Press.

[24]   Icimone B. Oliveira, F.E.C., José F. D. Chubaci, and Margarida M. Hamada, *Purification and Preparation of TlBr Crystals for Room Temperature Radiation Detector Applications.* IEEE Tranactions on Nuclear Science, 2004. **51**(3): p. 1224-1228.

[25]   Hitomi, K., *Radiation award by radiation science division of the Japanese society for applied physics.* Jpn. Soc. App. Phys. Intern., 2002. **6**.

[26]   Fougeres, P., Siffert, P., Hageali, M., Koebel, J.M., and Regal, R., *CdTe and Cd1-xZnxTe for nuclear detectors: facts and fictions.* Nuclear Instruments & Methods in Physics Research Section a-Accelerators Spectrometers Detectors and Associated Equipment, 1999. **428**(1): p. 38-44.

[27]   Chen, H., Awadalla, S.A., Iniewski, K., Lu, P.H., Harris, F., Mackenzie, J., Hasanen, T., Chen, W., Redden, R., Bindley, G., Kuvvetli, I., Budtz-Jorgensen, C., Luke, P., Amman, M., Lee, J.S., Bolotnikov, A.E., Camarda, G.S., Cui, Y., Hossain, A., and James, R.B., *Characterization of large cadmium zinc telluride crystals grown by traveling heater method.* Journal of Applied Physics, 2008. **103**(1): p. 5.

[28]   Carini, G.A., Bolotnikov, A.E., Camarda, G.S., and James, R.B., *High-resolution X-ray mapping of CdZnTe detectors.* Nuclear Instruments & Methods in Physics Research Section a-Accelerators Spectrometers Detectors and Associated Equipment, 2007. **579**(1): p. 120-124.

[29]   Kessick, R., Tepper, G., Lee, E., and James, R., *Contactless Thermally Stimulated Lifetime Measurements in Detector-Grade Cadmium Zinc Telluride.* Journal of Applied Physics, 2000. **87**(5): p. 2408-2412.

[30]   Eisen, Y., Shor, A., and Mardor, I., *CdTe and CdZnTe gamma ray detectors for medical and industrial imaging systems.* Nuclear Instruments and Methods in Physics Research A 1999. **428**: p. 158-170.

[31]   Franc, J., Hoschl, P., Belas, E., Grill, R., Hlidek, P., Moravec, P., and Bok, J., *CdTe and CdZnTe crystals for room temperature gamma-ray detectors.* Nuclear Instruments and Methods in Physics Research A   1999. **434**: p. 146-151.

[32]   Szeles, C., *CdZnTe and CdTe materials for X-ray and gamma ray radiation detector applications.* phys. stat. sol. (B), 2004. **241**(3): p. 783-790.

[33]   Ahmed, S.N., *Physics and Engineering of Radiation Detection*. 2007, San Diego, CA: Academic Press Inc.

[34]   Yang, J., Zidon, Y., and Shapira, Y., *Alloy Composition and Electronic Structure of Cd1−xZnxTe by Surface Photovoltage Spectroscopy.* Journal of Applied Physics, 2002. **91**(2).

[35]   Chu, M., Terterian, S., Ting, D., Wang, C.C., Gurgenian, H.K., and Mesropian, S., *Tellurium Antisites in CdZnTe.* Appl. Phys. Lett., 2001. **79**(17): p. 2728.

[36]   Zhou, D.X., Quan, L., Chen, X.Y., Yu, S.J., Zheng, Z.P., and Gong, S.P., *Preparation and characterizations of thallium bromide single crystal for room temperature radiation detector use.* Journal of Crystal Growth, 2009. **311**(8): p. 2524-2529.

[37] Zaletin, V.M., Barkov, I.P., Gazizov, I.M., Khrunov, V.S., Lisitskii, I.S., and Kuznetsov, M.S., *Use of TlBr crystals for x- and gamma-ray detectors.* Atomic Energy, 2009. **106**(4): p. 272-275.

[38] Hitomi, K., Onodera, T., Shoji, T., and He, Z., *Investigation of pixelated TlBr gamma-ray spectrometers with the depth-sensing technique.* Nuclear Instruments & Methods in Physics Research Section a-Accelerators Spectrometers Detectors and Associated Equipment, 2008. **591**(1): p. 276-278.

[39] Hitomi, K., Onodera, T., Shoji, T., Hiratate, Y., and He, Z., *TlBr gamma-ray spectrometers using the depth sensitive single polarity charge sensing technique.* Ieee Transactions on Nuclear Science, 2008. **55**(3): p. 1781-1784.

[40] Hitomi, K., Matsumoto, M., Muroi, O., Shoji, T., and Hiratate, Y., *Thallium bromide optical and radiation detectors for X-ray and gamma-ray spectroscopy.* Ieee Transactions on Nuclear Science, 2002. **49**(5): p. 2526-2529.

[41] Hitomi, K., Onodera, T., and Shoji, T., *Influence of zone purification process on TlBr crystals for radiation detector fabrication.* Nuclear Instruments & Methods in Physics Research Section a-Accelerators Spectrometers Detectors and Associated Equipment, 2007. **579**(1): p. 153-156.

[42] Churilov, A.V., Ciampi, G., Kim, H., Cirignano, L.J., Higgins, W.M., Olschner, F., and Shah, K.S., *Thallium Bromide Nuclear Radiation Detector Development.* IEEE Transactions on Nuclear Science, 2009. **56**(4): p. 1875-1881.

[43] Kim, H., Cirignano, L., Churilov, A., Ciampi, G., Higgins, W., Olschner, F., and Shah, K., *Developing Larger TlBr Detectors-Detector Performance.* Ieee Transactions on Nuclear Science, 2009. **56**(3): p. 819-823.

[44]   Hitomi, K., Muroi, O., Shoji, T., Suehiro, T., and Hiratate, Y., *Room temperature X- and gamma-ray detectors using thallium bromide crystals.* Nuclear Instruments & Methods in Physics Research Section a-Accelerators Spectrometers Detectors and Associated Equipment, 1999. **436**(1-2): p. 160-164.

[45]   Hitomi, K., Kikuchi, Y., Shoji, T., and Ishii, K., *Improvement of energy resolutions in TlBr detectors.* Nuclear Instruments & Methods in Physics Research Section a-Accelerators Spectrometers Detectors and Associated Equipment, 2009. **607**(1): p. 112-115.

[46]   Shah, K.S., Lund, J.C., Olschner, F., Moy, L., and Squillante, M.R., *THALLIUM BROMIDE RADIATION DETECTORS.* Ieee Transactions on Nuclear Science, 1989. **36**(1): p. 199-201.

[47]   Hofstadter, R., *Thallium halide crystal counter.* Physical Review, 1947. **72**(11): p. 1120-1121.

[48]   Shah, K.S., Lund, J.C., Olschner, F., Moy, L., and Squillante, M.R., *Thallium bromide radiation detectors.* IEEE Transactions on Nuclear Science, 1989. **36**(1): p. 199–202.

[49]   Owens, A., Bavdaz, M., Lisjutin, I., Peacock, A., Sipila, H., and Zatoloka, S., *On the development of compound semiconductor thallium bromide detectors for astrophysics.* Nuclear Instruments & Methods in Physics Research Section a-Accelerators Spectrometers Detectors and Associated Equipment, 2001. **458**(1-2): p. 413-417.

[50]   Bavdaz, M., Peacock, A., and Owens, A., *Future space applications of compound semiconductor X-ray detectors.* Nucl. Instrum. Methods Phys. Res. A, 2001. **458**: p. 123–131.

[51] da Costa, F.E., Rela, P.R., de Oliveira, I.B., Pereira, M.C.C., and Hamada, M.M., *Surgical gamma probe with TlBr semiconductor for identification of sentinel lymph node.* Ieee Transactions on Nuclear Science, 2006. **53**(3): p. 1403-1407.

[52] Hitomi, K., Muroi, O., Matsumoto, M., Hirabuki, R., Shoji, T., Suehiro, T., and Hiratate, Y., *Recent progress in thallium bromide detectors for X- and gamma-ray spectroscopy.* Nuclear Instruments & Methods in Physics Research Section a-Accelerators Spectrometers Detectors and Associated Equipment, 2001. **458**(1-2): p. 365-369.

[53] Hitomi, K., Murayama, T., Shoji, T., Suehiro, T., and Hiratate, Y., *Improved spectrometric characteristics of thallium bromide nuclear radiation detectors.* Nuclear Instruments & Methods in Physics Research Section a-Accelerators Spectrometers Detectors and Associated Equipment, 1999. **428**(2-3): p. 372-378.

[54] Wang, T., Jie, W.Q., and Zeng, D.M., *Observation of nano-scale Te precipitates in cadmium zinc telluride with HRTEM.* Materials Science and Engineering a-Structural Materials Properties Microstructure and Processing, 2008. **472**(1-2): p. 227-230.

[55] Yue Wanga, K.K., Yuko Inatomi, Rongbin Ji, Tetsuichi Motegi, *Growth and structure of CdZnTe crystal from Te solution with THM technique under static magnetic field.* Journal of Crystal Growth, 2005. **275**: p. 1551-1556.

[56] Rudolph, P., *Non-stoichiometry related defects at the melt growth of semiconductor compound crystals - a review.* Crystal Research and Technology, 2003. **38**(7-8): p. 542-554.

[57] Jackson, K.A., *Compound Semiconductor Devices: Structures and Processing.* 1998, Weinheim: Wiley-VCH.

[58]   Brice, J.C., *The Bridgeman and related methods. Crystal Growth Processes*. 1 ed. 1986, Glasgow: Blackie & Sons Limited : Bishopgriggs.

[59]   Lachish, U., *Semiconductor crystal optimization of gamma detection*. Journal of Crystal Growth 2001. **225**: p. 114-117.

[60]   Liao, P.K., Chen, M.C., and Castro, C.A. *Oral Presentation*. in *10th International Conference on Crystal Growth, Sun Diego, CA1992* 1992. Thousand Oaks, CA: American Association for Crystal Growth.

[61]   Miyake, H. and Hiramatsu, K., *THM Growth of Cu-III-VI2 Chalcopyrite Semiconductors*. Ternary and Multinary Compounds in the 21st Century, IPAP Books 1, 2001: p. 45-50.

[62]   Audet, N. and Cossette, M., *Synthesis of Ultra-High-Purity CdTe Ingots by the Traveling Heater Method*. Journal of Electronic Materials, 2005. **34**(6): p. 683-686.

[63]   Gille, P., Rossner, U., Puhlmann, N., Niebsch, H., and Piotroski, T.T., *Growth of Hg1-xMnxTe Crystals by the Travelling Heater Method*. Semicond. Sci. Technol., 1995. **10**: p. 353-357.

[64]   Yao, H., Lim, L.A., James, R.B., Schieber, M., and Natarajan, M., *Surface aging of HgI2 crystals studied by VASE and AFM*. Nuclear Instruments & Methods in Physics Research Section a-Accelerators Spectrometers Detectors and Associated Equipment, 1996. **380**(1-2): p. 26-29.

[65]   Melnikov, A.A., Sigov, A.S., Vorotilov, K.A., Davydov, A.A., Topalova, L.I., and Zhavoronkov, N.V., *Growth of CdZnTe single crystals for radiation detectors*. Journal of Crystal Growth, 1999. **197**(3): p. 666-669.

[66]   Zanio, K., Willardson, Beer, and Teatise, *Cadmium Telluride, Semiconductors and Semimetlas*. Vol. 13. 1978, San Diego: Academic Press.

[67] Luke, P.N., Amman, M., and Lee, J.S., *Factors affecting energy resolution of coplanar-grid CdZnTe detectors.* Ieee Transactions on Nuclear Science, 2004. **51**(3): p. 1199-1203.

[68] Elshazly, E.S. and Tepper, G., *Correlation of tellurium inclusions and carrier lifetime in detector grade cadmium zinc telluride.* Applied Physics Letters, 2008. **93**(4): p. 3.

[69] Ivanov, L.A.V., Dorogov, P., and Loutchanski, A., *Correlation Between Quality of CZT Crystals and Spectrometric Performance of Hemispherical Radiation Detectors.* IEEE Nuclear Science Symposium Conference, 2004: p. 4415-4419.

[70] Yue Wang, K.K., Yuko Inatomi, Rongbin Ji, Tetsuichi Motegi, *Growth and structure of CdZnTe crystal from Te solution with THM technique under static magnetic field.* Journal of Crystal Growth, 2005. **275**: p. 1551-1556.

[71] James, R.B., Brunett, B., Heffelfinger, J., Van Scyoc, J., Lund, J., Doty, F.P., Lingren, C.L., Olsen, R., Cross, E., Hermon, H., Yoon, H., Hilton, N., Schieber, M., Lee, E.Y., Toney, J., Schlesinger, T.E., Goorsky, M., Yao, W., Chen, H., and Burger, A., *Material properties of large-volume cadmium zinc telluride crystals and their relationship to nuclear detector performance.* Journal of Electronic Materials, 1998. **27**(6): p. 788-799.

[72] Chu, M.R., Terterian, S., Ting, D., Wang, C.C., Benson, J.D., Dinan, J.H., James, R.B., and Burger, A., *Effects of excess tellurium on the properties of CdZnTe radiation detectors.* Journal of Electronic Materials, 2003. **32**(7): p. 778-782.

[73] Duff, M.C., Hunter, D.B., Nuessle, P., Black, D.R., Burdette, H., Woicik, J., Burger, A., and Groza, M., *Synchrotron X-ray based characterization of CdZnTe crystals.* Journal of Electronic Materials, 2007. **36**(8): p. 1092-1097.

[74] Slater, J.C., *The Design of Linear Accelerators.* Reviews of Modern Physics, 1948. **20**(3): p. 473.

[75]   Tepper, G., Kessick, R., James, R., and Berg, L.v.d. *Contactless Measurements of Charge Traps and Carrier Lifetimes in Detector-Grade Cadmium Zinc Telluride and Mercuric Iodide* in *Hard X-Ray, Gamma-Ray, and Neutron Detector Physics II, Proceeding of SPIE*. 2000.

[76]   Hall, R.N., *Electron -Hole Recombination in Germanium.* Phys. Rev., 1952. **87**: p. 387.

[77]   Park, J.M., *Novel Power Devices for Smart Power Applications* 2004, Technical University of Vienna: Karlsplatz

[78]   Spieler, H., *Semiconductor Detector Systems*. 2005, New York: Oxford University Press.

[79]   Queisser, H.J., *Recombination at Deep Traps.* Solid State Electronics, 1980. **21**: p. 1495.

[80]   Pierret, R.F., *Advanced Semiconductor Fundamentals*. 2 ed. Vol. VI. 2002, New Jersey: Prentice Hall.

[81]   Schroder, D.K., *Semiconductor Material and Device Characterization*. 3 ed. 2006, New Jersey: John Wiley and Sons.

[82]   Sze, S.M., *Semiconductor Devices Physics and Technology*. 1985, New York: John Wiley and Sons.

[83]   *New Wave Research Inc, Minilase Nd:YAG Laser Operating Manual*. August 1997.

[84]   Heffelfinger, J.R., Medlin, D.L., James, R.B., *Structural and Chemical Analysis of Grain Boundaries and Tellurium Precipitates in Commercial Cd1-xZnxTe.* SPIE Conference on Hard X-Ray and Gamma-Ray Detector Physics and Applications, 1998. **3446**: p. 49.

[85]   Bolotnikov, A.E., Camarda, G.S., Carini, G.A., Cui, Y., Li, L., and James, R.B., *Modelling the effects of Te precipitates on the electron transport in CdZnTe radiation detectors.* Nuclear Instruments & Methods in Physics Research Section a-Accelerators Spectrometers Detectors and Associated Equipment, 2007. **579**(1): p. 125-129.

[86] Bolotnikov, A.E., Abdul-Jabbar, N.M., Babalola, O.S., Camarda, G.S., Cui, Y., Hossain, A.M., Jackson, E.M., Jackson, H.C., James, J.A., Kohman, K.T., Luryi, A.L., and James, R.B., *Effects of Te Inclusions on the Performance of CdZnTe Radiation Detectors.* Ieee Transactions on Nuclear Science, 2008. **55**(5): p. 2757-2764.

[87] Hage-Ali, M. and Siffert, P., *Semiconductors and Semimetals*. Vol. 43. 1995, San Diego: Academic Press. 219-257.

[88] Hossain, A., Bolotnikov, A.E., Camarda, G.S., Cui, Y., Yang, G., and James, R.B., *Defects in cadmium zinc telluride crystals revealed by etch-pit distributions.* Journal of Crystal Growth, 2008. **310**(21): p. 4493-4498.

[89] van Pamelen, M.A.J., Budtz-Jorgensen, C., and Kuvvetli, I., *Development of CdZnTe X-ray detectors at DSRI.* Nuclear Instruments & Methods in Physics Research Section a-Accelerators Spectrometers Detectors and Associated Equipment, 2000. **439**(2-3): p. 625-633.

[90] Szeles, C., Cameron, S.E., Ndap, J.O., and Chalmers, W.C., *Advances in the crystal growth of semi-insulating CdZnTe for radiation detector applications.* Ieee Transactions on Nuclear Science, 2002. **49**(5): p. 2535-2540.

[91] Bolotnikov, A.E., Camarda, G.S., Carini, G.A., Cui, Y., Li, L., and James, R.B., *Cumulative effects of Te precipitates in CdZnTe radiation detectors.* Nuclear Instruments & Methods in Physics Research Section a-Accelerators Spectrometers Detectors and Associated Equipment, 2007. **571**(3): p. 687-698.

[92] Brunett, B.A., Van Scyoc, J.M., Hilton, N.R., Lund, J.C., and James, R.B., *The performance effects of crystal boundaries in cadmium zinc telluride radiation spectrometers.* Ieee Transactions on Nuclear Science, 2000. **47**(4): p. 1353-1359.

[93] Carini, G.A., Bolotnikov, A.E., Camarda, G.S., Wright, G.W., James, R.B., and Li, L., *Effect of Te precipitates on the performance of CdZnTe detectors.* Applied Physics Letters, 2006. **88**(14).

[94] Babentsov, V., Franc, J., and James, R.B., *Compensation and trapping in large bandgap semiconductors: Tuning of the defect system in CdZnTe.* Journal of Crystal Growth, 2009. **311**(8): p. 2377-2380.

[95] Wang, T., Jie, W.Q., Zhang, J.J., Yang, G., Zeng, D.M., Xu, Y.D., Ma, S.Y., Hua, H., and He, K., *Study on the behaviors of impurities in cadmium zinc telluride.* Journal of Crystal Growth, 2007. **304**(2): p. 313-316.

[96] Lee, E.Y., James, R.B., Olsen, R.W., and Hermon, H., *Compensation and trapping in CdZnTe radiation detectors studied by thermoelectric emission spectroscopy, thermally stimulated conductivity, and current-voltage measurements.* Journal of Electronic Materials, 1999. **28**(6): p. 766-773.

[97] Zaletin, V.M., *Development of semiconductor Detectors Based on Wide-Gap Materials.* Atomic Energy, 2004. **97**(5): p. 773-780.

[98] Amman, M., Lee, J.S., and Luke, P.N., *Electron trapping nonuniformity in high-pressure-Bridgman-grown CdZnTe.* Journal of Applied Physics, 2002. **92**(6): p. 3198-3206.

[99] Babentsov, V., Franc, J., and James, R.B., *Compensation and Photosensitivity in CdTe Doped With Indium.* Ieee Transactions on Nuclear Science, 2009. **56**(4): p. 1724-1730.

[100] Zumbiehl, A., Mergui, S., Ayoub, M., Hage-Ali, M., Zerrai, A., Cherkaoui, K., Marrakchi, G., and Darici, Y., *Compensation origins in II-VICZT materials.* Materials

Science and Engineering B-Solid State Materials for Advanced Technology, 2000. **71**: p. 297-300.

[101]   Szeles, C., *CdZnTe and CdTe materials for X-ray and gamma ray radiation detector applications.* Physica Status Solidi B-Basic Research, 2004. **241**(3): p. 783-790.

[102]   Fiederle, M., Babentsov, V., Fauler, A., Witte, W., Benz, K.W., and James, R.B., *Semi-insulating cadmium telluride at low impurity concentrations.* Journal of Materials Research, 2004. **19**(2): p. 405-408.

[103]   Lee, E.Y. and James, R.B., *Effect of electron transport properties on unipolar CdZnTe radiation detectors: LUND, SpectrumPlus, and coplanar grid.* Journal of Electronic Materials, 1999. **28**(6): p. 843-849.

[104]   Lee, E.Y., Brunett, B.A., Olsen, R.W., Van-Scyoc, J.M., Hermon, H., and James, R.B., *Detection of electron and hole traps in CdZnTe radiation detectors by thermoelectric emission spectroscopy and thermally stimulated conductivity.* Proceedings of SPIE-The International Society for Optical Engineering (1998), (Hard X-Ray and Gamma-Ray Detector Physics and Applications), , 1998. **3446**: p. 40-48.

[105]   Schlesinger, T.E., James, R.B., Schieber, M., Toney, J., VanScyoc, J.M., Salary, L., Hermon, H., Lund, J., Burger, A., Chen, K.T., Cross, E., Soria, E., Shah, K., Squillante, M., Yoon, H., and Goorsky, M., *Characterization of lead iodide for nuclear spectrometers.* Nuclear Instruments & Methods in Physics Research Section a-Accelerators Spectrometers Detectors and Associated Equipment, 1996. **380**(1-2): p. 193-197.

[106]   Tepper, G. and Losee, J., *A compressed xenon ionization chamber X-ray/gamma-ray detector incorporating both charge and scintillation collection.* Nuclear Instruments and

Methods in Physics Research Section A: Accelerators, Spectrometers, Detectors and Associated Equipment, 1996. **368**(3): p. 862-864.

[107] Sullivan, C.J., He, Z., Knoll, G.F., Tepper, G., and Wehe, D.K., *A high pressure xenon gamma-ray spectrometer using a coplanar anode configuration.* Nuclear Instruments and Methods in Physics Research Section A: Accelerators, Spectrometers, Detectors and Associated Equipment, 2003. **505**(1-2): p. 238-241.

[108] Zhang, F., He, Z., Xu, D., Knoll, G.F., Wehe, D.K., and Berry, J.E., *Improved resolution for 3-d position sensitive CdZnTe spectrometers.* Ieee Transactions on Nuclear Science, 2004. **51**(5): p. 2427-2431.

[109] Kim, H., Cirignano, L., Churilov, A., Ciampi, G., Higgins, W., Olschner, F., and Shah, K., *Developing Larger TlBr Detectors—Detector Performance.* IEEE Transactions on Nuclear Science, 2009. **56**(3-2): p. 819-823.

[110] Madelung, O., Rossler, U., and Schultz, M., *Non-Tetrahedrally Bonded Elements and Binary Compounds*. 2006, Verlag: Springer

[111] Blackman, M. and Khan, I.H., *The Polymorphism of Thallium and Other Halides at Low Temperatures.* Proceedings of The Physical Society, 1961. **77**: p. 471-475.

[112] Elshazly, E.S., Tepper, G., and Burger, A., *Charge Trapping in Detector Grade Thallium Bromide and Cadmium Zinc Telluride: Measurement and Theory.* Nuclear Instruments and Methods in Physics Research A 2010. **620**: p. 279-284.

Appendix

Figure (A.1): Microwave cavity Perturbation (MCP) Electronics
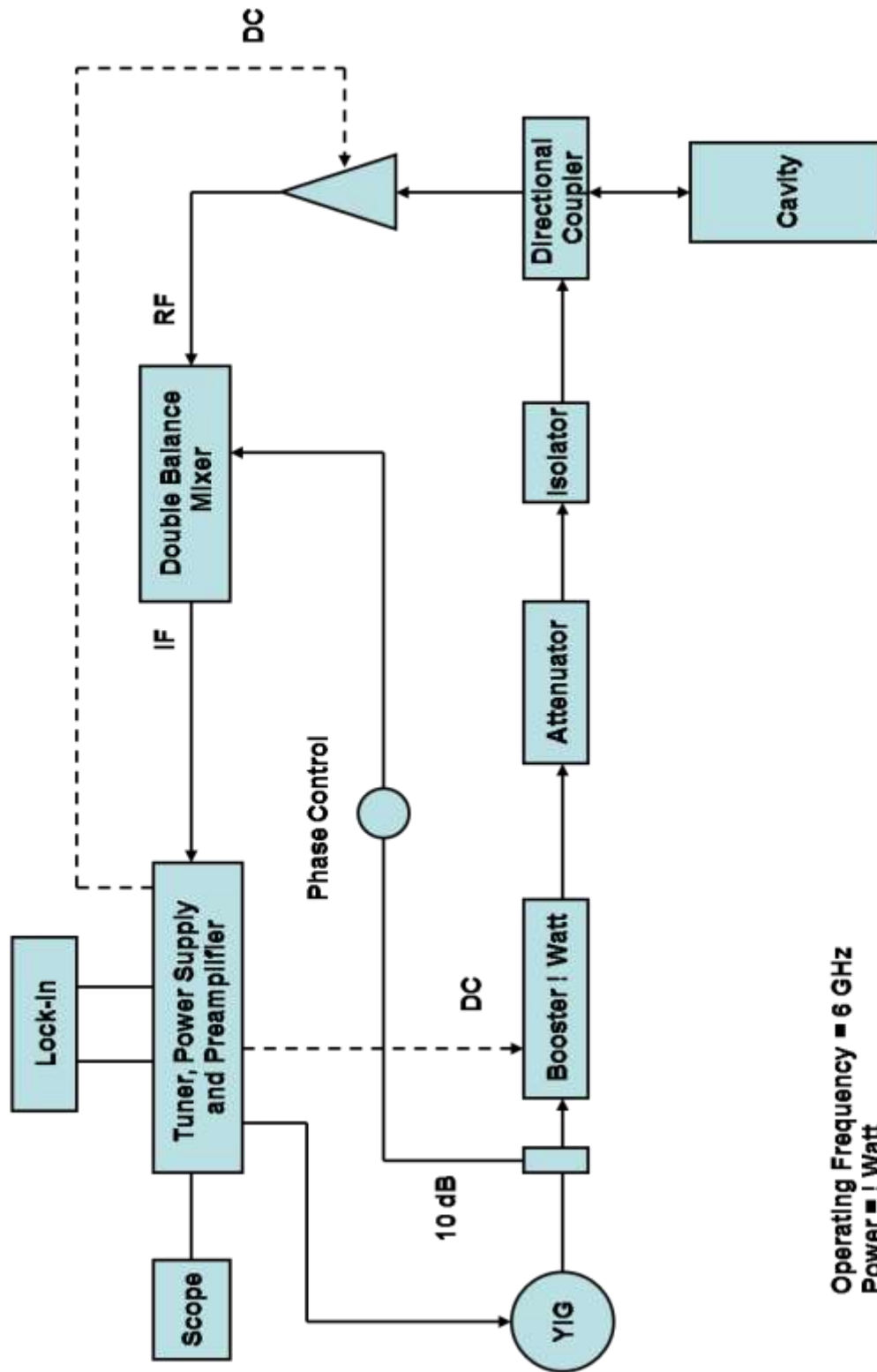
Operating Frequency = 6 GHz
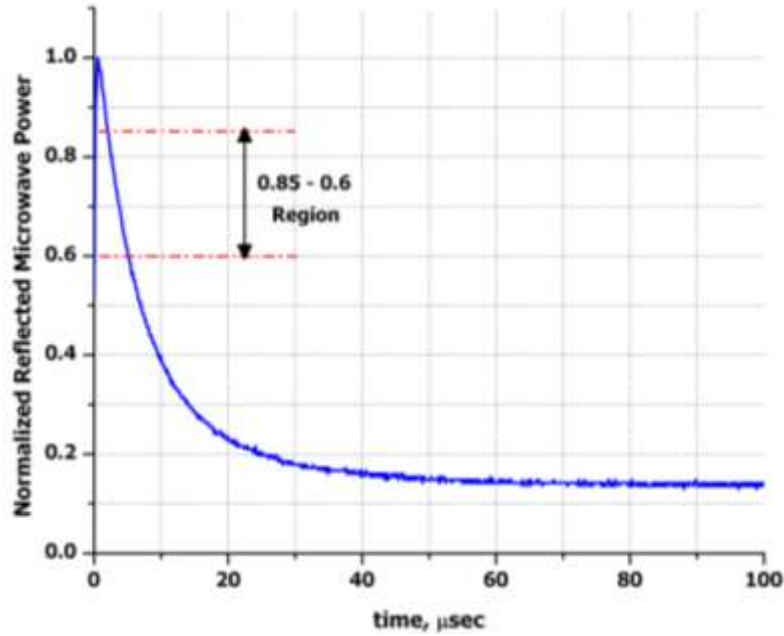Power = ! Watt

CALCULATION OF CARRIER OR DECAY TIME

Figure (A.2): Normalized Reflected Microwave Power versus time.

From the above pulse, at the 0.85 position on the y-axis the corresponding time (x-axis) value is determined, this is t_1. The same time value for $y = 0.6$ position is determined, this is t_2. For a first order decay the working equation is,
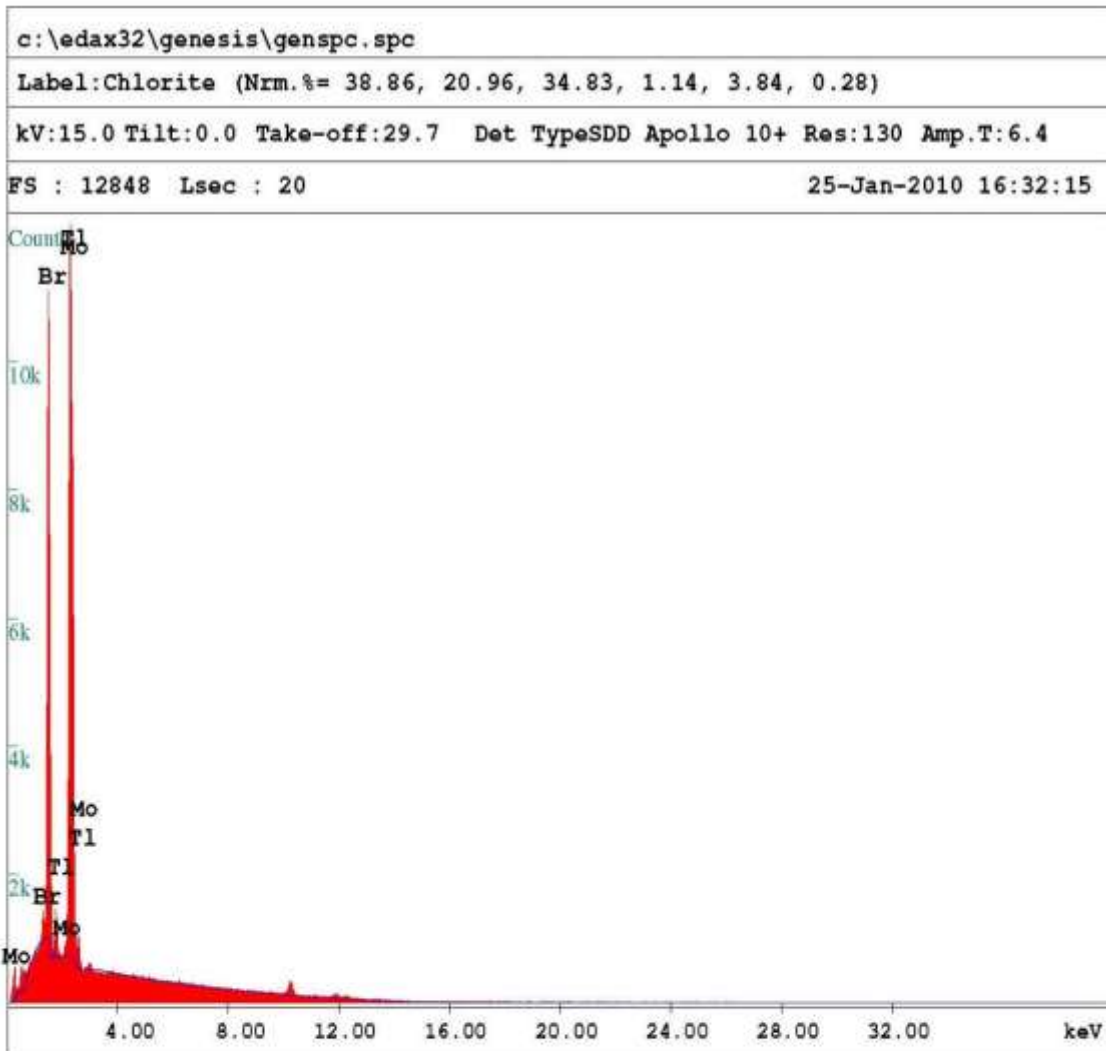
$$I(t) = I_o e^{-t/\tau}$$

$$I(t_1) = I_o e^{-t_1/\tau} \qquad\qquad I(t_2) = I_o e^{-t_2/\tau}$$

Setting the two equations equal to each other,

$$\frac{I(t_2)}{I(t_1)} = \frac{0.6}{0.85} = \frac{I_o e^{-t_2/\tau}}{I_o e^{-t_1/\tau}}$$

Therefore,

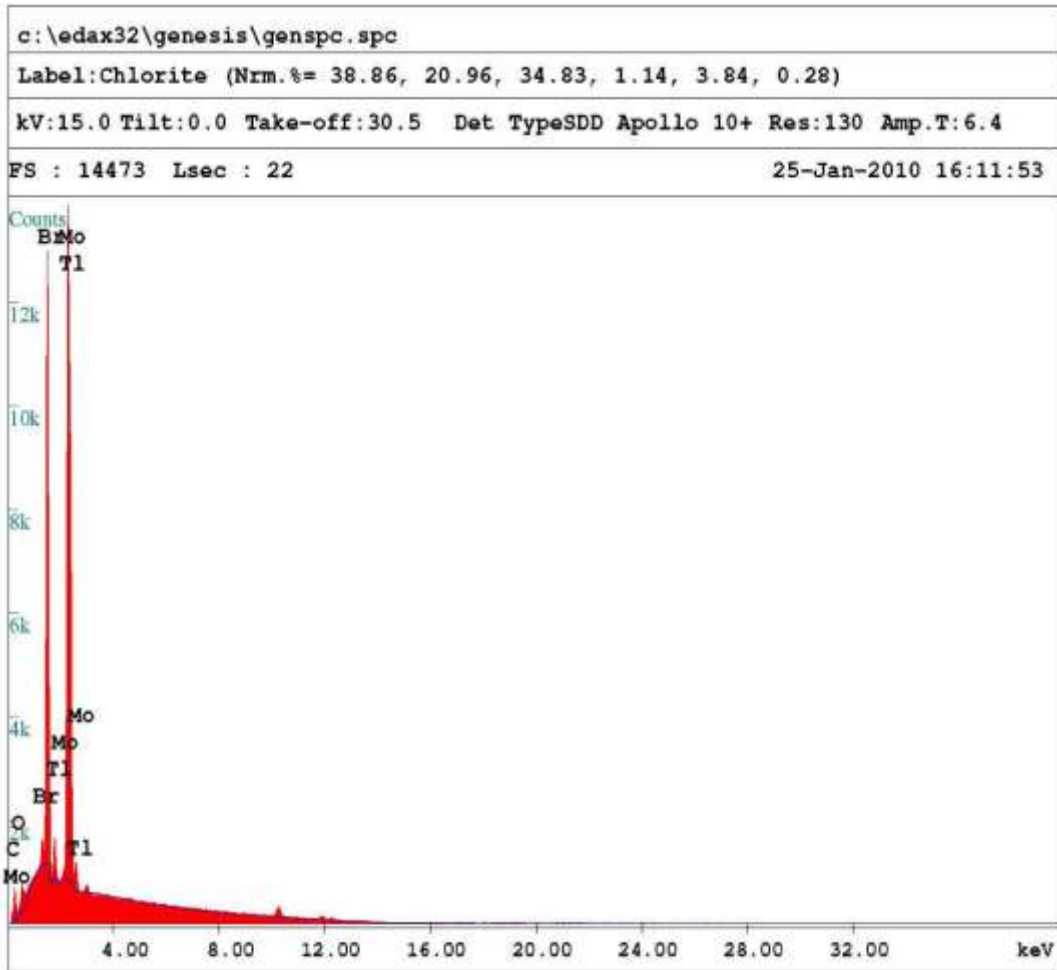$$\tau = \frac{(t_1 - t_2)}{\ln\left[\dfrac{I(t_2)}{I(t_1)}\right]}$$

104

```
c:\edax32\genesis\genspc.spc

Label:Chlorite (Nrm.%= 38.86, 20.96, 34.83, 1.14, 3.84, 0.28)

kV:15.0 Tilt:0.0 Take-off:29.7   Det TypeSDD Apollo 10+ Res:130 Amp.T:6.4

FS : 12848  Lsec : 20                          25-Jan-2010 16:32:15
```

EDAX ZAF Quantification (Standardless)
Element Normalized
SEC Table : Default

Element	Wt %	At %	K-Ratio	Z	A	F
BrL	31.92	47.23	0.2575	1.0697	0.7529	1.0017
TlM	47.62	27.55	0.3830	0.9115	0.8825	1.0000
MoL	20.47	25.22	0.1687	1.0530	0.7829	1.0000
Total	100.00	100.00				

Element	Net Inte.	Bkgd Inte.	Inte. Error	P/B
BrL	3818.59	459.84	0.39	8.30
TlM	3058.61	369.23	0.44	8.28
MoL	1759.72	332.09	0.61	5.30

Figure(A.3): EDX analysis of TlBr Single crystal

Figure (A.4): EDX analysis of Polycrystalline TlBr480
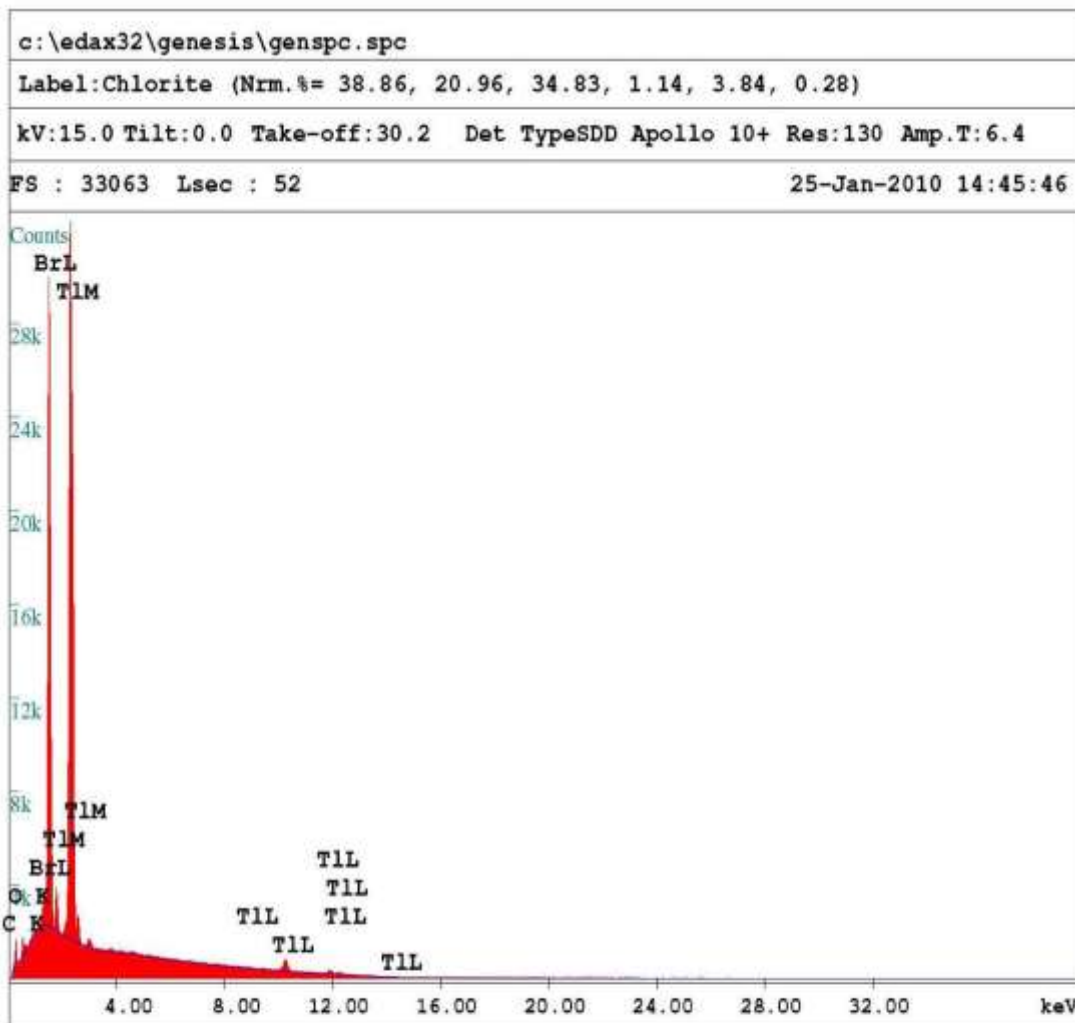
EDAX ZAF Quantification (Standardless)
Element Normalized
SEC Table : Default

Element	Wt %	At %	K-Ratio	Z	A	F
C K	1.96	19.03	0.0039	1.4219	0.1413	1.0000
O K	0.74	5.41	0.0018	1.3919	0.1772	1.0001
BrL	22.47	32.82	0.1739	1.0983	0.7048	1.0000
TlL	74.83	42.74	0.6806	0.9071	1.0027	1.0000
Total	100.00	100.00				

Element	Net Inte.	Bkgd Inte.	Inte. Error	P/B
C K	108.95	58.22	1.90	1.87
O K	77.54	106.58	3.02	0.73
BrL	4012.24	388.91	0.24	10.32
TlL	133.51	100.49	1.88	1.33

Figure (A.5): EDX analysis of Polycrystalline TlBr500
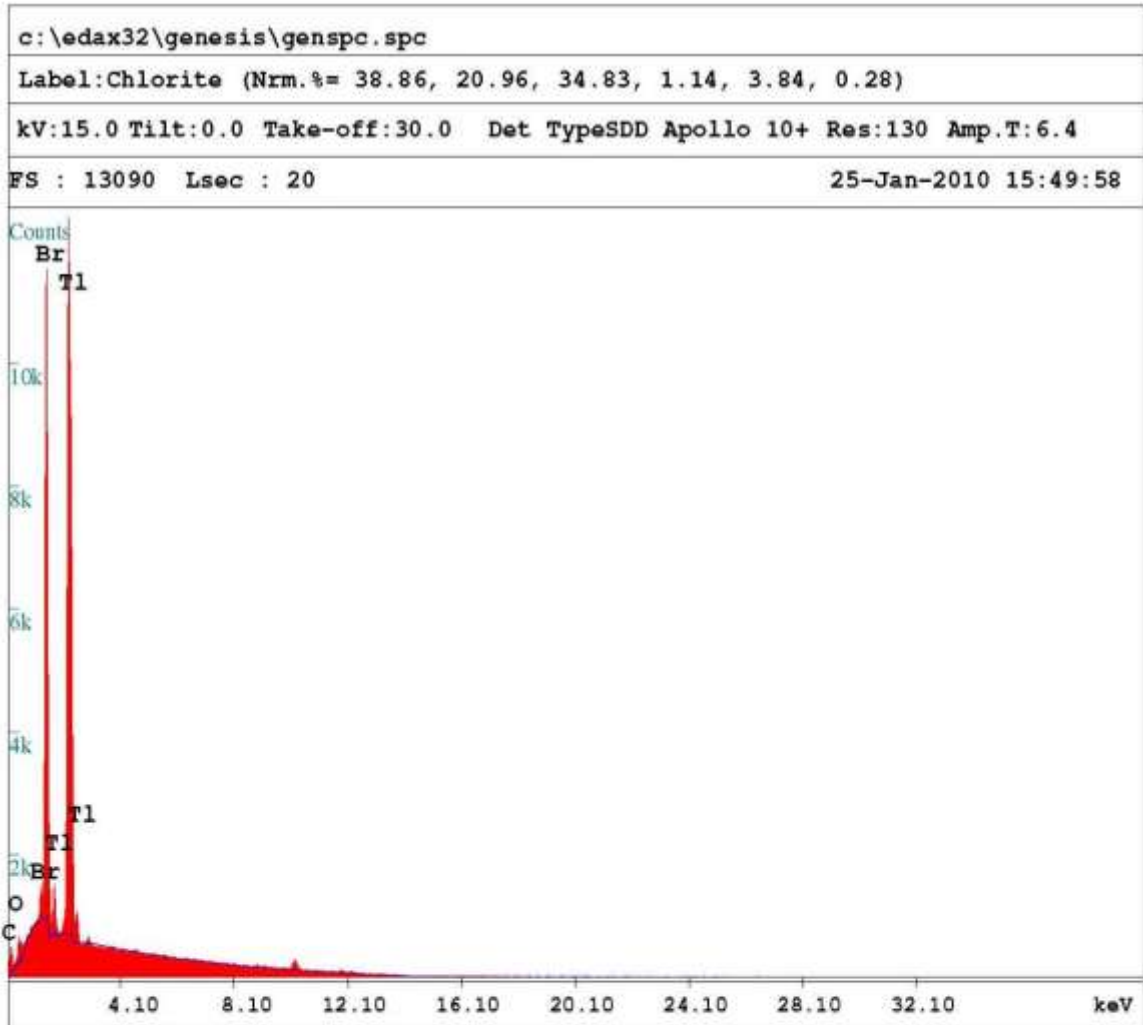
```
c:\edax32\genesis\genspc.spc

Label:Chlorite (Nrm.%= 38.86, 20.96, 34.83, 1.14, 3.84, 0.28)

kV:15.0 Tilt:0.0 Take-off:30.0   Det TypeSDD Apollo 10+ Res:130 Amp.T:6.4

FS : 13090   Lsec : 20                              25-Jan-2010 15:49:58
```


Figure (A.6): EDX analysis of Polycrystalline TlBr520

EDAX ZAF Quantification (Standardless)
Element Normalized
SEC Table : Default

Element	Wt %	At %	K-Ratio	Z	A	F
C K	2.94	24.03	0.0056	1.3948	0.1357	1.0000
O K	1.34	8.23	0.0033	1.3656	0.1798	1.0002
BrL	29.03	35.69	0.2286	1.0750	0.7326	1.0000
TlM	66.69	32.05	0.5413	0.9166	0.8856	1.0000
Total	100.00	100.00				

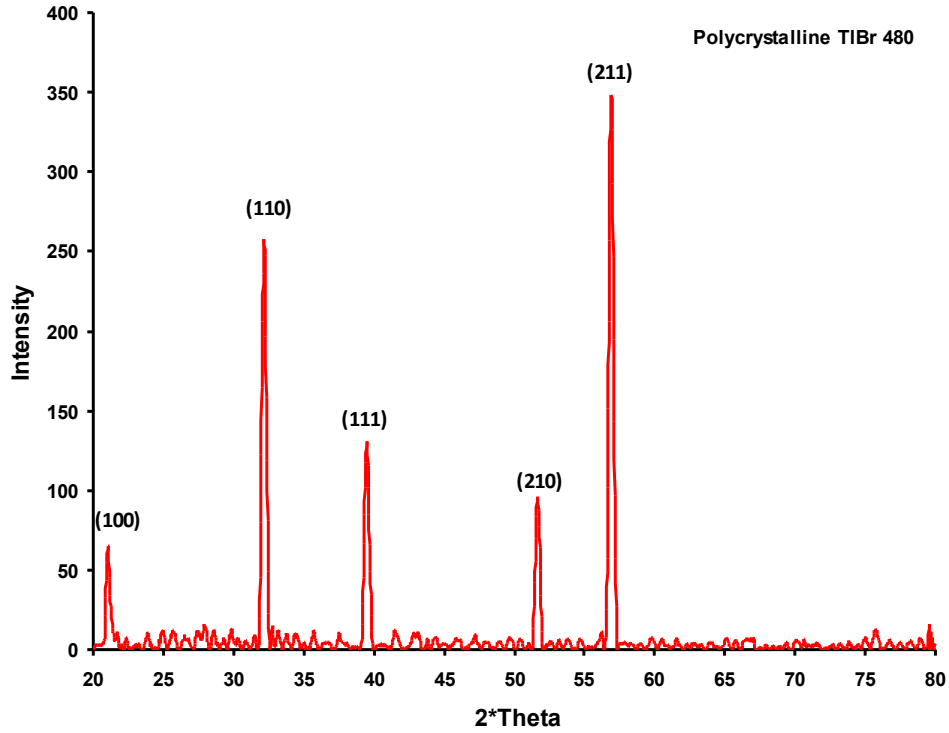| Element	Net Inte.	Bkgd Inte.	Inte. Error	P/B
C K	118.34	13.46	2.24	8.79
O K	107.35	75.50	3.29	1.42
BrL	4063.02	453.12	0.38	8.97
TlM	5180.34	365.42	0.33	14.18

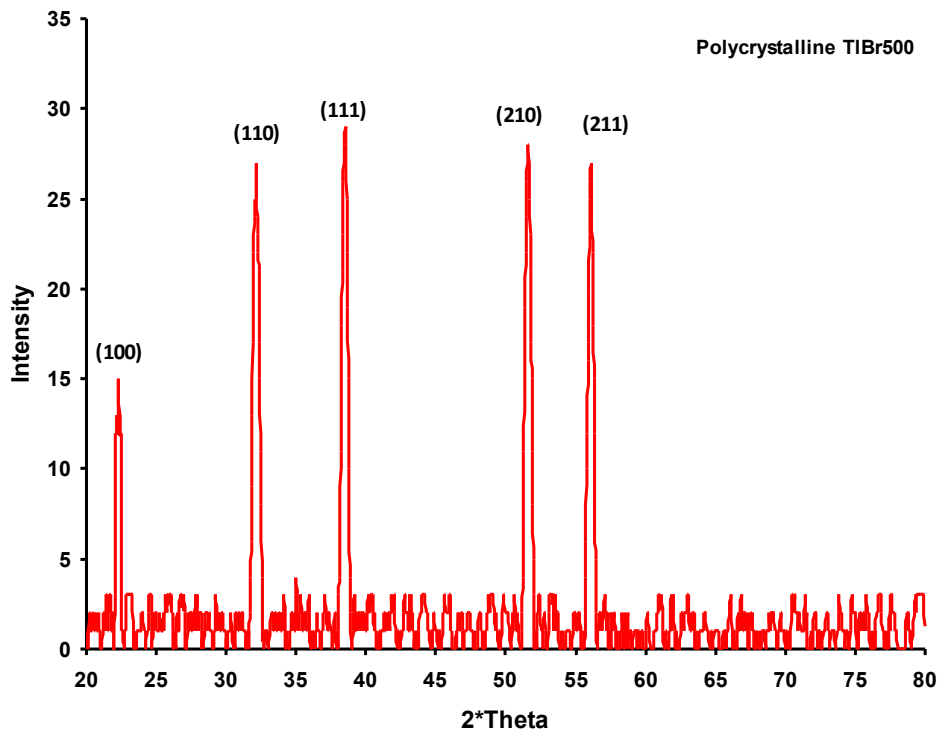Figure (A.7): XRD pattern of polycrystalline TlBr480 sample.

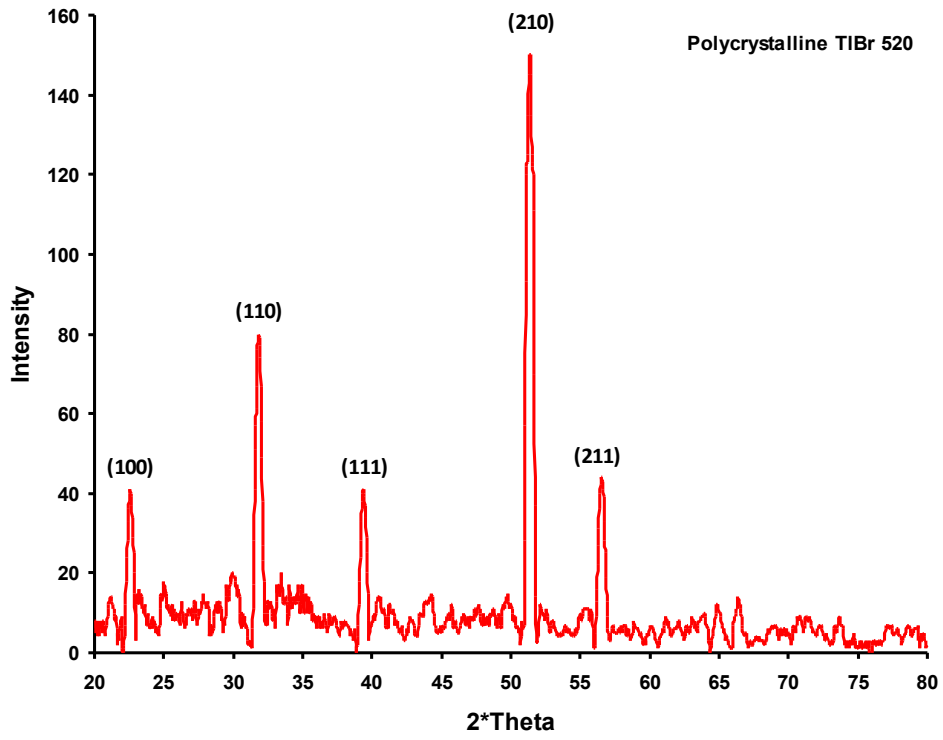Figure (A.8): XRD pattern of polycrystalline TlBr500 sample.

Figure (A.9): XRD pattern of polycrystalline TlBr520 sample.

VITA

Ezzat Salah El-Din Elshazly was born in Kalubia, Egypt. He received the degree of Bachelor of Science in Mechanical Engineering in January 1994 from Benha Higher Institute of Technology (BHIT), Egypt. He received the Master degree in Material Science from Imperial College of Science, Technology, and Medicine / London University, UK in December 1999. He also received the Master degree in Metallurgical Engineering from Cairo University, Egypt in December 2005. In August 2010, he completed his Doctor of Philosophy degree in Mechanical Engineering at Virginia Commonwealth University.

PERMANENT ADDRESS:

Ezzat S. Elshazly

Atomic Energy Authority

Nuclear Research Center

Metallurgy Department

P.O.Box 13759

Cairo / EGYPT

Personal E-mail address: ezzatelshazly@gmail.com

ACADEMIC APPOINTMENTS

- **2008 – PRESENT:** Lecturer Assistant of Material Science, Atomic Energy Authority /Nuclear Research Center / Metallurgy Department, Egypt.
- **2006 – PRESENT :** Ph.D student, Virginia Commonwealth University / School of Engineering, Department of Mechanical Engineering, USA.
- **1997 – 2008:** Mechanical Engineer, Atomic Energy Authority Nuclear Research Center / Metallurgy Department, Egypt.

EDUCATION:

- PhD Candidate, School of Engineering, Virginia Commonwealth University (Expected graduation: August, 2010)

- MSc. Material Science, Imperial College of Science, Technology and Medicine / London University – December 1999.
- MSc. Metallurgical Engineering, Cairo University – December 2005.
- Bachelor Degree in Mechanical Engineering, Benha Higher Institute of Technology (BHIT) - January, 1994.

PUBLICATIONS:

1) **Ezzat S. Elshazly**, M. El-Sayed Ali, and S. M. El-Houte, "Alumina Effect on The Phase Transformation of 3Y-TZP Ceramics", *Journal of Material Science and Technology*, Vol. 24 [6], 2008.

2) **Ezzat S. Elshazly**, and Gary Tepper, " Correlation of Tellurium Inclusions and Carrier Lifetime in Detector Grade Cadmium Zinc Telluride", *Applied Physics. Letters*, 93, 042112 (2008).

3) **Ezzat S. Elshazly**, Gary Tepper, and Arnold Burger, " Charge Trapping in Detector Grade Thallium Bromide and Cadmium Zinc Telluride: Measurement and Theory", Accepted on *Nuclear Instruments and Methods in Physics Research A* 620 (2010) 279–284

4) **Ezzat S. Elshazly**, S. M. El-Houte, and M. El-Sayed Ali, " Yttria Tetragonal Zirconia Biomaterials: Kinetic Investigation ", Submitted to *Journal of Materials Science and Technology*, Nov., 2009.

POSTERS AND PRESENTATIONS:

1) **Ezzat S. Elshazly**, Royal F. Kessick and Gary C. Tepper, " An Investigation of Defect Density and Carrier Lifetimes in Radiation Detector Grade Cadmium Zinic Telluride", *24th Watts Danial Symposium*, 16-17 October, 2007, Richmond, Virginia, USA.

AWARDS:

- VCU Graduate School Dissertation Fellowship: Dec., 2009 – Aug., 2010.
- Research Assistantship / VCU-School of engineering: Jan., 2009 – Dec., 2009.
- Teaching Assistantship / VCU-School of Engineering: Aug., 2008 – Jan., 2009.
- Research Assistantship / VCU-School of Engineering: Aug., 2006 – Aug., 2008.

MEMBERSHIP:

- Member in the American Physical Society (APS), 2008 - Present.
- Member in American Society of Mechanical Engineers (ASME), 2007 - Present.
- Graduate Student Association (GSA), Virginia Commonwealth University, USA, 2006 - Present.